THE UNIVERSITY OF ST. ANDREWS

Eclipse mapping and Doppler imaging of late-type single and binary stars

Tim Lister

Submitted for the degree of Ph.D.

September 2000

DECLARATION

I, Timothy Andrew Lister, hereby certify that this thesis, which is approximately 50000 words in length, has been written by me, that it is the record of work carried out by me and that it has not been submitted in any previous application for a higher degree.

September 2000

I was admitted as a research student in October 1997 and as a candidate for the degree of Ph.D. in October 1997; the higher study for which this is a record was carried out at the University of St. Andrews between 1997 and 2000.

September 2000

In submitting this thesis to the University of St. Andrews I understand that I am giving permission for it to be made available for use in accordance with the regulations of the University Library for the time being in force, subject to any copyright vested in the work not being affected thereby. I also understand that the title and abstract will be published, and that a copy of the work may be made and supplied to any *bona fide* library or research worker.

September 2000

I hereby certify that the candidate has fulfilled the conditions of the Resolution and Regulations appropriate for the degree of Ph.D. in the University of St. Andrews and that the candidate is qualified to submit this thesis in application for that degree.

September 2000

THE UNIVERSITY OF ST. ANDREWS

Eclipse mapping and Doppler imaging of late-type single and binary stars

Submitted for the degree of Ph.D.

September 2000

Tim Lister

ABSTRACT

The distribution of surface spot activity and long-term evolution on a variety of rapidly rotating cool stars is investigated. The techniques of Doppler imaging and eclipse mapping allow spectroscopic and photometric observations to be used to map the surface inhomogeneities on otherwise unresolvable active stars and binaries. Eclipse mapping makes use of high precision photometric observations and maximum entropy inversion methods to produce surface maps of eclipsing binary stars from data obtained on 1-metre class telescopes which compare well with those from high resolution spectroscopy which requires 4-metre class telescopes.

The stars examined span a range of rotation rate, type and tidal effects from the single K5 V dwarf star BD+22° 4409 (LO Peg) through two examples (GSC 2807-1423 and XY UMa) of the short period RS CVn class of active, detached binaries to the ultra-rapid rotation and extreme tidal torques of the W UMa contact binaries V523 Cas and TY UMa.

Using the indirect techniques of Doppler imaging and Eclipse mapping to derive surface maps for three of the five stars, we found evidence for a wide variety of spot activity on these stars. In the case of BD+22° 4409 we present the first images of this star, which is one of the latest in spectral type to have been imaged. The combination of rapid rotation and relative faintness of this target necessitated the use of Least-squares deconvolution to boost the S:N and enable surface maps to be produced. We also present the first spectroscopic study and surface maps of GSC 2807-1423 and considerably extend the baseline of surface maps for XY UMa.

In addition to the surface maps, in most cases it has been possible to collect data on a number of tracers of long-term activity variation. With the exception of BD+22° 4409 which has very little prior study, we have evidence for long-term changes in activity in the other four systems from archival photometry and times of eclipse minima.

ACKNOWLEDGEMENTS

I would like to thank my parents for unwittingly putting me off biology, and onto astronomy, which has proved to immensely enjoyable and satisfying and far better suited to me. Without their support throughout my education, I doubt I would have made it this far.

I would also like to thank my supervisor, Andrew Collier Cameron for his help and patience and my "pseudo-supervisor", Ron Hilditch, for a lot of valuable advice both related and unrelated to astronomy. A big thanks is due to the other members of the Cool Stars group at St. Andrews, for answering lots of dumb questions, often repeatedly, and those members of the group that have had to put up with me in the office over the years. I would especially like to thank John Barnes for the huge amount of help he has given me over the course of my thesis with the many obscurities of cool stars, Doppler imaging and data processing. I would also like to thank Dave James for two memorable observing trips including my first observing trip to La Palma which gave me a chance to lose so many games of pool on the mountain-top and taught me a lot about observational astronomy and the subsequent trip to the SAAO in South Africa. Thanks are also due to both Dave and John for obtaining the spectra of GSC2807-1423 during an Alpha Per run on the WHT.

The amounts of observational data that I have collected and reduced at St. Andrews would not have been possible without the superb efforts of Roger Stapleton, who runs one of the best-functioning astronomy computer systems I've ever used, and Jim Park and the other techs in the Electronics Workshop who have done so much to keep the James Gregory Telescope running with very minimal resources. They dealt effectively with all the problems I managed to bring them, even when it included setting fire to bits of equipment...

Many friends have helped and influenced me during my time at St. Andrews as both an undergraduate and postgraduate. Express thanks are due to Alasdair Allan for taking me under his wing and giving me my first taste of "big"-scope observing on the JGT, all the members of the AstroSoc and VirtualSoc committees I've known and served with but especially David Jackson (for the lessons to a newbie Observing Director), Nick Drake & Bronje Musgrave (for being wonderful academic parents among from many other reasons), Fiona Arnott (for making my job as VP such an interesting challenge...!), Micheal Willis

and Fraser Clarke. I also need to thank the owners and bar staff of my two favourite pubs in St. Andrews, the Cellar Bar and the Whey Pat Tavern, for giving me somewhere to escape to and relax in after work. So thanks to Barbera & Malcolm, Steve & Marjorie, Ellis, Big Andy, Alan, Karen, Ben and anyone else I've forgotten for doing their bit to keep me sane over the 7 years !

Big thanks are also due to the Comp. Sci. class of 1997, especially David Given, Stewart Waudby, Andrew Cook, Martin Bramley and Iain Merrick who have provided some great times over the years and who are all now earning far more than me... (but still send me computer problems at irregular intervals). I also need to thank the Honours Physics & Astronomy class of 96/97, who were a great bunch of people to work and study with and who made the whole experience of undergraduate astronomy so much richer. Of these people, I would most like to thank Helen Gossage for being such a wonderful friend over the years I have known her, and for always being there when I was struggling with some problem during my time as an undergrad. I always felt that I could talk to you about pretty much anything, and I regret the lapses in communications which have been due to tardiness on my part.

Last but certainly not least, the biggest thank you has to go to Rachel Street for putting up with me throughout the writing of this thesis and beyond. She has never failed to be there to support me and lift me when I would get down and thought I would never finish. Without her love and support to help me through the low points when it all seemed futile, I would never have made it this far. Thank you for sticking by me through the trying times and I would like to dedicate this thesis to you.

"Randy enrolled at another college with the aim of getting his master's degree in astronomy. This made him a grad student, and grad students existed not to learn things but to relieve the tenured faculty members of tiresome burdens such as educating people and doing research.

Within a month of his arrival, Randy solved some trivial computer problems for one of the other grad students. A week later, the chairman of the astronomy department called him over and said, "So, you're the UNIX guru." At the time, Randy was still stupid enough to be flattered, when he should have recognized them as bone-chilling words.

Three years later, he left the Astronomy Department without a degree, and with nothing to show for his labours except six hundred dollars in his bank account and a staggeringly comprehensive knowledge of UNIX."

Neal Stephenson *"Cryptonomicon"*

"Astronomers ... are paid to talk learnedly about a heavenly body's composition, weight, path - the irregularities of its conduct, the aberrations of its light - a sort of scientific scandal-mongering"

Joseph Conrad *"Lord Jim"*

CONTENTS

LIST OF FIGURES

LIST OF TABLES

CHAPTER 1

Introduction

1.1 Introduction

Although the Sun is our closest star by many orders of magnitude and despite having sunspot records stretching back to ancient China, our knowledge of the Sun's internal workings and its magnetic field is far from complete. Many of the manifestations of the Sun's magnetic field such as sunspots, flares and the corona are not fully understood.

In order to increase our understanding of magnetic fields on stars in general it is necessary to broaden our base of examples to include stars with a variety of ages, masses, rotation rates and try to draw a general consensus from as broad a range as possible.

Until such time as there is a significant improvement in the relatively new field of optical interferometric imaging, the tiny angular sizes of even nearby stars will make direct imaging of stellar surfaces impossible. This means that we will have to rely on indirect methods to obtain information about the surfaces of cool stars and their environment. Despite a history stretching back only 13 years, the method of Doppler imaging has been the most successful of the indirect methods and has provided a wealth of information on a wide variety of objects.

The Sun is variable in a wide variety of ways and on a large range of timescales. Somewhat surprisingly given the length of records of sunspots, the 11 year periodicity in sunspot number was identified about a century and a half ago (Schwabe 1843, Wolf 1856). Although the 11.1 year Schwabe cycle is the best known stellar activity cycle, the actual time between successive solar maxima, as measured from the eighteenth century up to the present day, varies between 8 and 15 years with a mean of 11 years (Eddy 1977). However

this is not the complete story as the magnetic field polarity in the sunspot groups reverses at the end of each 11 year cycle to produce Hale's 22 year magnetic cycle (Hale & Nicholson 1925). Other periodicities have also been detected such as the ~80 year Gleissberg cycle (Gleissberg 1944, Gleissberg 1971) and a longer period 190-yr cycle (Kuklin 1976).

On top of this regular cyclic behaviour are occasional absences of any activity for prolonged lengths of time. The most well known of these is the Maunder minimum (1645–1715), a period of approximately 70 years when almost no spots were observed on the solar surface which has been linked to a period of climate disruption on Earth. Other prolonged minima in solar activity have been identified in the past from sunspot records, auroral histories and radiocarbon records in tree rings (Ribes & Nesme-Ribes 1993 and references therein).

In order to understand the complex magnetic behaviour of the Sun and the timescales that they operate on, along with the occasional quenching of periodic behaviour, within a coherent framework, we need to determine which are the significant parameters and their relevant importance. Since our available data from the Sun can only ever cover a very limited region in this multi-dimensional parameter space, it is important to broaden the observational sample to include stars of other masses, temperatures, rotation, activity, age etc if we are to have any hope of identifying the critical parameters that give rise to the stellar dynamo and the enormous variety of magnetic behaviour seen on active stars.

1.2 Activity cycles

1.2.1 Single stars

The interest in using the Ca II H & K lines to track stellar activity cycles is due to Olin Wilson who became interested after seeing a plot of the Sun's 11 year cycle traced out in Ca II K emission. This led to the start of a 12 year program recording the variability of Ca II H & K fluxes on 91 stars that were "on or near the lower main sequence" which span a range of early F to early M (although there is only 1 example of the latter type) in spectral type. The results of this program were published in Wilson (1978). This work, which became the HK Project, has continued to the present day with an expansion to nightly observations in 1980, the inclusion of ~ 300 evolved giant stars from 1983 and in

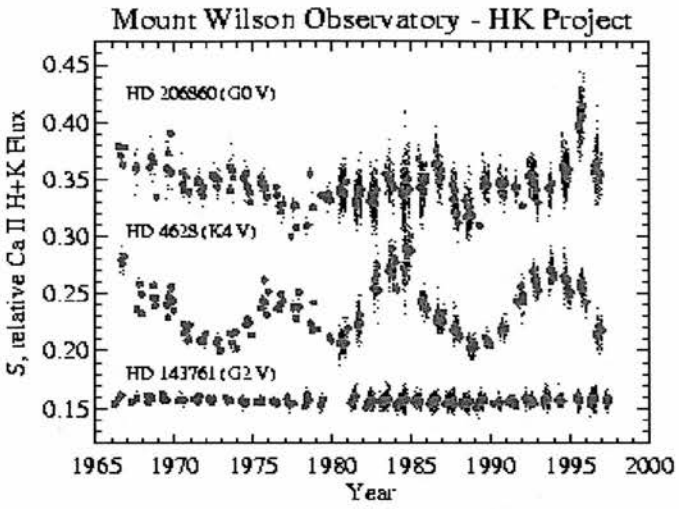

Figure 1.1: Three classes of Ca II variability: variable (top, HD 206860), cyclic (middle, HD 4628) and non-variable (bottom, ρ CrB). (From Baliunas *et al.* 1998).

1991, the start of monitoring of 120 stars with similar masses and magnetic activity to the Sun.

As discussed by Baliunas et al. (1998), Wilson found that the monitored stars fall into three broad classes of activity:

- *First*, smooth cycles with timescales of order of a decade (similar to the Sun's 11/22 year spot and magnetic cycles),
- *Second*, significant long-term variations but no obvious period,
- *Third*, inactive stars with no significant variation (either due to old age or possibly in a Maunder Minimum-like state)

Examples of each type of activity class are shown in Figure 1.1.

The increased baseline of observations since Wilson's first work have enabled the statistics on the amount and timescales of stellar magnetic variations to be improved.

Approximately 60% of the sample of stars show cyclic variations with periodic behaviour in their Ca II H and K fluxes and these cycles can occur in stars of all spectral types and any age. The upper limit on periods is 30 years which is set by the length of the observations and assumes that the stars showing systematic upwards or downwards

trends will eventually reverse. The older stars have a period cutoff at 7 years, with none of these stars having periods less than this value.

About 25% of the stars that have been monitored show variations but without any apparent periodicity. These tend to be the nearby analogues of the highly active, rapidly rotating dwarf stars found in young open clusters such as the Pleiades and α Per.

Finally, some 15% of the sample have records which are essentially flat and constant over the length of observation. It is likely that these stars are either old enough that the magnetic variability has declined to negligible or undetectable levels or the stars are in a long period of inactivity similar to the one the Sun experienced in the 17th century.

In addition to the chromospheric monitoring carried out by the HK Project, several programs have monitored the photometric variations of sun-like stars. There are several reasons for doing this. Experiments with space-based radiometers have show that during the Sun's 11 year sunspot cycle the increasing areal coverage of spots is accompanied by an increase in overall irradiance, presumed to be due to an increase in the bright faculae associated with the spots and it is important to contrast this with the behaviour on other stars. Another reason is that in very active, rapidly rotating stars the chromospheric emission saturates (Vilhu 1984) and so Ca II HK fluxes are no longer an effective proxy for magnetic variability.

However there are several reasons why the detection of long-term brightness variations in stars other than the Sun is not as simple as in the solar case. Firstly, the majority of the stars are far more active and heavily spotted, and in some cases, more evolved than the Sun and there is no reason to assume they will have strictly cyclic behaviour. In addition the long-term cycles are of relatively small amplitude and the photometric variation due to rotational modulation of spots is very much larger than it is on the Sun (up to $\Delta V = 0.6$ mag has been measured on HD 12545; Nolthenius 1991). This, coupled with the shorter-term irregularities caused by spot growth, decay and distribution tends to mask any long-term variations that are present. Finally the cycle periods for the evolved stars commonly found in RS CVn-type binaries tend to be much longer (cf. Sections 1.2.2.1 and 1.2.2.3) than the 7 to 21 years for solar-type stars found by Baliunas & Soon (1995).

Lockwood, Skiff & Radick (1997) reported on 12 years of photometric monitoring in Strömgren b, y of 41 program stars and 73 comparison stars. The program stars were

primarily main-sequence stars with the majority chosen from Wilson's targets and designed to bracket the Sun in temperature and mean chromospheric activity. The quantity used by Wilson to measure chromospheric emission observationally is known as the S-index which was developed into a chromospheric emission ratio, R'_{HK} by Noyes et al. (1984). This is defined as the chromospheric HK emission of a star normalized by the bolometric luminosity and also has the effect of correcting for a colour effect and the photospheric contribution present in the S-index. The program stars have spectral types spanning the range F3 to K7 and and mean chromospheric activity in the range $R'_{HK} = -4.23$ to -5.3 (cf. $R'_{HK} = -4.94$ for the Sun).

Early results from this program (Radick, Lockwood & Baliunas 1990) confirmed that the behaviour seen on the Sun of linked brightness and magnetic activity changes on time scales of activity cycles is also seen on other sun-like stars. The situation is somewhat different for stars which are younger than the Sun, as these stars show brightness and magnetic changes which are anti-correlated. This is presumably due to the much larger areas that spots on these stars cover (see e.g. Strassmeier 1999) meaning that the dimming due to the spots outweighs any brightening due to associated enhanced plage activity.

Another photometric monitoring program on active stars is being carried out by the Vienna and Catania groups with automatic photoelectric telescopes (Strassmeier et al. 1997b; Rodonò & Cutispoto 1994) located on Mt. Hopkins in Arizona and Mt. Etna in Sicily. Results for 23 stars of which 4 are solar type single stars, 2 are T Tauri stars, 4 are giants/subgiants and the remainder are RS CVn binaries, were presented by Strassmeier et al. (1997a).

The data of Strassmeier et al. (1997a) were combined with an additional three years of observations by Oláh, Kolláth & Strassmeier (2000) to study long-term behaviour. The single LQ Hya was included (along with 9 binary systems which are discussed further in Section 1.2.2) and they found a fairly smooth long-term variation which could be approximated by two periods of 11.4 and 6.8 years. The short period had higher power and is similar to the 7 year period mentioned by Strassmeier et al. (1997a).

Bondar' (1995) presented long-term studies of 29 red dwarf stars from measurements of archival plate collections, of which 10 objects had detectable or suspected long-term changes in their yearly mean magnitudes. Eight of these had long-term variations in the region of 0.2–0.5 mag and two (V833 Tau and PZ Mon) had variability of 0.6 and 1.0 mag

respectively.

Of these 10 stars only V833 Tau (discussed in the next section) and PZ Mon have actual cyclic behaviour where more than 1 complete cycle has been seen. The remainder, comprising 4 visual binaries (V577 Mon, FL Vir, V647 Her, HU Del), 1 single star (YZ CMi) and 3 spectroscopic binaries (BY Dra, CV Cnc[1] and CU Cnc[1]) will need further observation to derive unambiguous spot cycle periods.

PZ Mon is a relatively unstudied active star that was shown by Bondar' (1992) to have the greatest photometric variability of any of the BY Dra dwarf stars. A long-term spot cycle of $P_{cyc} \sim 50$ yrs was presented by Bondar' (1995). The evolutionary state was revised by Saar (1998) who used the archival photometry in conjunction with the *Hipparcos* parallax and high resolution spectra to assign a spectral type of K1 III to PZ Mon, making it a probable RS CVn system similar to σ Gem and consistent with the low level of flaring that had been observed. Further spectroscopic observations would be needed to determine whether PZ Mon is actually a binary.

The number of active single giants is quite a lot smaller than the number of dwarf stars. The General Catalogue of Variable Stars (Kholopov et al. 1985) lists only 4 members of the FK Comae class of rapidly-rotating active giant stars of which one (UZ Lib) turned out to be binary (Bopp et al. 1983, Strassmeier 1996b) and two (V642 Mon and V645 Mon) are unconfirmed. A few other candidates for this class have been suggested (see e.g. Gondoin 1999) but most will require additional data to determine conclusive membership of the FK Comae class.

The only FK Comae stars that have been studied well enough for any chance of cycle determination are the class prototype FK Comae Berenices (G2 III) itself and HD 199178 (=V1794 Cyg; G5 III-IV). Korhonen et al. (1999) presented results from surface images of FK Com that suggested that the same spot group had persisted for the 11 months between observations and had moved 0.2 in phase. They also collated and analysed all the available photometric data from 1980 and determined that the photometric minimum moves between the two active longitudes previously determined by Jetsu, Pelt & Tuominen (1993). The occupation of a given active longitude lasts 1–2 years with the changeover to the other active longitude taking a similar time. There is some evidence of a 6.5 year

[1]Although classified as a single flare star and a SB2 binary respectively by Bondar' (1995), CV Cnc and CU Cnc are actually part of the GJ 2069 quadruple system (Delfosse et al. 1999)

cycle in the behaviour of the active longitudes but additional data will be needed for 1996–present to confirm this possible cycle.

V1794 Cyg is another star which is well confirmed as a member of the FK Com class and magnetic activity has been detected at all wavelengths from the radio to the X-ray (Strassmeier et al. 1999 and references therein). 20 years of $UBVRI$ photometry were analysed by Jetsu, Pelt & Tuominen (1999) who found no significant activity cycles in either the mean magnitude or the total amplitude of the seasonal light curves. They also found no active longitudes that were statistically significant upon applying the same tests that found active longitudes on FK Com and 4 RS CVn binaries (Jetsu 1996). The proposed explanation for the non-detection of active longitudes was strong differential rotation indicated by the short-term period changes which implied differential rotation 3 times stronger than in FK Com (Jetsu, Pelt & Tuominen 1993). By contrast the yearly period changes were surprisingly regular with the suggestion of 3.3 year cycle representing the butterfly diagram of V1794 Cyg, although no significant correlation with mean magnitude was found.

There is obviously a need for continued monitoring of the known active single dwarf and giant stars and additional efforts should be put into finding and confirming additional examples, especially of the FK Comae class. The new generation of X-ray satellites such as *AXAF* and *XMM-Newton* with their greatly increased collecting area, throughput and sensitivity should make this task easier by virtue of being able to reach fainter X-ray flux levels. This should enable a larger volume of space to be probed and fainter examples of the FK Comae class found.

1.2.2 Binary stars

1.2.2.1 Photometric variations

The original chromospheric survey of main-sequence stars (Wilson 1978) was selected to exclude any known spectroscopic binaries and only a few visual binaries were included. Although it is well established that the mean magnetic activity level decreases gradually with age and rotation, as shown by Baliunas et al. (1998) for the Sun, the long-term surface magnetic variability leads to an apparent uncertainty in the solar age of 3–8 billion years. In order to study the amount of long-term variability, binaries are important since each

Table 1.1: Binary stars with long-period photometric variations. (Adapted from Oláh, Kolláth & Strassmeier 2000).

Star	Spectral class	P_{orb} (days)	P_{rot} (days)	τ_1 (yrs)	τ_2 (yrs)	τ_3 (yrs)	Time base (yrs)
V833 Tau	K5 V	1.7880	1.7936	trend(60?)	6.4	2.5	11.3
EI Eri	G5 IV	1.9472	1.9527	trend	16.2	2.4	18.5
V711 Tau	G5 IV+K1 IV	2.8377	2.841	-	16.5	3.5:	22.0
BY Dra	K4 V+K7 V	5.7951	3.8285	trend(55?)	13.7	2.7:	27.8
HU Vir	K0 III–IV	10.3876	10.42	trend	-	5.6	16.0
IL Hya	K0 III–IV	12.908	12.791	trend	13.0	-	27.3
VY Ari	K3–4 IV–V	13.198	16.199	-	15.3	-	22.2
HK Lac	K0 III	24.4284	24.378	≥ 34.2	13.0	6.8	30.3
IM Peg	K2 III	24.6488	24.494	≥ 48.3	-	-	27.2

component should have the same age. A sample of visual binaries were measured by Donahue (1998) who found a mean age discrepancy of 1.1 Gyr, although 70% of all the binaries and 60% of those over ~ 2.2 Gyr had an age discrepancy < 1 Gyr. The large age discrepancies that arise for older binaries are thought to be due to one of the components being in a "Maunder Minimum"-like state of prolonged inactivity.

The long-term behaviour of 10 rapidly-rotating active stars (including one single star - LQ Hya) was studied by Oláh, Kolláth & Strassmeier (2000) using the large collection of photometric data collected by Strassmeier et al. (1997a), supplemented by an additional 3 years of photometric data collected with the Vienna automatic photoelectric telescopes (Strassmeier et al. 1997b). They determined cycle lengths for nine of the ten stars studied and found double or multiple time-scale variations for six of the nine cyclic stars and the results, along with the basic stellar data, are summarized in Table 1.1. Here P_{orb} is the orbital period and P_{rot} is the rotational period, which can be different from the orbital period even in the case of orbital synchronization because of the effect of the spots at different latitudes and rotational velocities on the light curve. In the table, $\tau_{1,2,3}$ are the significant resulting periods from their analysis in order of decreasing length.

They found that the long-term brightness variations on active stars are primarily caused by changes in the overall spot coverage and that spot migration (if present) does not

change the shape or length of the cycles. In several cases there was good agreement between the cycle lengths determined from photometry and those determined by other means such as O-C curves, Doppler imaging and total spot areas, orbital period fluctuations or periods of a third body and alternating minima changes.

Of the stars studied by Oláh, Kolláth & Strassmeier (2000), two of them-V833 Tau and BY Dra-were also studied by Bondar' (1995) (cf. Section 1.2.1) for long-term trends.

V833 Tau is a dK5e BY Dra-type variable in a 1.778 day orbit (Griffin et al. 1985) with an unseen companion which is thought to be sub-stellar, with a minimum mass of only $0.05\,M_{\odot}$ (Hartmann et al. 1981). There is no evidence that the star has been spun up to synchronous rotation by tidal torques and although it can effectively be considered as single we choose to consider it here. The long-term sinusoidal cycle of ~ 60 years found by Bondar' (1995) from photographic observations shows up in the photometric data of Oláh, Kolláth & Strassmeier (2000) as a long-term trend, along with a shorter period of 6.4 years with the possibility of another period of 2.5 years.

BY Dra is the prototype for the class of active dwarf stars which show spot modulation and flaring activity at many wavelengths. It is a non-eclipsing spectroscopic binary (dK5e + dK7e, $P = 5.795\,\mathrm{d}$) with an inclination of about 30°and pseudosynchronous rotation but a non-circular orbit ($e = 0.3$), possibly indicating youth. There is a long history of observation with photographic records stretching back to 1898. Investigations of long-term trends have been carried out based on photographic observations (Phillips & Hartmann 1978, Bondar' 1995) and on photoelectric data by many authors (e.g. Pettersen, Oláh & Sandmann 1992, Kővári 1999).

Bondar' (1995) found long-term variations of the order of 0.3–0.5 mag. with a duration of ~ 60 years with a shorter period of $\sim$ 8–9 years and lower amplitude superimposed. Pettersen, Oláh & Sandmann (1992) found cyclic behaviour on a timescale of $\sim$ 13–14 years, a result confirmed by Oláh, Kolláth & Strassmeier (2000) who found a timescale $\tau_2 = 13.7$ years but no evidence of the longer cycle found by Bondar' (1995).

1.2.2.2 Active longitudes

Preferred longitudes for spot activity have been found on a number of systems and have been known about for many years. Zeilik and collaborators have found evidence for per-

sistent active longitudes on a variety of short-period RS CVn systems; SV Cam (Zeilik et al. 1988b), RT And (Zeilik et al. 1989), WY Cnc (Zeilik et al. 1990a), BH Vir (Zeilik et al. 1990c) and CG Cyg (Zeilik et al. 1994). The short-period RS CVn EI Eri ($P = 1.95$ d) was found to have active longitudes and switching between them by Berdyugina & Tuominen (1998). A similar result was found by Jetsu (1996) for V711 Tau (=HR 1099, $P = 2.8$ d). Among longer period binaries active longitudes have been identified on HK Lac ($P = 24.4$ d; Oláh, Hall & Henry 1991, Oláh et al. 1997), II Peg ($P = 6.7$ d; Lazáro, Arévalo & Fuensalida 1987, Jetsu 1996, Berdyugina et al. 1998b), λ And ($P = 20.5$ d; Jetsu 1996), σ Gem ($P = 19.6$ d; Oláh et al. 1989, Jetsu 1996).

Active longitudes and activity cycles on four RS CVn (EI Eri, II Peg, σ Gem and HR 7275) binary systems were presented by Berdyugina & Tuominen (1998) from their reanalysis of archival photometry. This work followed on and extended the period analysis work of Jetsu (1996) which in turn used the photometric data of Henry et al. (1995). They found active longitudes on all 4 systems and all separated by 180° (0.5 in phase) to within the errors. They found no preferable orientation of the active longitudes with respect to the line of centres in the binaries implying that they are not synchronized with the orbital motion. The exception to this was σ Gem where synchronization was observed and the active longitudes were located along the binary line of centres.

Most of these stars showed similar behaviour in that one longitude is usually more active than the other and this persists for several years. In most cases there is evidence for a "flip-flop" or switching of activity in the active longitudes, which happens in a much shorter timescale of a few months. Multiple switching events were observed on EI Eri (3 switches, $P_{cycle} = 9.0$ yrs), II Peg (5 switches, $P_{cycle} = 9.3$ yrs), σ Gem (2 switches, $P_{cycle} \simeq 14.9$ yrs) and HR 7275 (=V1762 Cyg, 2 switches, $P_{cycle} \simeq 17.5$ yrs). These are similar to that observed on FK Comae (Korhonen et al. 1999) (cf Section 1.2.1). This switch in active longitude was thought to be due to spot migration in the orbital reference frame rather than spot evolution within the active longitude regions, a view which was reversed subsequently by Korhonen et al. (1999) and Berdyugina et al. (1998b) who attributed the switch to spot evolution.

The cyclic behaviour observed on these binaries seems to be very different from that on the Sun as the structure is highly nonaxisymmetric. Another difference is that the latitudinal motion of the spots seems to be very small because of the almost linear migration

of the spots in phase. Theoretical calculations of nonaxisymmetric dynamo models by Moss & Tuominen (1997) have shown that close late-type binaries which have orbitally synchronized components should show large-scale nonaxisymmetric magnetic fields with maxima at the conjunctions, corresponding to the longitudes 0°and 180°.

This is observed for σ Gem but not for the other three long period systems studied by Berdyugina & Tuominen (1998). The shorter-period RS CVn systems with $P \leq 1$ day appear to contradict this model also by having active longitudes located preferentially at 90°and 270°. Clearly further observational results and improved theoretical calculations of dynamo models and flux tube evolution in binary systems will be required before the formation, evolution and persistence of active longitudes in binary systems is understood.

1.2.2.3 Orbital period variations

Long-term observations of eclipsing binaries and their times of minima have shown evidence for orbital period variation on a wide variety of binary systems including members of the RS CVn, Algol, contact (W UMa) and cataclysmic variable (CV) classes and even binary pulsars (Arzoumanian, Fruchter & Taylor 1994). These variations tend to be quasi-periodic rather than strictly sinusoidal with amplitudes up to $\Delta P/P \simeq 3 \times 10^{-5}$ and periods of a few decades to a few centuries in RS CVn and Algol systems. The use of the sophisticated timing techniques used in the field of millisecond pulsar study has led to the discovery of period changes of $\Delta P/P \sim 10^{-7}$ in the binary pulsar PSR B1957+20 which consists of a 1.6 ms pulsar and a 0.025 $M_\odot$ companion.

The suggestion that these long-term period changes could be related to magnetic activity was put forward by Hall (1989) who found that in a sample of 101 Algol systems, only those with secondaries having a spectral type later than F5 showed orbital period variations which varied in sign. Other possible explanations for period change such as mass transfers/ejection, gravitational radiation, magnetic braking via a stellar wind or thermal relaxation oscillations would produce period changes of fixed sign or with timescales orders of magnitude longer than what is observed.

A number of systems have been identified which show long-period cyclic orbital period changes and these are shown in Table 1.2. These have been taken primarily from the compilation of 46 (including 10 CV systems) eclipsing binaries studied by Lanza &

Table 1.2: Binary stars with long-period orbital period variations covering at least one complete cycle. (Adapted from Lanza & Rodonò 1999).

Star	Spectral class	P_{orb} (days)	τ_1 (yrs)	τ_2 (yrs)	Time base (yrs)
β Per (Algol)	B8 V+K4 IV	2.8673	32.0	-	195.3
RS CVn	K2 IV+F5 V	4.7979	trend (112.0?)	39.0	102
AR Lac	G2 IV+K0 IV	1.983	36.0	-	98
AB And	G5 V+G5 V	0.3319	86.5	-	92
CG Cyg	G9.5 V+K3 V	0.6311	50	-	90
RT Lac	G5+G9 IV	5.0740	80.7	12.06	101.4
W Del	A0+G2	4.8060	50.9	-	97.5
WW Dra	G2 IV+K0 IV	4.6296	79.3	-	97
U Sge	B8 V+G4 IV	3.3806	39.0	-	95
XZ And	A4 IV–V+G5 III	1.3573	36.8	-	104
X Tri	A3 V+G3 IV	0.9715	18.75	-	76
VV UMa	A2 V+G6	0.6874	22.28	-	65
AP Leo	F8 V+F8 V	0.4304	43.0	-	100

Rodonò (1999). We have adopted a more cautious approach than Lanza & Rodonò (1999) in that we have only included systems where at least one complete cycle of variation has been seen and where the majority of the cycle is not based on older, less accurate visual times of minima. We have also excluded from the table those systems which have a degenerate component such as V471 Tau (K2 V + WD) and the eclipsing binary pulsar systems mentioned earlier. The table includes 6 Algol systems (β Per, W Del, U Sge, XZ And, X Tri and VV UMa), 5 RS CVn systems (RS CVn, AR Lac, CG Cyg, RT Lac and WW Dra) and 2 W UMa systems (AB And and AP Leo).

In addition there are some systems such as CF Tuc (Anders et al. 1999), SZ Psc (Kalimeris et al. 1995) and several contact systems (see e.g. Kalimeris, Rovithis-Livaniou & Rovithis 1994) which have quasi-periodic O-C diagrams but there is an insufficient timebase in the majority of cases for a thorough analysis. A summary of these systems is presented in Table 1.3 which lists each star, its binary class, orbital period and most likely timescale for variation, τ_1 (taken either from Lanza & Rodonò 1999 or the quoted

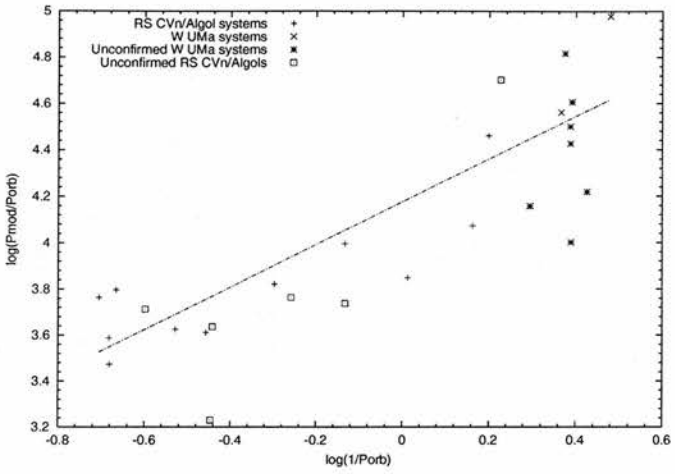

Figure 1.2: $\log(P_{mod}/P_{orb})$ against $\log(P_{orb})$ for the binary systems listed in Table 1.2 with a straight line fit to the data. Also shown are the unconfirmed cycles of the systems in Table 1.3.

Table 1.3: Binary stars with long-period orbital period variations that could be confirmed with a small amount of additional observations.

Star	Binary Type	P_{orb} (days)	τ_1 (yrs)	V mag	Reference
RW Tau	Algol	2.7688	32.8	8.0–11.5	Šimon (1997a)
TV Cas	Algol	1.813	28.8	7.2–8.2	Khalesseh & Hill (1992)
Z Dra	Algol	1.3574	20.3	10.8–14.1	Rafert (1982)
SV Cam	RS CVn	0.5931	82.0	8.4–9.2	Applegate (1992)
CF Tuc	RS CVn	2.798	13.0	7.0–7.3	Anders et al. (1999)
SZ Psc	RS CVn	3.9658	56.0	7.2–7.7	Kalimeris et al. (1995)
OO Aql	W UMa	0.5068	20.0	9.3–10.3	Demircan & Gürol (1996)
AK Her	W UMa	0.4215	75.7	8.3–8.8	Rovithis-Livaniou et al. (1992)
V566 Oph	W UMa	0.4096	35.6	13.8–15.5	Kalimeris et al. (1994)
AH Vir	W UMa	0.4075	11.2	9.0–9.6	Demicran, Derman & Akalin (1991)
V839 Oph	W UMa	0.4090	30.0	8.8–9.4	Akalin & Derman (1997)
SS Ari	W UMa	0.4060	30.0	10.4–10.9	Demircan & Selam (1993)
U Peg	W UMa	0.3748	17.0	9.2–10.0	Zhai, Zhang & Leung (1984)

reference).

The variation of P_{mod}/P_{orb} (with τ_1 normally taken as P_{mod}, except in the case of RT Lac) against P_{orb} is shown on a logarithmic scale in Figure 1.2 where both sets of systems have been included. There is evidence for a correlation but little evidence for the 2 parallel branches seen by Oláh, Kolláth & Strassmeier (2000) (their Fig. 13). Clearly additional systems need to be found and the probable cycles of the systems in Table 1.3 confirmed before we can say with any certainty whether the ratio of P_{mod}/P_{orb} has any physical meaning as has been suggested by Soon, Baliunas & Zhang (1993).

These systems would be the most suitable for future monitoring to obtain additional times of eclipse minima as all the systems are bright ($V \leq 12$ mag with the exception of Z Dra and V566 Oph) and many have deep, easily detectable primary eclipses. The orbital periods are for the most part short and, for the W UMa systems in particular, at least 1–2 minima could be obtained in a single night of observing using photoelectric photometers or CCD detectors on small telescopes. In addition, the W UMa systems in Table 1.3 show a variation in τ_1 covering $\sim$ 11–76 years with a corresponding range in P_{orb} of only 0.13 day. The confirmation and refinement of these cycle periods will be important for determining what fundamental parameters govern long-term stellar activity.

The wide variety of long term periods and period changes seen in binary systems has been given a possible theoretical explanation by Applegate & Patterson (1987) and Applegate (1992). Those authors propose that the orbital period modulation can be explained a coupling of the binary orbit to changes in the gravitational quadrupole moment of the magnetically active star in the system as it goes through an activity cycle. The gravitational quadrupole moment is sensitive to the speed of rotation of the outer part of the star and the required shape change of the star can be produced by the cyclic transfer of angular momentum from the inner to the outer part of the star. The required torque to produce this transfer can by supplied by a magnetic field beneath the surface of several kilogauss, which is of the order of those known on the Sun and other active stars.

The model requires variability at the $\Delta L/L \simeq 0.1$ level and a variable differential rotation of $\Delta\Omega/\Omega \simeq 0.01$ in order to explain orbital period variation of the order of $\Delta P/P \simeq 10^{-5}$. The mechanism has several predictions which should be testable. Firstly the luminosity variation should have the same period as the orbital period modulation and any other magnetic indicator such as starspot amplitudes, coronal X-ray luminosity

or chromospheric lines must also have the same period. Additionally the star should also be hottest and bluest at its most luminous, although this may be difficult to decouple from time-variable spot effects.

Applegate (1992) applied the presented model to Algol, three RS CVn-type binaries SS Cam, SV Cam and RS CVn itself as well as a pre-CV, V471 Tau. Applegate found that the model produces a good fit to all of the systems with the exception of RS CVn. Confirmation of the predictions of the Applegate model were provided for the eclipsing RS CVn binary CG Cyg by Hall (1991b) who found that the mean brightness outside of eclipse and the orbital period vary with the same cycle length of $\sim$ 50 years. Also the light curve and O-C curve are in phase with the maximum light and a period increase, with both occurring in early 1980. In addition the chromospherically active star became bluer in phase with the brightening.

Rodonò, Lanza & Catalano (1995) analysed 34 V band light curves of RS CVn (K2 IV + F5 V) obtained between 1949 and 1993 by means of an iterative χ^2 optimization technique which divided the stellar surface into elements $9^\circ \times 9^\circ$ on a side, adjusting the specific intensities until a good fit was found. They found satisfactory fits by assuming that spots were only located on the K2 IV component. Fourier analysis of the spot area over time gave a cycle period of 19.7 ± 1.9 years. In addition they analysed the variation of the orbital period by means of times of minima going back to 1890 and found a long-term modulation with a period of 122.15 years. When this was removed, a shorter period variation of 38.8 years was found and they noted that this was almost exactly double the activity cycle period found from the analysis of the spot area.

These results produced a generalization of the Applegate mechanism by Lanza, Rodonò & Rosner (1998) who considered the effect of the Lorentz force which was found to lower the energetic requirements by a factor of two. They applied this to RS CVn and found a substantial improvement in agreement between the theory and observational data. A further generalization of the treatment of the magnetic field was proposed by Lanza & Rodonò (1999) and applied to a sample of 46 binaries of the Algol, RS CVn, W UMa and CV types.

Further observational tests of the Applegate mechanism have been carried out on the Algol-type binaries RW Tau (Šimon 1997a), SW Cyg and U Sge (Šimon 1997b). Šimon (1997a) analyzed over 100 years worth of minima times for RW Tau (B8 V + K0 III–IV,

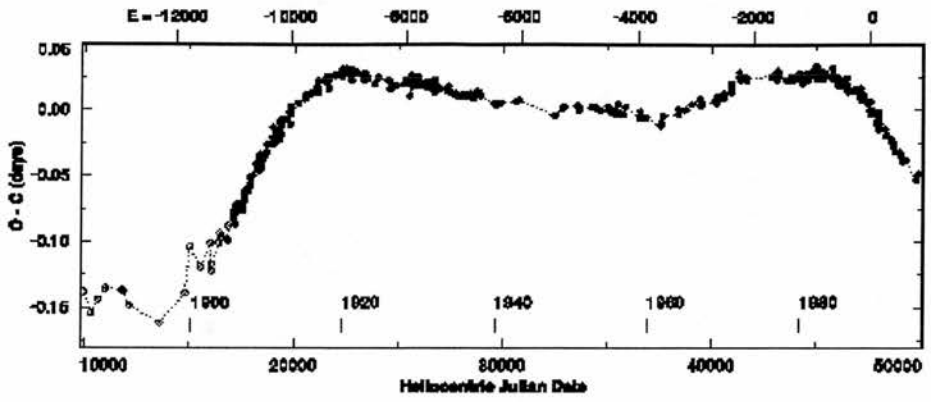

Figure 1.3: O-C diagram for RW Tau. (From Šimon 1997a).

P=2.77 days) and found that O-C curve was quite complex with 2 seasons of activity lasting 13000 and 15000 days with an interval between of $\sim$ 12000 days where the period was almost constant (see Figure 1.3). Comparison of Strömgren photometry with the O-C data was hampered by some incompleteness but some coincidence of brightness minima and abrupt changes of orbital period are apparent.

The identification of mass-transfer events with the period changes is very difficult since data for the former are scarce, requiring spectroscopic observations on larger telescopes than for minima timing. Plavec (1962) noted distortions of the RV curve due to the gas stream during 1939–1947 during which time the orbital period was almost constant.

It is difficult to interpret the RW Tau results within the framework of the Applegate model since the orbital period changes are far from periodic and the (admittedly limited) photometry is inconclusive. However traditional explanations of period change have even less success explaining the observations. Apsidal motion is definitely ruled out as orbital circularization would have occurred long before the mass transfer began. The long baseline of O-C timings rules out the third body with a period of 88 years cited by Frieboes-Conde & Herczeg (1973) to explain the period changes. Mass transfer in the conservative case (see e.g Huang 1963, Hilditch 2001) can only lead to a period increase and non-conservative mass transfer, where a temporary accretion disc forms and/or matter is lost through the L_2 point, requires a complex formulation with a large number of free parameters. Any mass transfer that is taking place in the system was inferred from the strength of the H α emission to be of the order of $10^{-9}\,\mathrm{M_{\odot}yr^{-1}}$ and the orbital period remained constant even during the times when enhanced emission was seen.

One possible explanation is that an Applegate-type mechanism is operating along

with mass-transfer and that during 1923–1955 when the period was almost constant, the orbital changes due to the magnetic cycle and the (possibly enhanced) mass-transfer roughly balanced out. Another possibility is that the dynamo in the secondary star somehow "switched off" and entered a short "Maunder Minimum"-like phase, leaving only the small effect of the mass-transfer on the orbital period. Since the period is currently decreasing, future monitoring should determine if the period change reverses indicating cyclical behaviour.

Similar results were found for SW Cyg and U Sge (Šimon 1997b) with a correlation of the changes in the orbital period P and the luminosity of the late-type loser star L_{los}. He proposed that the changes were due to changes in the apsidal motion constant k_{22} of the loser star (Matese & Whitmire 1983, Petrova 1995) which is very sensitive to the density profile. The highly erratic mass transfer in Algol systems could then cause disturbances in the outer convective layers and k_{22} on the diffusion time scale, similar to the observed period variations.

Although the baseline of observations of minima times can exceed a century in the case of the bright Algol and RS CVn systems, with periodic timescales of variation on the order of several decades this is only barely enough. In addition, the majority of the minima times are based on older, less accurate visual and photographic observations. However what is mostly critically needed for discriminating tests of the Applegate or other mechanisms is high precision minima times *combined with* long-term photometric monitoring, preferably in more than 1 colour, to confirm that orbital period and brightness variations are in step.

1.3 Surface imaging results

1.3.1 Single stars

In order to understand the nature of magnetic fields on the Sun and the stellar dynamo in general, we need more examples of single stars spanning a range of masses, rotation rates and evolutionary states. An obvious place to look to increase the number of suitable stars for Doppler imaging would be among the open clusters where photometric and spectroscopic work (e.g. Stauffer & Hartmann 1987; van Leeuwan, Alphenaar & Meys

1987; Stauffer, Hartmann & Jones 1989; Soderblom et al. 1993) has shown that there is a significant population of rapid rotators ($v\sin i > 40$ km s^{-1}) among the lower main sequence in clusters such as the Pleiades and α Persei. The most significant result is that, while rapid rotators of spectral types G-M are found in α Persei (age $\sim$ 50 Myr), by the age of the Pleiades ($\sim$ 70 Myr) only K or later type are found and at the age of the Hyades ($\sim$ 600 Myr) rapid rotators are restricted to M dwarfs. This large variation in spin-down timescale from $\sim$ 20 Myr for the G dwarfs to $\geq$ 500 Myr for the M dwarfs is a serious challenge for rotational spin-down models to explain, although recent models of angular momentum evolution for low-mass stars (e.g Bouvier, Forestini & Allain 1997) have narrowed the gap between models and the observations.

Although Doppler imaging has recently been pushed out to the nearby clusters of the Pleiades (Stout-Batalha & Vogt 1999) and α Persei (Barnes et al. 1998), it is still difficult to obtain spectra with high enough S:N, while keeping the exposure time short enough to minimise phase-blurring on these faint rapid rotators.

However, several stars much closer than the cluster dwarfs have been found in recent years of comparable age to those in the young clusters. They have usually been identified by having similar space motions to the Pleiades cluster and high photospheric lithium abundances. To date seven of these nearby single, main-sequence stars have been Doppler imaged: the Pleiades age K2-dwarf LQ Hya (Strassmeier et al. 1993; Rice & Strassmeier 1998), the ZAMS K0-dwarf star AB Dor, (Collier Cameron & Unruh 1994; Collier Cameron 1995; Unruh, Collier Cameron & Cutispoto 1995; Hussain, Unruh & Collier Cameron 1997; Donati & Collier Cameron 1997), the late-PMS/ZAMS K3-dwarf Speedy Mic (Barnes et al. 2000a), the young K5-dwarf BD+22°4409 (Lister, Collier Cameron & Bartus 1999), the G1.5-dwarf EK Dra (Strassmeier & Rice 1998) and the PMS star PZ Tel (Barnes et al. 2000b). In addition 6 stars in open clusters have been Doppler imaged, two low-mass Pleiades stars HII 686 (K4V) and HII 3163 (K0V) by Stout-Batalha & Vogt (1999) and four α Persei G-dwarfs He 699, He 520 (Barnes et al. 1998), AP 149 and AP 193 (Barnes 1999).

In addition to the dwarf stars, 3 single giant stars have been Doppler imaged. Two of these giants are members of the FK Comae Berenices (V1794 Cyg (HD 199178) and FK Com) and the other (CM Cam) is an effectively single giant star with a very long-period ($\sim$ 10 years) companion (Strassmeier et al. 1998). The parameters of these stars

are summarized in Table 1.4.

Table 1.4: Single stars that have been Doppler imaged. (Adapted from Strassmeier 1996a).

Star	M-K class	$v \sin i$	P_{rot}
Year(s) of obs.	i	Spots[1]	Reference
LQ Hya	K2 V	26.5 km s^{-1}	1.606 d
Feb 1991	70°	P, H, I, L	Strassmeier et al. (1993)
Feb 1991	75°	P, H, I, L	Saar et. al. (1994)
May 1991	75°	H, I, L	Saar et. al. (1994)
May 1993	75°	P, H, L	Saar et. al. (1994)
Mar 1995	65°	(P), H, L	Rice & Strassmeier (1998)
1992–96 (5 maps)	60°	P, H, I, L	Donati (1999)
AB Dor	K0 V	91 km s^{-1}	0.514790 d
Feb 1989	60°	H, I, L	Kürster et. al. (1994)
Jan 1992	60°	P, H, I, L	Collier Cameron & Unruh (1994)
Dec 1992	60°	P, H, I, L	Collier Cameron (1995)
Nov 1993	60°	(P), H, I, L	Unruh et. al. (1995)
Dec 1995	60°	P, H, I, L	Donati & Collier Cameron (1997)
Dec 1996	60°	P, H, I, L	Donati et al. (1999)
RX J1508.6-4423	G2 V	115 km s^{-1}	0.31 d
May 1998	30°	P, H, I, L	Donati et al. (2000)
HII 686	K4 V	64 km s^{-1}	0.397 d
Dec 1993	51°	(P), H, I, L	Stout-Batalha & Vogt (1999)
HII 3163	K0 V	70 km s^{-1}	0.42 d
Dec 1993	58°	P, H, I, L	Stout-Batalha & Vogt (1999)
EK Dra	G1.5 V	17 km s^{-1}	2.605 d
Mar 1995	60°	(P), H, I, L	Strassmeier & Rice (1998)
He 520	G6 V	91 km s^{-1}	0.607903 d
Nov 1996	75°	H, I, L	Barnes et al. (1998)
He 699	G2 V	96.5 km s^{-1}	0.490798 d
Oct 1996	65°	P, H, I, L	Barnes et al. (1998)
Nov 1996	65°	P, H, I, L	Barnes et al. (1998)

continued on next page

continued from previous page

Star	M-K class	$v \sin i$	P_{rot}
Year(s) of obs.	i	Spots[1]	Reference
AP 149	G8 V	102 km s^{-1}	0.32 d
Dec 1998	30°	(P), H, I, (L)	Barnes (1999)
AP 193	G5–6 V	64 km s^{-1}	0.7483 d
Dec 1998	55°	(P), H	Barnes (1999)
Speedy Mic	K3 V	128 km s^{-1}	0.38 d
July 1998	55°	H, I, L	Barnes et al. (2000a)
PZ Tel	K0 V	68 km s^{-1}	0.94 d
July 1999	60°	P, H, I, L	Barnes et al. (2000b)
BD+22° 4409	K5 V	69 km s^{-1}	0.4236 d
Aug 1993	50°	P, H, L	Lister et. al. (1999)
RE 1816+541	M1–2 V	61.6 km s^{-1}	0.4586 d
June 1996	70°	H, I, L	Barnes & Collier Cameron (2000)
FK Com	G2 III	155 km s^{-1}	2.39960 d
1989	75°	H, L	Piskunov & Huenemoerder (1994)
August 1994	60°	H	Korhonen et al. (1999)
July 1995	60°	H	Korhonen et al. (1999)
Jun–Jul 1996	60°	I,(L)	Korhonen et al. (2000)
Jul–Aug 1996	60°	I,L	Korhonen et al. (2000)
April 1997	60°	H,I	Korhonen et al. (2000)
June 1997	60°	H,I	Korhonen et al. (2000)
HD 199178	G5 III-IV	71.5 km s^{-1}	3.3286 d
1985	80°	P, L	Vogt (1988)
1989–90	40°	P, H, L	Strassmeier et al. (1999)
April 1997	40°	P, H, I, L	Strassmeier et al. (1999)
CM Cam	G8 III–II	47 km s^{-1}	16.053 d
March 1994	60°	P, H, I, L	Strassmeier et al. (1998)
Feb–March 1995	60°	(P), H, I, L	Strassmeier et al. (1998)
Jan 1996	60°	H, I, L	Strassmeier et al. (1998)
April 1997	60°	H, I, L	Strassmeier et al. (1998)

continued on next page

continued from previous page

Star	M-K class	$v \sin i$	P_{rot}
Year(s) of obs.	i	Spots[1]	Reference
YY Men	K2 III	50 km s^{-1}	9.55 d
Jan 1987	65°	H, L	Piskunov et. al. (1990)
Sep 1990	35°	P, H, I, L	Kürster & Dennerl (1993)

[1]P = Polar spot, H = High-latitude spots (latitudes 90°–60°), I = Intermediate-latitude spots (latitudes 60°–30°), L = Low-latitude spots (latitudes ≤30°). Brackets denote inconclusive evidence for that type of spot.

1.3.2 Detached binaries

A large number of detached binary systems, primarily RS CVn systems with giant or sub-giant primary components of spectral type G–K and an unseen secondary component, presumably of late spectral type, have been Doppler imaged over the years. There are several reasons for this preponderance of RS CVn systems. The presence of a giant or sub-giant component ensures that the system will be fairly bright and the short periods allow a large phase coverage within a reasonable amount of telescope time. On the other hand, the $v \sin i$ values are not so high that the signal-to-noise has to be compromised to avoid phase-smearing.

The exceptions to this are V824 Ara which is a pre-main sequence binary and YY Gem which is a double M-dwarf binary. Both of these systems are important since they broaden the sample space of studied systems. Details of the systems are shown in Table 1.5.

Table 1.5: Detached binary stars that have been Doppler imaged. (Adapted from Strassmeier 1996a). Where two values of $v \sin i$ appear, this indicates that both components were imaged.

Star	M-K class	$v \sin i$	P_{rot}
Year(s) of obs.	i	Spots[1]	Reference
HR 1099	K1 IV	41 km s^{-1}	2.84 d
Oct 1981	33°	P, L	Vogt & Penrod (1983)

continued on next page

continued from previous page

Star	M-K class	$v \sin i$	P_{rot}
Year(s) of obs.	i	Spots[1]	Reference
Sep 1983	33°	H	Gondoin (1986)
1984–1985	33°	P, L	Vogt (1988)
1988-91	33°	P, L	Donati et al. (1992)
Dec 1989	33°	P, L	Jankov & Donati (1995)
Dec 1992	33°	P, L	Jankov & Donati (1995)
1981–92 (23 maps)	33°	P, L	Vogt et al. (1999)
1991–96 (5 maps)	40°	P, I, L	Donati (1999)
Nov–Dec 96 (37 maps)	40°	P, I, L	Strassmeier & Bartus (2000)
SV Cam	G2 V + K5 V	117 km s^{-1}	0.59307133 d
1993–94	90°	H, I	Hempelmann et al. (1997)
σ **Gem**	K1 III	27 km s^{-1}	19.4 d
1991–92	60°	H, L	Hatzes (1993)
HU Vir	K0 III–IV	25 km s^{-1}	10.4 d
1991–92	65°	P, H	Strassmeier (1994)
Jan 1995	55°	P, H, I	Hatzes (1998)
DM UMa	K0–1 IV–III	50 km s^{-1}	7.50 d
Jan 1993	40°	P, H, I, L	Hatzes (1995c)
II Peg	K2 IV–V	22.6 km s^{-1}	6.724333 d
1992–94	65°	P, H, I, L	Hatzes (1995a)
1992–96 (9 maps)	60°	H, I	Berdyugina et al. (1998a)
1997–98	60°	H, I	Berdyugina et al. (1998b)
UX Ari	K0 IV	39 km s^{-1}	6.44 d
1983–84	60°	H, I	Noah, Bopp & Fekel (1987)
1986	60°	P, L	Vogt & Hatzes (1991)
IN Com	G5 III–IV	67 km s^{-1}	5.92 d
Mar 1994	45°	P, H, L	Strassmeier et. al. (1997)
UZ Lib	K0 III	69 km s^{-1}	4.74 d
Mar 1994	30°	P, L	Strassmeier (1996b)
HD 12545	K0 III	21 km s^{-1}	23.96924 d

continued on next page

continued from previous page

Star	M-K class	$v \sin i$	P_{rot}
Year(s) of obs.	i	Spots[1]	Reference
Dec 1997–Jan 1998	60°	P, H, I	Strassmeier (1999)
V824 Ara	G5 IV + K0 V	37, 34 km s^{-1}	1.681646 d
Sep 1990	49°	P, H, L	Hatzes & Kürster (1999)
May 1996	52°	P, H, L	Strassmeier & Rice (2000)
IL Hya	K0 III–IV	26 km s^{-1}	12.90513 d
Mar 1994	55°	P, H, I, L	Weber & Strassmeier (1998)
Feb–Mar 1995	55°	H, I, L	Weber & Strassmeier (1998)
EI Eri	G5 IV	50 km s^{-1}	1.95 d
1984–87	46°	P, H	Hatzes & Vogt (1992)
1987–88	46°	P, H, L	Strassmeier et al. (1991)
Jan 1996	46°	P, H, I, L	Washuettl et al. (1998)
Nov–Dec 1996	46°	P, H, I	Washuettl et al. (1998)
YY Gem	M1 V + M1 V	48, 48 km s^{-1}	0.8214 d
Dec 1992–Feb 1993	87°	I, L	Hatzes (1995b)
HD 291095	K0–2 IV	41 km s^{-1}	3.8584 d
Apr 1997	50°	P, H, I	Strassmeier (2000)
Apr 1998	50°	P, H, I	Strassmeier (2000)
Feb 1999	50°	P, H, I, L	Strassmeier (2000)
IM Peg	K2 III	26.5 km s^{-1}	24.6488 d
Aug–Oct 1996	70°	H, I	Berdyugina et al. (2000)
Nov–Dec 1996	70°	H, I	Berdyugina et al. (2000)
Jun–Oct 1997	70°	H, I	Berdyugina et al. (2000)
Oct–Dec 1997	70°	H, I	Berdyugina et al. (2000)
Jul,Oct 1998	70°	(P), H, I	Berdyugina et al. (2000)
Oct–Nov 1998	70°	H, I	Berdyugina et al. (2000)
May–Sep 1999	70°	H, I	Berdyugina et al. (2000)
Aug–Nov 1996	70°	H, I	Berdyugina et al. (2000)

[1]P = Polar spot, H = High-latitude spots (latitudes 90°–60°), I = Intermediate-latitude spots (latitudes 60°–30°), L = Low-latitude spots (latitudes $\leq$30°). Brackets denote inconclusive evidence for that type of spot.

Several of the active giant stars in the RS CVn binary systems listed above have shown evidence from surface images and simultaneous photometry for levels and scales of magnetic activity that completely dwarf the Sun and many other active stars. Berdyugina et al. (2000) observed IM Peg spectroscopically shortly after it had displayed its largest ever photometric variability ($\Delta V = 0.36$ mag on a star of $V = 5.6$) and in their image obtained in Aug–Oct 1996, found an active region of linear size $6.5\,R_\odot \times 10.5\,R_\odot$ with the radius of IM Peg being $\sim 13\,R_\odot$. With a period of 24.64 days and $v \sin i = 26.5$ km s^{-1}, IM Peg is one of the slowest rotators to have been Doppler imaged (although it is still rotating at ~ 13 times solar), but this is clearly no hindrance to the generation of enormous active regions.

Using the temperature sensitive ratio of two of the TiO bandheads at 7055 Å and 8860 Å O'Neal, Saar & Neff (1996) found evidence for starspot coverage of 43%–55% on the visible hemisphere of II Peg and large photometric variabilities of up to $\Delta V = 0.5$ mag (Strassmeier et al. 1997a) have been observed on this star. However, Strassmeier (1999) found a light curve amplitude of $\Delta V = 0.63$ mag and a spot of $12\,R_\odot \times 20\,R_\odot$ ($\sim 10,000$ times the areal coverage of the largest sunspot group) on HD 12545, making this the most active star known to date. Like IM Peg, HD 12545 is only a moderately fast rotator with a $v \sin i = 20.8$ km s^{-1}and period of 23.97 days.

1.3.3 Contact binaries

The set of close binaries that have actually evolved into a contact configuration have the potential to provide some of the challenging tests of theories of magnetic fields. The very rapid stellar rotation imposed by the short orbital periods and synchronization is expected to lead to strong dynamo activity. This is coupled with the strong departure from spherical geometry and the possibility of mass and/or energy transfer through the neck region and the corresponding effect on the convective processes and sites of dynamo generation.

Unfortunately the conditions that lead to strong dynamo activity also cause serious problems for Doppler imaging. The combination of comparatively faint magnitudes and large rotational velocities makes obtaining high S:N spectra at high dispersion very difficult to achieve without phase blurring.

Along with the generally poor quality of the system parameters for many contact

Table 1.6: Contact binary stars that have been Doppler imaged.

Star	M-K class	$v \sin i$	P_{rot}
Year(s) of obs.	i	Spots[1]	Reference
AE Phe	G0 V	118, 257 km s^{-1}	0.36323718 d
Nov 1989	88°	H, L	Maceroni et al. (1994)
Nov 1990	87°	H, L	Maceroni et al. (1994)
YY Eri	G2 V	112, 280 km s^{-1}	0.31249510 d
Nov 1989	82°	H, L	Maceroni et al. (1994)
Nov 1990	82°	H, L	Maceroni et al. (1994)
VW Cep	K0 V	97, 246 km s^{-1}	0.27830818 d
Mar 1991	64°	P, H, I, L	Hendry & Mochnacki (2000)
Nov 1991	64°	P, H, I, L	Hendry & Mochnacki (2000)
Jun 1992	64°	P, H, I, L	Hendry & Mochnacki (2000)
Aug 1992	64°	P, H, I, L	Hendry & Mochnacki (2000)
Nov 1992	64°	P, H, I, L	Hendry & Mochnacki (2000)
Feb 1993	64°	P, H, I, L	Hendry & Mochnacki (2000)
May 1993	64°	P, H, I, L	Hendry & Mochnacki (2000)

[1]P = Polar spot, H = High-latitude spots (latitudes 90°–60°), M = Mid-latitude spots (latitudes 60°–30°), L = Low-latitude spots (latitudes $\leq$30°). Brackets denote inconclusive evidence for that type of spot.

systems, this is the main reason why only three W UMa systems have been Doppler imaged to date. AE Phe and YY Eri were Doppler imaged by Maceroni et al. (1994), who used the older equivalent width technique, rather than a full inversion of line profiles. They also used the Hα line, which is known to be strongly affected by chromospheric activity and so these results can be more correctly classed as an attempt at chromospheric rather than photospheric mapping. Maceroni et al. (1994) did not quote the values of $v \sin i$ used in their reconstructions and we have used the values given by Duerbeck (1978) and Nesci et al. (1986) for AE Phe and YY Eri respectively.

The first proper Doppler images of a contact binary have been produced by Hendry & Mochnacki (2000) who presented 7 Doppler images of the contact binary + long-period companion system VW Cep obtained over a baseline of $\sim$ 2 years. The reconstructions were based on observations of the Na I D line, which is also affected by chromospheric activity, though not to the degree of Hα (see e.g. Unruh & Collier Cameron 1997). A summary of the three contact systems that have been Doppler imaged is presented in Table 1.6.

Hendry & Mochnacki (2000) found a large off-centre polar spot on the primary and a smaller, more centralised, polar spot on the secondary and a distribution of unresolved starspots over most of the surface of both components. They found a large degree of spot coverage on both components with an average of 66% of the surface on the primary and 55% on the secondary covered with cool spots. These values are high, although not unreasonable given the large photometric variation seen on RS CVn systems such as II Peg and the results of spot coverage measurements made using the TiO bandheads (Neff, O'Neal & Saar 1995, O'Neal, Saar & Neff 1996).

From high and low-latitude spot migrations they determined a differential rotation of $\alpha = -1.1 \pm 0.4 \times 10^{-4}$ where α is the ratio of the difference in the polar and equatorial angular velocities to the equatorial angular velocity, i.e.

$$\alpha = \frac{\Omega_{equator} - \Omega_{pole}}{\Omega_{equator}} \tag{1.1}$$

However to get a better understanding of the rate of surface shear caused by the differential rotation it is more informative to express this in terms of $\Delta\Omega$. Unfortunately there is very little consistency among authors on how the differential rotation is defined and expressed. In order to achieve some sense of consistency and to enable the differential

rotation results presented in this section and others to be compared, we have elected to express everything in terms of $\Delta\Omega$ and provide appropriate relations for the other quantities.

Assuming a solar-type differential rotation law given by

$$\Omega(l) = \Omega_0 - \Delta\Omega \sin^2 l \tag{1.2}$$

where l is the latitude and we define

$$\Omega_0 = \frac{2\pi}{P_{rot}} \tag{1.3}$$

Since the spots that produce the largest photometric signal and therefore often define the rotation period are close to the equator and the absence of detailed latitude distributions for some of the differential rotation results, we shall assume that $\Omega_{equator} = \Omega_0 = \Omega_{phot}$. Therefore we have the following relations

$$\Delta\Omega = \frac{2\pi}{\text{lap time}} \tag{1.4}$$

$$\Delta\Omega = \alpha\Omega_0 = (\Omega_{equator} - \Omega_{pole}) \tag{1.5}$$

We can now re-express the differential rotation value found by Hendry & Mochnacki (2000) using Eqns. (1.3) and (1.5) as $\Delta\Omega = -0.00248$, indicating a very small amount of differential rotation.

This is in the opposite sense to the Sun (cf. $\Delta\Omega = +0.052$ (Lang 1992) for the Sun), in the sense that the equator rotates slower than the poles. The small value and opposite sign of the differential rotation on VW Cep is perhaps not surprising given the strong effect of the tidal torques on the significantly non-spherical components.

1.3.4 Summary of surface imaging results

Single stars

The dwarf single stars span a range of spectral class from G1.5–M1V and a wide range in velocity from the relatively slow rotating EK Dra at 17 km s^{-1} to the 110 km s^{-1} of Speedy Mic which is one of the fastest rotating late-type single stars known. Virtually all the observations for each star show polar or high-latitude spots along with low-latitude

spots near the equator. This is in marked contrast to the Sun where spots are only found within $\pm 30°$ of the equator.

An explanation for the proliferation of polar spots among rapid rotators was first put forward by Schüssler & Solanki (1992). They suggested that the rapid rotation and the resulting Coriolis force leads to deflection of the magnetic flux tubes towards the poles as they rise through the convection zone. This was modelled in detail by Schüssler et al. (1996) who extended the approach of Caligari, Moreno-Insertis & Schüssler (1995), which had worked successfully on the Sun, to rapid rotators. Similar results were found by DeLuca, Fan & Saar (1997). A limitation of these models is that they only considered stars of 1 solar mass and as Table 1.4 shows, there are now a wide variety of objects which have been surface imaged.

The models were extended to higher and lower stellar masses (1.7 $M_{\odot}$–0.4 $M_{\odot}$) by Granzer et al. (2000) who found that for 0.6 $M_{\odot}$ PMS and 0.4 $M_{\odot}$ ZAMS models, the probable spot locations span a latitude range of 45°–75° for rotation rates of 4–63 times solar. At slower rotation rates, the lower latitude limit extended down to $\sim 25°$. The situation is similar for 1 $M_{\odot}$ PMS and 0.6 $M_{\odot}$ ZAMS models with latitude ranges of 35°–70° and a preference for higher latitudes in the PMS models and lower latitudes in the ZAMS case. Only for 1 $M_{\odot}$ ZAMS and 1.7 $M_{\odot}$ PMS models (which become fully radiative upon reaching the main-sequence) at rotation rates less than or equal to a few times that of the Sun have spots which reach to the equator.

These models are therefore unable to explain the bimodal distribution of spots at high and low-latitude that are seen on most of the rapidly-rotating dwarfs such as LQ Hya, AB Dor, BD+22° 4409 and the α Per dwarfs He520 and He699. The model does predict that low-mass M-dwarfs with rotation rates greater than 4 times solar should show spots no lower than 50°. At present the only suitable M-dwarfs are HK Aqr (dM2e, $v \sin i = 70$ km s^{-1}, $P = 0.43$ d; Young et al. 1990), RE1816+541 (dM1–2e, $v \sin i = 61$ km s^{-1}, $P = 0.4589$ d; Jeffries, James & Bromage 1994, Robb & Cardinal 1995b), G165-08 (=GJ3079, dM4e, $v \sin i = 51.5$ km s^{-1}, $P = 0.108$ d; Robb, Balam & Greimel 1999, Delfosse et al. 1998), G188-38 (dM4e, $v \sin i = 29.6$ km s^{-1}, $P = 0.448$ d; Greimel & Robb 1998, Delfosse et al. 1998) and GJ 791.2 (dM4.5, $v \sin i = 32.1$ km s^{-1}; Delfosse et al. 1998). With the increase in sensitivity of Doppler imaging through use of techniques such as least-squares deconvolution, the arrival of 8-metre telescopes and the increased number

of M-dwarfs that will be found by surveys such as 2MASS (Skrutskie et al. 1998, Beichman et al. 1998) and DENIS (Epchtein et al. 1994, Epchtein 1998), the prospects for surface imaging down to the M-dwarf regime and testing this prediction are good.

The first steps have been taken to extend Doppler imaging into the M dwarf regime with the Doppler images of the rapidly rotating M1–2 dwarf RE 1816+541 produced by Barnes & Collier Cameron (2000). They used least-squares deconvolution to boost the S:N of archival echelle observations to ~ 350 and the resulting surface maps show spots at all latitudes from the equator to $\sim 80°$, but without strong evidence for a polar spot. Obviously it would be unwise to infer anything about activity on M dwarfs in general on the basis of one set of images on one object, and further observations will be needed.

The situation for single giants is somewhat confused. FK Com has never shown a polar spot in 7 separate surface images despite having the highest $v \sin i$ of any single or binary star that has been Doppler imaged. The majority of spots appear at high and intermediate latitudes with only the very occasional extension of spots to latitudes below 30°. In contrast V1794 Cyg and CM Cam have consistently shown polar and low-latitude spots, despite having $v \sin i$ approximately 1/2 and 1/4 that of FK Com respectively. This suggests that whatever controls the dynamo in giant stars, it cannot be solely related to rotation rate.

Differential rotation results have been obtained from the cross-correlation of constant latitude strips for AB Dor (Donati & Collier Cameron 1997, Donati et al. 1999), RX J1508.6-4423 (Donati et al. 2000) and PZ Tel (Barnes et al. 2000b) which give values of $\Delta\Omega = 0.057$, $\Delta\Omega = 0.13$ and $\Delta\Omega = 0.0626$–0.0871 respectively, despite stellar rotation rates up to 50 times quicker.

The differential rotation has been modelled theoretically by Kitchatinov & Rüdiger (1995) and Kitchatinov & Rüdiger (1999) who have produced models for G2 and K5 dwarfs and a series of models for an evolving $2.5\,M_\odot$ giant, covering approximately G2 to K1. They found that for dwarfs, the normally used scaling relation, given by a power law:

$$\frac{\Delta\Omega}{\Omega} = \frac{\Omega_{eq} - \Omega_{pole}}{\Omega_0} \sim \Omega^{-n'},$$

gave values of $n' = 1.56$ for solar rotation down to $n' = 1$ for $P_{rot} = 1$ day, with a mean of $n' = 1.15$ for the G2 model. The corresponding values for the K5 model were 1.21, 0.95 and 1.04 respectively. This value of $n' \simeq 1$ for rapidly-rotating stars does not differ

too much from the value found by Hall (1991a), who estimated differential rotation rates from the range of spot rotation periods, given by $\delta P/P$, found from photometry on a large sample of variable stars.

The value of differential rotation found Donati & Collier Cameron (1997) for AB Dor was $\Delta\Omega/\Omega \simeq 4.6 \times 10^{-3}$ which corresponded to within a factor 2 with the extrapolated model, which is quite good agreement given the mismatch of spectral type and the extreme rotation rate.

The results for the giant models indicate that the predicted differential rotation is quite large and several times solar for G2 stars, rising even further towards later spectral types. However there have been no definite measurements of differential rotation on single giants that could not be more simply interpreted as a mismatch between the average rotation period determined from a long baseline of photometric observations and the rotation period that applies at the time which is determined by the different latitudes of the spot distribution. When this was corrected for, Korhonen et al. (2000) found an upper limit to the differential rotation of $\Delta\Omega = 0.00026 \pm 0.00052$, a result consistent with solid body rotation. Obtaining an unambiguous differential rotation measurement would require surface images derived from high-resolution spectroscopy separated by a suitable gap to allow differential rotation to be detectable but short enough that substantial spot evolution doesn't occur.

Binary stars

The binary stars also span a similar range in spectral class as the single stars and a wide range in rotational velocity from the 24 km s^{-1} of II Peg up to 117 km s^{-1} for SV Cam. Most of the systems show polar spots and a good many show low-latitude structure as well. While some of the long-period, low $v \sin i$ ($\leq$ 30 km s^{-1}) systems such as HU Vir and IL Hya show polar spots, some of the other systems such as σ Gem and IM Peg do not. Conversely among systems with higher $v \sin i$, systems such as SV Cam and YY Gem do not show polar spots, although it should noted that both of these systems have high inclinations.

This is not explained by the models of rising flux tubes in rapid rotators (Schüssler et al. 1996; DeLuca, Fan & Saar 1997; Granzer et al. 2000) which predict that the Coriolis

force should deflect the flux tubes so that they emerge at high latitudes only. However all the models of flux tube behaviour that have been produced so far have been for single stars and the effect of a secondary star has been neglected. The additional tidal torques on the convective envelope, which could alter meridional flows and inhibit differential rotation, could well affect the dynamo and flux tube production and evolution.

As noted in Section 1.3.2, there is a trend for large amounts of spot activity and large photometric variability on the slower rotating RS CVn systems. In Table 1.7 we have collected the maximum observed photometric variability in the V band from the literature for the RS CVn systems that have been Doppler imaged and these are plotted in Figure 1.4. There appears to be a definite trend towards lower photometric variability as $v \sin i$ increases, but there could well be luminosity-related systematic effects present and we do not attach any great significance to what may be nothing more than a curiosity.

A number of differential rotation detections have been claimed on binary systems with at least three systems having differential rotation in the opposite sense to the Sun (UX Ari by Vogt & Hatzes 1991, HU Vir by Strassmeier 1994, HR 1099 by Vogt et al. 1999 and VW Cep by Hendry & Mochnacki 2000).

However the UX Ari result is based on images which have incomplete phase coverage and are separated by a 5 month interval. Also the number of observations per dataset is very small and one dataset contained 5 images taken over a 2 month period. This means that there is likely to have been a significant degree of spot evolution both within the individual datasets themselves and in the gaps between datasets, making the correlations between spots needed to derive the differential rotation somewhat suspect. Similar comments apply to the result by Vogt et al. (1999) who derived a value of $\alpha = -0.0035 \pm 0.0004$, equivalent to $\Delta\Omega = -0.0077 \pm 0.0009$ i.e. opposite to the Sun but several times smaller in magnitude. However these results are also based on the re-identification of features in annual or at best bi-annual images.

It has been shown by Barnes et al. (1998) that cross-correlation maps produced from Doppler images of the α Per G dwarf He 699 taken a month apart show no correlation due to the evolution of the small-scale surface features. While it is possible that the tidal torques in a binary system may slow the disruption of spot groups by differential rotation, as suggested by the evidence for longer lap times on binaries, it is unknown what effect binarity may have on the emergence and decay of spots. This makes any result based

Table 1.7: Photometric variability for RS CVn systems that have been Doppler imaged.

Star	ΔV (mag)	$v \sin i$ (km s^{-1})	P_{rot} (days)
σ Gem	0.17	27.0	19.4
HU Vir	0.25	25.0	10.4
DM UMa	0.2	26.0	7.5
UX Ari	0.3	39.0	6.44
IN Com	0.11	67.0	5.92
XX Tri	0.63	20.8	23.97
EI Eri	0.15	50.0	1.95
IL Hya	0.2	26.5	12.73
IN Vir	0.2	24.0	8.2
UZ Lib	0.30	67.0	4.77
IM Peg	0.36	26.5	24.65
II Peg	0.5	22.6	6.72
SV Cam	0.1	117.0	0.593
HD 291095	0.25	41.0	3.87

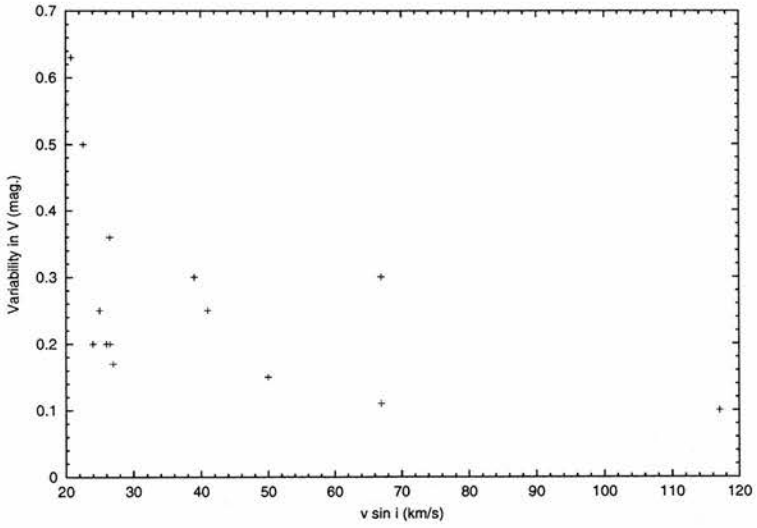

Figure 1.4: ΔV as a function of $v \sin i$ for the RS CVn systems that have been Doppler imaged.

on the identification of similar-looking features in a series of Doppler images to derive differential rotation somewhat suspect, given the caveats listed above.

The differential rotation result on HU Vir (Strassmeier 1994) is based on spot modelling of photometric variations and so there is an additional problem of assigning latitudes to the spots and with the non-uniqueness of solutions.

None of the theoretical differential rotation work (e.g. Kitchatinov & Rüdiger 1995; Kitchatinov & Rüdiger 1999) has considered the effect of a close secondary component on the differential rotation pattern. Results for a giant model (Kitchatinov & Rüdiger 1999) predict a large amount of differential rotation, but observations, although far from conclusive, seem to be indicating very small values and possibly in the opposite sense to the Sun, with the equator rotating slower than the poles. Further observational and theoretical effort will be required for a definitive answer to the question of strength and sign of differential rotation on binary systems. We note here the suitability of the short-period sub-class of RS CVn systems ($P_{\rm orb} \leq 1$ day e.g. CG Cyg, SV Cam, XY UMa and UV Leo) as "laboratories" for testing differential rotation, being reasonably bright, having short enough periods that they can be fully mapped in 1–2 nights but not so rapid that phase blurring becomes a problem, and proven short-term spot evolution. In addition, they can be compared with differential rotation results obtained on single dwarfs such as AB Dor and PZ Tel which have comparable rotation periods.

1.4 Summary

In this section we try to draw together the single and binary systems that have appeared in more than one of the previous sections on photometric or orbital period variations, active longitude and surface imaging results. The systems are generally those with a long or active observational history or ones which could contribute significantly to our theoretical undertstanding.

The selected stars are:

- **LQ Hya** (single, K2 V, $P_{\rm rot}$ = 1.6 d) - Long-period photometric variations with timescales of 11.4 and 6.8 years (with a possible shorter period of 2.8 years) were found by Oláh, Kolláth & Strassmeier (2000). The star has also been extensively

surface imaged, particularly by the technique of Zeeman-Doppler Imaging (ZDI) and 5 maps were presented by Donati (1999), who also found evidence for a magnetic cycle. LQ Hya, as a young, rapidly-rotating active star, is predicted to have almost rigid rotation like AB Dor, and therefore a global magnetic field driven by a α^2-dynamo. However this should produce nonaxisymmetric and steady magnetic fields which is not supported the observations. This has been modelled theoretically by Kitchatinov, Jardine & Donati (2000) who considered a distributed dynamo and found comparable strength radial and azimuthal field which were axisymmetric, in agreement with the observations. They also found oscillations with $P_{\rm cyc} \simeq 3.2$ yrs, almost half the shorter period found by Oláh, Kolláth & Strassmeier (2000). Further observations, especially of the magnetic field components, will be needed before the picture becomes clearer.

- **FK Com** (single, G2 III, $P_{\rm rot} = 2.4$ d) - Switching between active longitudes with a possible $P_{\rm cyc} \simeq 6.5$ yrs was found from photometry by Korhonen et al. (1999). From this and Doppler images (Korhonen et al. 1999, Korhonen et al. 2000), it has been determined that both spot evolution and migration is occurring and producing the switches.

- **V711 Tau** (=HR 1099, binary, K1 IV, $P_{\rm rot} = 2.84$ d) - This was the first cool star to be Doppler imaged and has been a prime target ever since. Long series of Doppler images were discussed by Vogt et al. (1999) who found some evidence for an approximately 3 yr cycle in the total spotted area and by Strassmeier & Bartus (2000) who claimed to have detected a latitudinal migration rate of $+0.41 \pm 0.23$ °/day, but this could well be an artifact of spot re-arrangement and the poor latitude resolution of Doppler images. Photometric variations with timescales of 16.5 and 3.5 years were found by Oláh, Kolláth & Strassmeier (2000) and it remains to be seen whether this agreement with the period of Vogt et al. (1999) is coincidental. A 16 year cycle was also found by Henry et al. (1995) from long-term photometric monitoring and the same dataset was used to search for active longitudes by Jetsu (1996), who only found firm evidence for one active longitude.

  A 6-yr time series of ZDI maps was presented by Donati (1999) who found evidence for strong azimuthal components in all images indicating the dynamo is likely to be distributed throughout the convective zone. There is evidence for long-term changes in the radial and azimuthal field structures, which could be cyclic, but no more

than half a cycle has been observed so far and more data will be needed. They also found that the orbital period is varying non-linearly with time and could be described by a sine curve of period 18 ± 2 yr and amplitude of $4.2 \pm 0.1 \times 10^{-4}$ d. A third body is ruled out by the large variation in the systemic velocity which is not observed and the fact that the body would have a minimum mass of 7.3 $M_{\odot}$, which is simply not seen. This agrees well with the longer period found by Oláh, Kolláth & Strassmeier (2000) from photometry and the results were shown by Donati (1999) to be compatible with the updated Applegate mechanism (Lanza, Rodonò & Rosner 1998) in terms of the required magnetic field and change in angular rotation rate. Again, only half the cycle has been observed and further observations will be needed to confirm and refine the periodic change.

- **EI Eri, II Peg, σ Gem, IL Hya, IM Peg, HK Lac, HU Vir** (binaries, $P_{\rm rot}$ = 1.95–24.6 d) - Despite having a large range in rotation periods and a somewhat smaller range in spectral type, these objects are actually quite similar. Long-period photometric variations have been found on EI Eri (16.2 and 2.4 yrs), IL Hya (13.0 yrs), HK Lac (13.0, 6.8 yrs and a trend $\geq$ 34.2 yrs), IM Peg (trend $\geq$ 48.3 yrs) and HU Vir (5.6 yrs) by Oláh, Kolláth & Strassmeier (2000) and on II Peg (11.0 and 4.4 yrs) and σ Gem (8.5 yrs) by Henry et al. (1995). Active longitudes with switching between them have been found on EI Eri (switch time of 9.0 yrs), II Peg (9.3 yrs) and σ Gem (14.9 yrs) by Berdyugina & Tuominen (1998) and on HK Lac ($\sim$ 6.5 yr) by Oláh, Hall & Henry (1991). All of the stars have Doppler imaging results and show spots over intermediate and high latitudes. All of the stars apart from the two slowest rotators (σ Gem and IL Hya) show polar spots as well and a fair number show spots at the equator and low-latitudes as well.

There is a very wide variety of activity taking place, on timescales of weeks to centuries and across a large section of the Hertzsprung-Russell diagram. Great progress is being made at linking up different areas of cool star study, both observationally and theoretically to examine cyclic and periodic behaviour on stars. Tantalizing tie-ups between periods from different methods are beginning to emerge for some of the best studied objects and more data and longer baselines will result in confirmation and refinement of these results and the addition of others.

However contradictions still exist between theory and observation and between dif-

ferent observations. Examples of the former are the axisymmetric and cyclic dynamos suggested by Zeeman-Doppler images of young active stars and nonaxisymmetric and steady state dynamos suggested by the Mount Wilson H&K Project observations and some theories. On the observational side there are disagreements between cycle lengths from photometric and photographic sources and the question of differential rotation on binary stars is still uncertain in both sign, magnitude and relevant parameters.

CHAPTER 2

Doppler Imaging, Least-squares deconvolution and Eclipse mapping techniques

2.1 Early History

Although the first attempt to map surface anomalies on stars was due to Deutsch (1958), this was limited by the use of a sharply truncated spherical harmonic expansion to describe the distribution of elements on chemically peculiar Ap stars. The use of the low order spherical expansion and simple treatment of the line physics combined with the photographic data available at the time meant that the resolution on the stellar surface was very low. After this pioneering work there was a lull of a decade before any further work and during this time the emphasis moved towards using the information in the rotationally broadened line profiles rather than variations in line strength.

In the 1970s Falk & Wehlau (1974) used the spherical harmonic technique of Deutsch to give a formal method of recovering surface anomalies from Doppler-broadened profiles and despite the limitations of the method, this was probably the first "Doppler imaging" in the modern sense of the word. The subject was put on a firmer footing in the mid 1970s with the development by Russian astronomers (Goncharsky et al. 1982) of the first computer codes for solving the inverse problem of recovering a stellar surface image from line profile information. This led to the understanding that stellar imaging is, at the fundamental level, an ill-posed problem. This means that, when inverting the line profiles to obtain the surface map, there is a large number of possible surface maps that would give a good fit to the data as measured by some parameter such as χ^2.

The solution to this problem requires the use of additional constraints on the pos-

sible surface maps to give a unique solution. This is usually done by means of some form of penalty function such as the Tikhonov regularizing function (Tikhonov 1963), which minimises image gradients, or the image entropy function (Narayan & Nityananda 1986), which minimises spurious correlations between pixels. The purpose of this penalty function is to prevent over-fitting of the data and give the smoothest image within the constraints of the data. The differences between the two are discussed in more detail in Piskunov, Tuominen & Vilhu (1990) and Rice, Wehlau & Khokhlova (1989) but the choice of regularizing function is not important if the data are of sufficient quality.

The reason for this somewhat odd result is that, despite the fact that entropy regularization discourages correlations between pixels and Tikhonov regularization encourages them, there is smoothing built into the image-data transformation by the finite width of the line profile that emerges from the stellar photosphere. Therefore unless the data are of very low quality (in which case their value for surface imaging is questionable), the image is principally constrained by the χ^2 criterion and tends to be naturally smooth. The regularizing function should normally only make its presence felt when the data are being overfit. Tikhonov regularization keeps the image smooth even when poorly constrained by the data, whereas entropy regularization tends to cause the map to break up and become 'pixelated' when over-fitted.

This intrinsic non-broadened line profile emerging from all points on the stellar surface is what sets the ultimate limits on what is imageable by the Doppler imaging method. The Doppler-broadened rotational profile needs to be significantly broader than this local line profile, which includes the contribution of a wide variety of mechanisms ranging from the atomic level to the granulation effect on scales of 10^6 m. This photospheric "noise" has already started to set a lower limit of ~ 2 m s^{-1} on the accuracy of the radial velocity searches for extra-solar planets (e.g. Saar, Butler & Marcy 1998, Santos et al. 2000).

The practical lower limit on $v \sin i$ is ~ 20 km s^{-1} for Doppler imaging. Fortunately, since rotation is one of the key components in the operation of the magnetic dynamo, all of the potential targets with enough spot area to be resolvable by these methods tend to be rapid rotators, almost by definition. Very rapid rotation, as found in short period binaries, causes its own problems as the lines become very broad and shallow and the challenge is to obtain enough S:N to resolve the small spot bumps within these shallow lines, without causing phase blurring.

Since Doppler imaging is not sensitive to small, unresolved spots or the temperature of the dark spots on the surface, it tends to underestimate the total spot area. This has been shown by a number of authors who have used Doppler images to produce synthetic photometric light curves for comparison with simultaneous or near-simultaneous photometric observations. The light curve shape is nearly always well-reproduced but the spot amplitude is always too small.

For these reasons Doppler imaging should ideally be carried out in conjunction with another method which is more temperature-sensitive. The simplest is to use contemporaneous broad-band photoelectric or CCD photometry in several bands which will be sensitive to the relative temperatures of the spots and the unspotted photosphere. The first images based on a regularized technique that incorporated spectroscopy and photometry were the Rice & Wehlau maps published in Strassmeier et al. (1991).

An alternative and often complementary method is to arrange the spectroscopy to cover the temperature sensitive ratio of TiO bandheads at 7055Å and 8860Å (O'Neal, Saar & Neff 1996). Since these bands should only be present in the spots and not in the photosphere (except for the very coolest Doppler imaging targets), this will provide a good handle on the total spot coverage. Results presented by O'Neal, Saar & Neff (1996) suggest that the total spot coverage can be greater than 50%, which is many times the amount found in Doppler imaging results.

2.2 Cool Stars and Maximum Entropy Methods

The extension of the technique of Doppler imaging to the field of cool stars came with the work of Vogt, Penrod and Hatzes in a trial and error approach to the mapping of the primary of the RS CVn binary HR 1099 (Vogt & Penrod 1983). They showed that moving bumps caused by starspots could be observed in the line profiles, and this could be used to derive a stellar surface image. These absorption line profiles will have irregularities caused by the dark areas on the stellar surface which will vary in time as the star rotates. This effect is illustrated schematically in Figure 2.1.

The apparent bright bump caused by the starspot is the effect of an overall depression of the continuum caused by less of the brighter photospheric flux reaching us, which is offset by the smaller amount of line absorption within the spot.

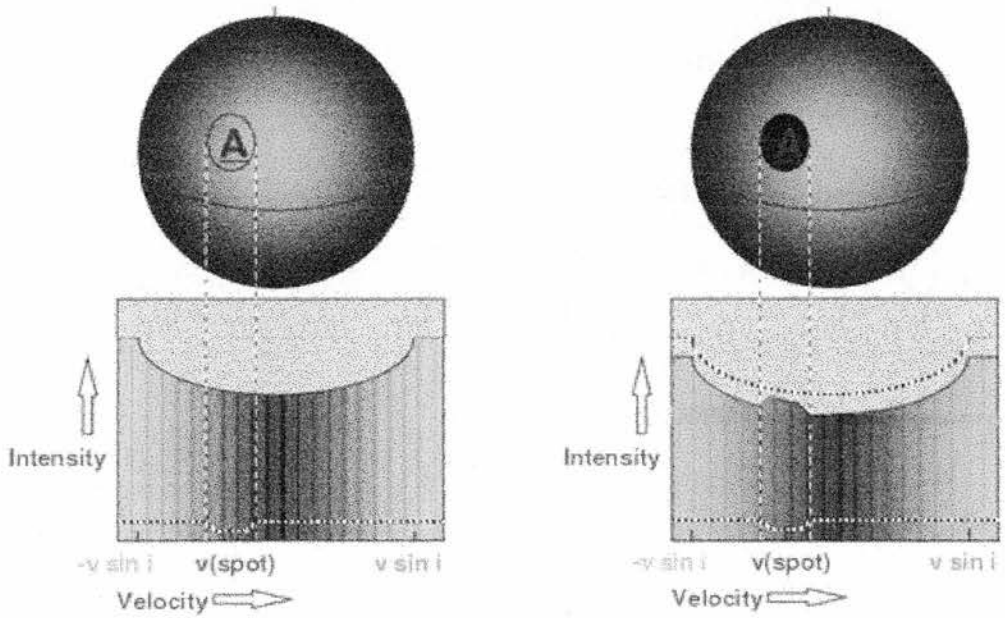

Figure 2.1: Schematic illustration of the effect of a starspot on a rotationally-broadened line profile.

As the star rotates these bumps travel across the line profile at a rate that depends on the projected distance from the rotation axis. The fraction of the rotation period that the spot is visible for depends on the spot latitude and on the inclination of the star to our line of sight. If the stellar inclination is known or can be deduced, then the spot latitude can be determined and from the time when the spot bumps cross the centre of the line profile, the longitude can be determined.

2.2.1 The forward problem (Image→Data transformation)

The initial ad-hoc approach of inversion of Vogt & Penrod (1983) was followed later (Vogt, Penrod & Hatzes 1987) by a formal inversion method making use of the maximum entropy code of Skilling & Bryan (1984) (MEMSYS). This casts the problem into the form of a matrix transformation between the image space, $\mathbf{f}$, which is a grid of image parameters on the star, and the data space, $\mathbf{D}$, which is the observed data (spectral line profiles and/or photometry) which fulfil the requirements for Doppler imaging.

Written in matrix form this becomes $\mathbf{fR} = \mathbf{D}$, where $\mathbf{R}$ is a transformation matrix which corresponds to the transformations needed to obtain a synthetic spectral line profile or photometric flux from a star where the properties of the stellar atmosphere are known.

From a naïve or mathematical point of view it would be expected that this equation could be written as $\mathbf{f} = \mathbf{D}\mathbf{R}^{-1}$ to obtain the image. The matrix $\mathbf{R}$ will not generally be invertable since it is unlikely to be a square matrix and it will not satisfy the condition that a certain number of rows are independent.

2.2.1.1 Choice of mapping parameter

In the above we have not specified what form the image parameters that produce $\mathbf{f}$ can take. The image $\mathbf{f}$ is a vector of parameter values $f_i, i = 1, \ldots, N$ which describes the brightness of the image on a suitable surface grid and several quantities can be used as image parameters.

If entropy regularization is being used, this image parameter should be both additive and positive, which means that the flux received from a set of pixels is proportional in a linear way to the area-weighted sum of the image pixel values. Temperature does not fit these criteria, but bolometric surface brightness and spot filling factors (discussed later) do.

Bolometric surface brightness was the first quantity to be used for representing image brightnesses in Doppler imaging codes (e.g Vogt, Penrod & Hatzes 1987, Rice, Wehlau & Khokhlova 1989, Jankov & Foing 1992) and has also been used more recently by Berdyugina (1998) in the new Occamian approach. This requires a grid of synthetic spectra spanning the temperature range that is expected to be computed in advance, but no restriction is placed on the mix of dark or bright features in the image.

An alternative development due to Collier Cameron (1992) was the use of starspot filling factor rather than bolometric flux. This prevents problems with stars where the inclination means that part of the star always faces away from the observer and is never seen. In these cases, if bolometric flux is used as the image parameter, it is necessary to assign a default value for the surface flux. In principle this could be determined from the unspotted photosphere when magnetic activity is at a minimum, however most active stars have not been observed long enough for any sort of 'stellar cycle' to be detected and so this default is essentially arbitrary.

Collier Cameron (1992) also showed that, when using the bolometric surface flux as the image parameter, this implicitly assumes that each pixel in the image can be assigned

a unique temperature. This in turn assumes that we can resolve all the temperature variations on the stellar surface, but because of the tradeoff between longer exposures to obtain a high S:N ratio and the rotational blurring that occurs with long exposures this is not possible. When the pixels are rotationally smeared, the surface brightnesses must go up to compensate for the dilution of the flux into a larger area. This leads to excess flux in the synthesized profiles which does not correspond to any true temperature on the star and results in 'hot spots' that appear interspersed with the genuine starspots.

The disadvantage of this approach is the restriction to dark spots of a single temperature. This is inappropriate for systems such as T Tauri stars which may have accretion hotspots as well as dark starspots or other systems with bright faculae. It may also be inappropriate for close binary systems where there is strong irradiation of one or both of the components. A similar approach of utilizing a two-temperature model was developed by Kürster (1993) who used a CLEAN-like algorithm and applied it to AB Dor (Kürster, Schmitt & Cutispoto 1994).

2.2.1.2 Local line profiles and renormalization

Each pixel on the model star produces a specific intensity that depends on the value of the pixel, the angle between the surface normal and the line of sight to the observer and, in the case of spectroscopy, on the Doppler shift of the pixel. The projected area, surface normals and Doppler shifts of the image pixels will vary as the star or binary system rotates and so must be computed at each rotation phase that is present in the data. Since the departure from a spherical shape can be quite significant at the rotation speeds of Doppler imaging targets, a Roche model is normally used for single stars and binary systems.

It is still too computationally expensive to compute the synthetic spectra and photometry at each rotation phase and the specific intensities are normally pre calculated on a grid of wavelength, temperature and direction cosine (the angle between the outward normal of a pixel and the observer's line of sight). Interpolation is then performed using this lookup table when specific intensity values are required. In our Doppler imaging code DOTS these intensity profiles are derived from observations of slowly rotating "template" stars which have a similar spectral type to the star we wish to Doppler image. For the intensity profiles at the spot temperature we use spectra of a slowly rotating M dwarf. This is due to the problems of generating an accurate stellar atmosphere that correctly

reproduces the many different opacities present at the cool temperatures of starspots (see e.g. Unruh & Collier Cameron 1995, Allard et al. 1997, Leggett et al. 2000).

If synthetic specific intensities are being used then the modelling of the stellar atmosphere depends quite critically on the atomic parameters such as the oscillator strengths and damping parameters and these are most conveniently taken from the Vienna atomic line database (VALD: Piskunov et al. 1995, Kupka et al. 1999). Photometric intensities are computed for an effective wavelength range corresponding to each filter and stored in a similar lookup table to the synthetic spectra. This normally requires limb-darkening coefficients such as the grids of Wade & Rucinski (1985) or more up-to-date tabulations such as Diaz-Cordoves, Claret & Giménez (1995) and Claret, Diaz-Cordoves & Giménez (1995). The profiles in the lookup table are then scaled at 10 limb-angles calculated for the appropriate linear limb darkening coefficient.

If the transformation between the image and the computed model of the data, denoted by $\mathbf{f}$ and $\mathbf{C}$ respectively, was linear then it could be written as above as $\mathbf{C} = \mathbf{R}.\mathbf{f}$. However, the relation between the value of a pixel and its contribution to the computed data is non-linear and a function of temperature and the limb angle. In addition, since the spectra are not in general spectrophotometric we cannot determine the observed continuum flux exactly and we must renormalize the synthetic profiles with inverse variance weighting so that they match the observed profiles. A similar procedure is necessary for the photometric data in each band so that the mean value, weighted by the inverse variances, matches the observed values. This introduces a further non-linearity since there is a dependence of the renormalization scaling factor on the values of the computed data. The details of the renormalization procedure have been given by Collier Cameron, Jeffery & Unruh (1992) and Collier Cameron (2000) and will not be repeated here.

2.2.2 The inverse problem (Data→Image transformation)

If we cannot find the exact solution to the equation by inverting to find a unique image, then we must search through all the possible images and find the one that fits the observed spectra, $\mathbf{D}$, within the errors in the data, while not introducing excess structure and overfitting the data. This is expressed in matrix form as

$$\chi^2(\mathbf{f}) = (\mathbf{D} - \mathbf{C}(\mathbf{f}))^T.\mathrm{Diag}[\sigma^2].(\mathbf{D} - \mathbf{C}(\mathbf{f})) \tag{2.1}$$

where $\mathbf{C}$ is the synthetic spectrum and photometry computed from the model image. The matrix transpose is used as an approximation for the incomputable matrix inverse, which helps to determine which image pixels most affect which data points.

One logical criterion for obtaining the "best" image is to find the smoothest or simplest image. From information theory, this corresponds to the image with the least amount of information, or alternatively the maximum entropy. For a filling-factor model (cf. Section 2.2.1.1, this takes the form

$$S = \sum_i (-f_i \ln \frac{f_i}{m_i} - (1 - f_i) \ln \frac{(1 - f_i)}{(1 - m_i)}) \tag{2.2}$$

and

$$S = \sum_i (f_i - m_i - f_i \ln \frac{f_i}{m_i}) \tag{2.3}$$

if a bolometric surface brightness model is utilized. In both cases m_i is the default value for a pixel in the absence of any constraint by the data.

An alternative regularization scheme that has been used by some authors is the Tikhonov scheme (Tikhonov 1963) which seeks to minimise image gradients by the functional

$$T = -\sum_i \|\nabla f_i\|^2 \tag{2.4}$$

In any case the code will move back and forth between the image and data spaces adjusting the pixel values as it iterates, seeking to maximise

$$Q(\mathbf{f}) = S(\mathbf{f}) - \lambda\chi^2(\mathbf{f}), \tag{2.5}$$

where S is the entropy (in the Tikhonov approach T is substituted) and λ is a Lagrange multiplier which acts as a scaling parameter. The convergence to a unique solution is achieved in a relatively small number of iterations (typically 20–30) by starting with a high value of λ and using a six dimensional search to lower λ until a suitably low value for χ^2 is reached. Conjugate gradient methods are then used to find the point where the ∇S and $\nabla\chi^2$ vectors are parallel, which corresponds to the unique solution.

2.3 Testing

In order to Doppler image a star various assumptions have to be made about the parameters and this can lead to errors in the reconstruction. Important tests of Doppler imaging with regard to errors have been covered by many authors. The early papers such as Vogt, Penrod & Hatzes (1987) covered the intrinsic limits of recovering Doppler images with regard to the S:N required, phase coverage, instrumental resolution and the north-south ambiguity in high inclination systems. Later work such as Piskunov (1991) and Unruh (1996) attempted to quantify the limits of errors in the assumed parameters such as $v \sin i$, inclination, atomic parameters for the line and gaps in the phase coverage. Unruh, Collier Cameron & Cutispoto (1995) and Unruh (1996) were the first to consider the effect of blended lines on the line profile. They found that close blends are relatively unimportant, but as the distance from the blend to the line centre increases banding artefacts can appear, even mimicing polar spots.

Polar and high-latitude spots have been a controversial feature of many Doppler reconstructions since the first images of Vogt, Penrod & Hatzes (1987). Finding spots at high latitudes and even straddling the pole was a surprise since spots on the Sun appear in a band of about $\pm 30^{\circ}$ of the solar equator. It was thought that the flat-bottomed profiles associated with polar spots were caused by incorrect treatment of the line physics (Byrne 1996), but improved testing has proven that polar spots are genuine. Bruls, Solanki & Schüssler (1998) have carried out an investigation into the effects of chromospheric in-filling producing flatter bottoms in 14 of the photospheric lines most commonly used for Doppler imaging. They conclude that chromospheric effects can lead to some in-filling of the profiles but this is a small effect which only affects some of the lines and is unlikely to fully account for the appearance of a polar spot.

Recently, attempts have been made to treat the stellar parameters in a more consistent way. Rice & Strassmeier (1998) in their study of LQ Hya derived values of $v \sin i$ and i by optimising the fits to the data and combining this with the rotation period to give a stellar radius. By combining this with their simultaneous photometric data in three bandpasses, this provided an additional constraint on the image by ensuring the correct flux was obtained, given the star's known parallax.

This was taken one step further by Hendry & Mochnacki (2000) who incorporated

many of the "extra" parameters such as the binary orbit and the sizes of the stars into the iteration procedure itself so that they were adjusted along with the image. They also incorporated the observed distance modulus to predict and match the stellar surface flux with the observed V magnitude at each epoch.

2.4 Later developments

2.4.1 Eclipsing binaries

Although many of the systems that have been Doppler imaged (cf. Section 1.3) are binary systems, in the vast majority of cases (cf. Table 1.5) the secondary star is not seen in the spectrum and only one component has been imaged.

The extension of Doppler imaging to eclipsing binary systems was first examined by Vincent, Piskunov & Tuominen (1993). They found in particular that information derived from spectral line-profile variations during eclipse can resolve the mirroring of features between hemispheres that causes problems in Doppler imaging of high-inclination objects, and gives better latitude resolution near the stellar equator than normal Doppler imaging. This technique has been employed by Piskunov (1996) to produce temperature maps of the eclipsing RS CVn system ER Vul which show clear evidence of the reflection effect due to mutual heating of the components' inner faces.

Despite the benefits from the additional information contained in the eclipses, only 1 additional Doppler imaging result on an eclipsing binary system has been presented to date by Hempelmann et al. (1997) on SV Cam. Clearly this is an important technique which will allow the parameter space to be broadened and enable the study of magnetic field structure and evolution at the higher rotational velocities found in short-period binaries.

2.4.2 Zeeman-Doppler Imaging

A recent extension to the field of Doppler imaging is Zeeman-Doppler Imaging where we attempt to recover a magnetic field map along with the temperature map (cool stars) or an abundance map (Ap stars) (see Semel 1989; Donati, Semel & Praderie 1989). This technique is important in trying to prove whether starspots detected by the Doppler imag-

ing method coincide with active magnetic regions. The first attempts to detect magnetic fields on solar-type stars (see, for example, Vogt 1980; Brown & Landstreet 1981; Borra, Edwards & Mayor 1984) tried to analyze integrated circularly polarized light using a conventional Zeeman analyzer. However the complex magnetic structures formed by bipolar magnetic regions such as starspots leads to inconclusive results. Measurements of Zeeman broadening (Robinson 1980) were shown by Saar (1988) to only be trustworthy for rotation velocities below 8 km s^{-1}. However it is rapidly rotating stars that are the most active and of the greatest interest for magnetic studies.

Zeeman-Doppler Imaging (ZDI) can be described simplistically as Doppler imaging using circularly polarized light. The idea is to take measurements with high spectral and temporal resolution over many rotation phases. The changing positions of distortions in the polarization profile with phase allows construction of 2 dimensional magnetic images from one dimensional magnetic measurements. This is analogous to the reconstruction of a temperature map in conventional Doppler imaging from distorted one dimensional spectral profiles. This enables the use of ZDI to magnetically map rapid rotators (Donati et al. 1992; Donati & Collier Cameron 1997).

The problem with Zeeman-Doppler imaging is that the polarization signatures are a very small fraction of the continuum, typically about 0.1%. This small signal would be undetectable using the conventional single or three-line Doppler imaging technique and would limit the potential of ZDI to the few brightest active stars which could produce high enough S:N without phase-blurring. To solve this problem Donati et al. (1997) introduced the new technique of Least-squares deconvolution to give a large multiplex gain and boost the S:N and make ZDI possible. Least-squares deconvolution is described in more detail in Section 2.4.3.

Results using this technique have been used to investigate the magnetic topology, prominences and surface differential rotation on AB Dor (Donati & Collier Cameron 1997, Donati et al. 1999) and the magnetic structure and long-term cyclic behaviour on LQ Hya and HR 1099 (Donati 1999).

These results, and in particular the detection of strong azimuthal field components at high latitudes on all the stars that have been studied significantly with ZDI, has implications for the dynamo process in these stars. This coupled with the fact that the poloidal and toroidal components are of comparable strength indicates that the dynamo processes

occuring in these rapid rotators operate throughout the entire convective stellar envelope, rather than being confined to the overshoot layer at the base of the convection zone, as is thought to occur in the Sun. Further magnetic maps obtained over the length of an activity cycle (if it exists) will provide valuable input into improved dynamo models for active stars, a process which has begun with the work of Kitchatinov, Jardine & Donati (2000).

2.4.3 Least-squares deconvolution

In order to increase the sample space of Doppler imaged systems, it is necessary to push the magnitude limit to fainter levels without compromising the need for high S:N data for reliable mapping. Similar problems occur with binary star targets where the high rotational velocities limit the maximum exposure time that can be used without adverse blurring effects. In ZDI the challenge is to obtain a high enough S:N to detect the very small Zeeman signatures produced by the stellar magnetic field.

To solve this problem Donati et al. (1997) introduced the new technique of Least-squares deconvolution which makes use of the large number (typically 1000 – 4000) of photospheric lines contained in an echelle spectrum on a large CCD detector. The method works by treating the observed stellar spectrum as a convolution of a mean line profile with an absorption line pattern represented by δ - functions taken from an appropriate linelist. Weak lines with central depths less than 0.4 (in normalised units) are not included since they tend to be become indistinguishable from the continuum in the relatively low S:N spectra of rapid rotators. We also remove from the linelist those spectral regions which are badly affected by telluric line absorption, since the telluric lines tend to be much stronger and deeper than photospheric lines and only serve to add noise to the deconvolution process. Lines that also strongly affected by chromospheric absorption such as the Na I D (5889.95 Å – 5895.92 Å) and Mg I b (5163.50 Å – 5186.86 Å) lines and the surrounding regions are also removed.

If we write the deconvolved profile as $\mathbf{z}(v)$ with elements z_k, then the predicted data, $\mathbf{p}$, formed by the convolution of the mean line profile with the absorption line pattern is given by

$$p_j = \sum_k A_{jk} z_k \tag{2.6}$$

The elements A_{jk} of the convolution matrix $\mathbf{A}$ are obtained for each line i by

$$A_{jk} = \sum_i w_i \Lambda \left[\left(v_k - c\frac{(\lambda_j - \lambda_i)}{\lambda_i} \right) / \Delta v \right] \tag{2.7}$$

where w_i is the line weight, λ_i is the wavelength of line i, λ_j the wavelength of the j^{th} spectrum pixel, v_k is the radial velocity of the k^{th} bin in the deconvolved profile and Δv the velocity increment in the deconvolved profile and where the triangular interpolation function is given by

$$\Lambda(x) = \begin{cases} 1 + x & \text{for } -1 < x \leq 0, \\ 1 - x & \text{for } 0 < x < 1, \\ 0 & \text{for all other } x \end{cases} \tag{2.8}$$

The line weights w_i that are incorporated in the convolution matrix $\mathbf{A}$ are proportional to the central depths of the lines as obtained from a Kurucz model atmosphere of the appropriate spectral type. The velocity increment Δv is set at the average velocity resolution of the extracted object spectrum and is normally determined by the size of the CCD pixels in the echelle spectrograph. The width of the deconvolved profile ($\pm \Delta v \frac{k}{2}$ km s^{-1}) is normally set wider than the $v \sin i$ of the object to allow some continuum to be included. Determination of the deconvolved profile $\mathbf{z}(v)$ via least-squares requires the minimisation of the misfit vector between the observed and predicted spectrum $|\mathbf{r} - \mathbf{p}|$ (where $\mathbf{p} = \mathbf{A}.\mathbf{z}$),

$$\chi^2 = (\mathbf{r} - \mathbf{A}.\mathbf{z})^T.\mathbf{Q}.(\mathbf{r} - \mathbf{A}.\mathbf{z}) \tag{2.9}$$

Here the inverse variances σ_j^2 associated with the N elements r_j of the residual spectrum $\mathbf{r}$ are incorporated via the diagonal matrix

$$\mathbf{Q} = \text{Diag}\left[1/\sigma_1^2, \ldots, 1/\sigma_N^2\right] \tag{2.10}$$

The least-squares solution for $\mathbf{z}$ is obtained by solving the matrix equation

$$\mathbf{A}^T.\mathbf{Q}.\mathbf{A}.\mathbf{z} = \mathbf{A}^T.\mathbf{Q}.\mathbf{r} \tag{2.11}$$

which, since the square matrix $\mathbf{A}^T.\mathbf{Q}.\mathbf{A}$ is symmetric and positive-definite, the problem can be solved using efficient methods such as Cholesky decomposition (Press et al. 1992), rather than a $O(N^3)$ matrix inversion. Errors on the points of the deconvolved profile are obtained from the diagonal elements of the covariance matrix

$$\mathbf{C} = \left[\mathbf{A}^T.\mathbf{Q}.\mathbf{A}\right]^{-1} \tag{2.12}$$

By combining all these lines with appropriate weighting for the different line strengths and the continuum level into a single least-squares profile it is possible to obtain the equivalent of an average of all the line profiles to boost the S:N ratio of the object spectrum in question. The multiplex gain from this technique should be equal to the square root of the number of lines recorded in the echellogram but in practice the variations in line depth and the continuum level, along with residual flat-fielding errors conspire to produce less than the theoretical gain. Nevertheless increases in S:N of factors of 30 over a single line have been obtained which corresponds to an increase in sensitivity of up to ~ 4.5 mag for Doppler imaging purposes. This increases the number of potential Doppler imaging candidates by opening up a greater volume of space that is accessible without any change in telescope equipment.

The least-squares technique has the advantage that line blends are treated simultaneously without producing any sidelobes that would result from cross-correlation or other techniques. The disadvantage lies in the assumption that all lines have a similar mean profile which forfeits any temperature sensitivity that arises from the different line strengths. This could be worked round by using subsets of lines with different excitation potentials, at the cost of a slightly lower gain in S:N.

2.5 Eclipse mapping

Normally only full Doppler imaging from high resolution spectroscopic data can give accurate spot locations. The only exception to this rule is the special case where cool spots are present within the region on the inner face of the hotter star that is occulted by the cooler secondary during the course of primary eclipse. Any spots in this region will give rise to distortions in the primary eclipse profile that should be easily detectable in broad-band optical photometry with high precision and sufficient time resolution.

Although the technique of Doppler imaging has been used for several years, the extension to eclipsing binary systems was only first examined in 1993 by Vincent, Piskunov & Tuominen (1993), as discussed in more detail in Section 2.4.1. However they did not examine the possibility of using photometric data on its own.

It was first noted by Hall (1991a) that photometry of eclipsing spotted stars during secondary eclipse would be a powerful tool for determining spot latitudes. He made the

comment that this technique had good potential and had been under-utilized.

Unfortunately this situation did not change until the extension of an existing photometric and spectroscopic Doppler imaging code (DOTS) to handle eclipse mapping by Collier Cameron (1997b). This enabled the use of maximum entropy techniques to be used to resolve far finer detail and with greater reliability than is possible with the traditional one or two spot modelling techniques (see e.g. Budding & Zeilik 1987, Banks 1989).

These techniques are normally used to remove the gross distortion effects of starspots on the light curve in order to derive more reliable system parameters. Even in the presence of more than one or two spot groups on the surface, the summed rotational modulation signal rarely contains any significant power beyond the frequencies of 2nd-order Fourier terms. This is observed in the light curves of spot-affected stars which never show more than 2 minima or maxima at any one time.

The converse of this is that almost any arbitrary spot distribution can be modelled by a two spot model that will give a satisfactory fit to a light curve, with the possible inclusion of a high-latitude polar spot to produce an unmodulated depression in the light curve. However there is very little independent information in a photometric light curve and it is not possible to solve for spot latitude, longitude and radius simultaneously with traditional spot modelling techniques. The normal procedure adopted by practitioners of these methods is to fix either the spot latitude (usually at 45° latitude) or the spot radius at arbitrary values.

While these methods are fine for determining system parameters of binary systems they say very little about the detailed spot distribution or its possible evolution. The development of maximum entropy techniques for use with photometric data means that it is possible to obtain similar surface resolution with photometric observations taken on a 1-metre telescope as with traditional spectroscopic Doppler imaging on a 4-metre. Eclipse mapping has an advantage over spectroscopic imaging in that it is most sensitive near the equatorial regions, where spectroscopic Doppler imaging has poor latitude resolution. However it is insensitive to high latitude structure and polar spots as these produce no photometric modulation.

The eclipse mapping method was applied to observations of the short-period RS CVn binary XY UMa by Collier Cameron & Hilditch (1997) who found evidence for time-

variable surface structure on the primary star between observations taken in 1992, 1995 and 1996. In 1992 they found an extended distribution of spots with low filling factor from longitude 270°–110° in good agreement with Hilditch & Bell (1994) who used photometry alone to infer a belt of dark spots. This suggested a relatively uniform coverage of unresolved spots on the star. In the later observations, activity was primarily concentrated the near the quadratures (longitudes 90° and 270°) and, in some cases, large apparently resolved spots with filling factors near unity and extending over several pixels in the eclipsed region near the sub-stellar point. Further observations and eclipse mapping results of XY UMa are presented in Chapter 5 and for GSC2807-1423 in Chapter 4.

CHAPTER 3

Doppler imaging of BD+22° 4409 (LO Peg) using Least-squares Deconvolution

The work in this chapter is published in Monthly Notices of the Royal Astronomical Society, "Doppler imaging of BD+22° 4409 (LO Peg) using least-squares deconvolution" *MNRAS (1999) 307, 685* .

3.1 Introduction

As discussed in Section 1.3.1, understanding the nature and the temporal evolution of the magnetic field on the Sun and other stars requires a sample of single stars covering a range of parameters such as age, mass and rotation rate. The open clusters provide a convenient place to find large numbers of single stars that normally have determined ages and rotational speeds that are rapid enough to allow Doppler imaging. With the advent of 8–10 metre telescopes and new analysis techniques the nearby clusters of the Pleiades (Stout-Batalha & Vogt 1996) and α Persei (Barnes et al. 1998) have been brought within range of Doppler imaging. However, it is still difficult to obtain spectra with high enough S:N, while keeping the exposure time short enough to minimize phase-blurring on these faint rapid rotators.

However in recent years several stars much closer than the cluster dwarfs have been found with comparable ages to those in the young clusters. The main technique for detecting this type of objects is to make use of the fact that the magnetic activity is connected to the rotation rate. For rapidly rotating, late-type stars the coronal X-ray/EUV flux is expected to reach 10^{-3} of the bolometric luminosity (see e.g. Jeffries

& Jewell 1992; Dobson & Radick 1989). This means that optical follow-up of objects detected with X-ray all-sky surveys can produce a good source of rapidly rotating single and binary stars. Their relative youth is confirmed by their space motions which are similar to the Pleiades cluster and their high photospheric lithium abundances. Several of these stars have now had Doppler imaging follow up and these results are summarized in Section 1.3.

Recently Donati & Collier Cameron (1997) and Barnes et al. (1998) have used the method of *least-squares deconvolution* (LSD) to make use of the large number (typically 1000 - 3500) photospheric lines contained in an echelle spectrum on a large CCD detector. By combining all these lines with appropriate weighting, into a single least-squares profile, it is possible to boost the S:N ratio of the object spectrum in question. The multiplex gain from this technique corresponds to an increase in sensitivity of up to ~ 4.5 mag for Doppler imaging purposes. This increases the number of potential Doppler imaging candidates by opening up a greater volume of space that is accessible without any change in telescope equipment. Further details of least-squares deconvolution are given in Section 3.4 and Section 2.4.3.

We apply this technique to the nearby rapidly rotating K dwarf BD+22° 4409 (=LO Peg) to produce maps of the starspot distribution. This star was detected during the *ROSAT* WFC EUV all-sky survey and also by the *Extreme Ultraviolet Explorer (EUVE)* survey (Malina et al. 1994) on account of the coronal X-ray/EUV flux. Spectroscopic and photometric observations by Jeffries et al. (1994) showed BD+22° 4409 to be a chromospherically active, rapidly rotating, single K5V–K7V star with $v_{eq} \sin i = 69$ km s^{-1}. From the comparatively high lithium abundance and a trigonometric parallax they also concluded that the star is young and a likely member of the Local Association. From their photometry Jeffries et al. (1994) were unable to discriminate between two possible rotation periods of 10.17±0.08h and 9.22±0.08h. They preferred the longer period, but they noted that the shorter period is still physically reasonable and produced a light curve with very little scatter.

Further photometric observations were obtained by Robb & Cardinal (1995a) in 1995 July, who determined an ephemeris of HJD of Maxima = $2449909.8059(33) + 0.4236(4)E$. This confirmed the longer period of Jeffries et al. (1994) and improved the determination of the period by approximately a factor of 10.

Table 3.1: Observations of BD+22° 4409 in 1993 August. The average S:N after deconvolution is also listed for each group of the object spectra.

Object	UT Start	UT End	Exp time	No. of	Comments
	1993 Aug 4/5		[s]	frames	
Gliese 673	21:32:38	21:38:38	360	1	K5V template
Gliese 820A	21:52:09	21:54:09	120	1	K5V template
Gliese 820B	21:59:31	22:02:31	180	1	K5V template
BD+22° 4409	22:10:40	00:05:10	200	22	Mean S:N = 1195
BD+22° 4409	00:10:42	02:03:57	200	22	Mean S:N = 1265
BD+22° 4409	02:12:55	04:00:06	200	20	Mean S:N = 1285
BD+22° 4409	04:06:15	04:41:46	200	7	Mean S:N = 1200
HD 214923	04:48:50	04:59:12	30	5	B8V tell. std.
Gliese 15A	05:05:31	05:17:31	720	1	M1V template
Object	UT Start	UT End	Exp time	No. of	Comments
	1993 Aug 5/6		[s]	frames	
Gliese 687	20:41:13	21:01:13	1200	1	M3V template
Gliese 786	21:06:43	21:26:43	1200	1	K5V template
Gliese 649	21:38:01	22:08:01	1200	1	M1V template
BD+22° 4409	22:07:32	00:02:15	200	21	Mean S:N = 1025
BD+22° 4409	00:07:55	02:00:49	200	21	Mean S:N = 1165
BD+22° 4409	02:06:54	04:21:27	200	24	Mean S:N = 1125
BD+22° 4409	04:27:27	05:15:52	200	9	Mean S:N = 915
BD+22° 4409	05:26:43	05:46:05	200	4	Mean S:N = 835
HD 22928	05:57:17	06:05:21	30	5	B5III tell. std.

3.2 Observations

BD+22° 4409 was observed on the nights of 1993 August 4 to 5 with the *Utrecht Echelle Spectrograph* (Walker et al. 1986) on the 4.2 m *William Herschel Telescope*. These data were taken from the La Palma Data Archive formerly operated by the Royal Greenwich Observatory and now run by the UK Astronomy Data Centre. A total of 71 and 79 spectra of 200 s exposure time were obtained on the first and second nights with spectral standard stars being observed at the beginning and end of the nights. Table 3.1 shows the journal of observations for the two nights. The 1280 x 1180 pixel EEV6 CCD detector was used in conjunction with the 31.6 grooves mm^{-1} echelle grating. This was centred at a wavelength of 5372 Å in order 106 of the grating. This gave a total of 46 extractable orders and a wavelength range of 4530 Å – 7150 Å.

Three spectra from the first night and four from the second night were of low quality and were discarded. These spectra were mainly ones that immediately preceded or followed arc-frames and so contamination from the lamp seems a likely cause of the poor quality. This gave a total of 68 and 75 object spectra for the first and second nights respectively. Several template stars with spectral types and temperatures similar to the photosphere and spots of BD+22° 4409 were observed for later use in the Doppler imaging process. Observations of B stars were also obtained to provide a relatively featureless spectrum for order tracing.

3.3 Data reduction

3.3.1 Preparation

Bias-subtraction, trimming, rotating and flat-fielding were carried out on the raw CCD frames using the Starlink package FIGARO (Shortridge et al. 1995) prior to extraction.

3.3.2 Extraction

The spectra were extracted using ECHOMOP, the echelle reduction package developed by Mills (1994). Pixel to pixel variations were removed using flat-field exposures taken with an internal tungsten reference lamp. ECHOMOP initially had trouble with the width and

changing slope of the UES orders when order tracing on the usually recommended flat-field frame. Much better results were obtained with an order trace on frames of late B-type telluric standards.

Cosmic ray rejection was not used during the extraction since it removed relatively few events, while slowing the processing down significantly. The deconvolution process dealt with any cosmic ray hits within a spectral line sufficiently well that any cleaning of the extracted frames was unnecessary. Orders were extracted using ECHOMOP's implementation of the extraction algorithm developed by Horne (1986) and extended by Marsh (1989). Wavelength calibration was carried out in ECHOMOP using Thorium-Argon arc-frames, which were treated in a similar manner to the object and standard frames. Error statistics, based on the readout and photon noise, were propagated through the reduction process by ECHOMOP.

3.3.3 Continuum fitting

As found by Collier Cameron & Unruh (1994) and Barnes et al. (1998), the shape of the continuum in the echelle orders can be well approximated by a n^{th} order polynomial. By fitting to a slowly rotating star of close spectral type, it is possible to get a good match to the continuum shape without the problems of rotationally broadened lines and ill-defined continuum windows in rapid rotators. For these UES spectra it was found that polynomial fits of order 7 to the slowly rotating K5V star Gliese 673 (= HD157881) were required to give satisfactory results when the object frames were divided by the fits.

3.4 Least-squares deconvolution

BD+22° 4409 at magnitude $m_v \sim 9.5$, is on the limit of what could be Doppler imaged using the traditional single or three-line techniques with the fast rotation imposing strong constraints on the maximum exposure length if phase blurring is to be avoided. Binning of the data in order to increase the S:N ratio would result in a lack of resolution on the stellar surface.

Fortunately modern CCD detectors and echelle spectrographs can capture a large range of the stellar spectrum in one exposure. The wavelength range of $\sim$ 2600 Å of the

EEV chip & UES used for these observations is not exceptional and contains of the order of 2000 photospheric lines in one spectrum. Least-squares deconvolution (Donati et al. 1997, Donati & Collier Cameron 1997) is a means of combining the information from all these lines into one high S:N profile. By treating the stellar spectrum as a convolution between a pattern of δ - functions from the linelist and a similar line profile for each line, extracting the average line profile becomes a least-squares solution to a matrix equation. The result of this procedure is a profile with a high S:N which is suitable for use in Doppler imaging. Cosmic ray hits can also be removed effectively during this process. The process is described in more detail in Section 2.4.3.

The linelists used in the procedure were generated by Donati et al. (1997) from a full LTE spectral synthesis based on the ATLAS9 model atmospheres of Kurucz (1993). We used a K5 linelist and removed from it the regions of wavelength range which are badly affected by the telluric lines at the red end of the spectrum. These are usually much stronger than the photospheric lines in this part of the spectrum and would only distort and add noise to the deconvolved profile. The region around the strong Mg I b lines (5163.50 Å - 5186.86 Å) at the blue end was also excluded.

3.4.1 Errors

One change in our deconvolution program, SPDECON, from that used by Barnes et al. (1998) and Donati & Collier Cameron (1997) is the addition of error propagation through to the output deconvolved profiles. Further details are given in Section 2.4.3

3.4.2 Construction of specific intensity lookup tables

For the purposes of our implementation of Doppler Imaging, the star consists of only two temperature components, the clean photosphere and the spots. To produce the lookup tables for the specific intensity that is required in the Doppler Imaging process, template spectra of the M1 dwarf Gliese 649 (photospheric temperature similar to that of the spots, T~3500 K) and the K5 dwarf Gliese 673 (photospheric temperature similar to BD+22° 4409) were deconvolved in the same manner as the object spectra using the same standard continuum to minimise equivalent width mismatches.

The lines were scaled at ten linearly spaced limb angles (i.e. 0.1, 0.2... 1.0) according

to the mean continuum scaled intensity value and the relative central intensity, I_0, for each temperature and then combined into the lookup table.

The central wavelength was calculated from the lines in the linelist, weighted with respect to the line strength and deviation from the standard continuum fit used in SPDECON. This was used to obtain values for the relative central intensities from Kurucz (1993) ATLAS9 LTE models for temperatures corresponding to the spots and the photosphere of 3500K and 4250K respectively.

3.5 Image reconstruction

3.5.1 Fine tuning of parameters

As has been shown by Collier Cameron & Unruh (1994) and Unruh (1996), the reconstructed image is sensitive to the values chosen for the stellar parameters. Spurious features can be produced if the parameters have a small error and the maximum entropy method will usually fail to converge in the case of serious deviations from the correct values. Sets of reconstructions were carried out for different values of one of the parameters of equivalent width, radial velocity, inclination and $v \sin i$, while keeping the others fixed. The initial aim was to minimise the spot area to produce the image with maximum entropy (the smoothest image) as had been done in previous investigations (Collier Cameron & Unruh 1994). The problem with the maximum entropy method is the difficulty of converging each run to the same end conditions. Differences in the value of the MEM TEST statistic, which is a measure of the convergence of the iteration process, will mean changes in the amount of spot area left on the surface at the end of iteration.

We have found that the initial χ^2 produced by DOTS upon loading a blank stellar image, is a smoother and better diagnostic for fine-tuning the stellar parameters. We illustrate this in Fig. 3.1 with plots of spot coverage and initial χ^2 as functions of geocentric radial velocity, $v \sin i$ and inclination along with parabolic fits to each set of points. The scatter of the spot area points about the best fit line is most likely due to the problem, mentioned above, of converging to a fixed entropy value in all cases. From the χ^2 fits, we found the best fits when $v \sin i$ = 69 km s^{-1} and v_{rad} = -19.25 km s^{-1} for the night of 1993 August 04/05 and $v \sin i$ = 69.5 km s^{-1} and v_{rad} = -23 km s^{-1} for the night of 1993

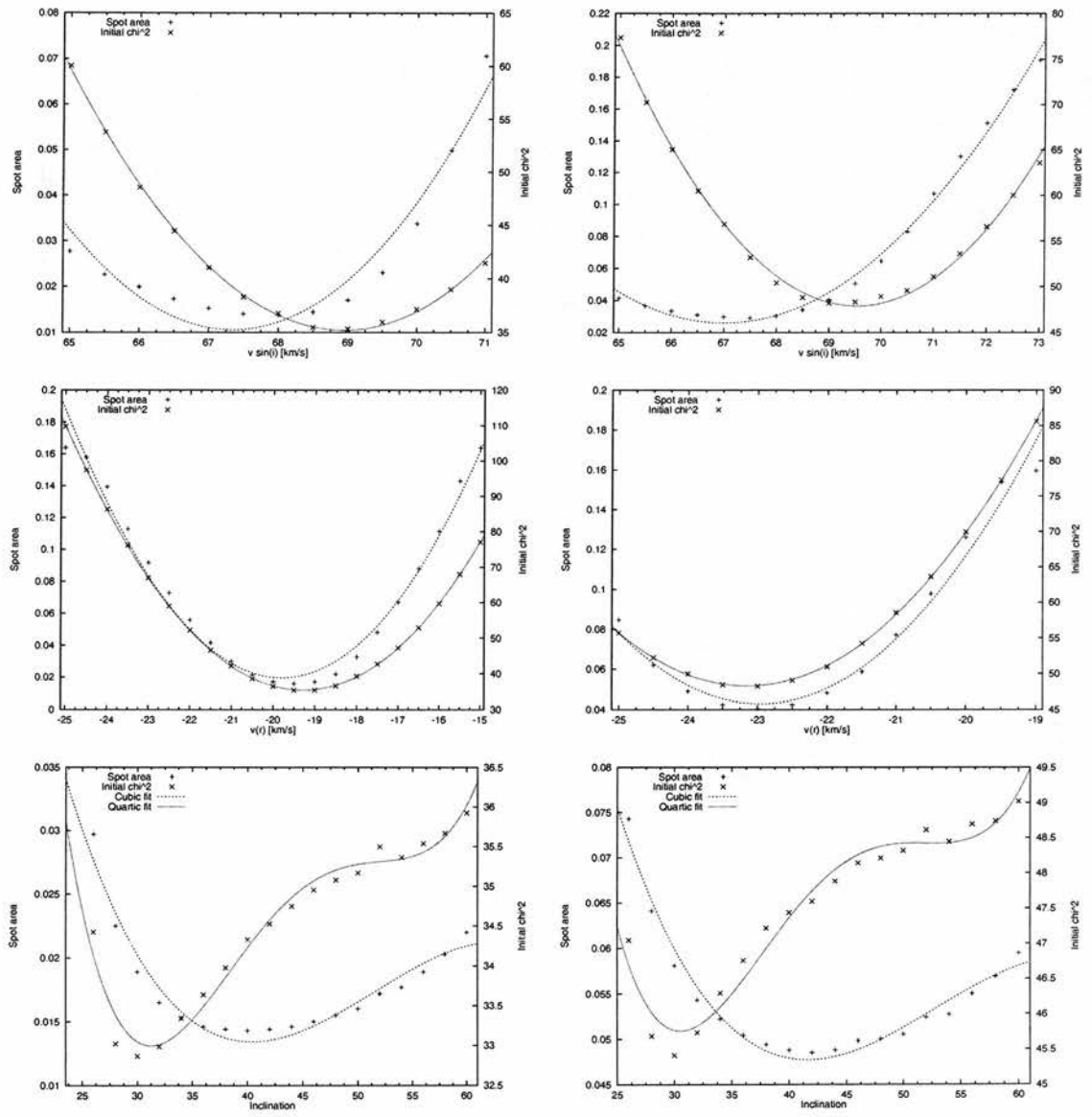

Figure 3.1: The plots on the left show the spot coverage and the initial χ^2 as a function of (top to bottom) $v \sin i$, radial velocity and inclination for the first night. The plots on the right are the same but for the second night.

August 05/06, which agree with the values of Jeffries et al. (1994). The reconstructed images with parameters from χ^2 minimisation showed no significant differences from those that used parameters from the spot area minimisation.

We also performed a trial grid of reconstructions using the method suggested by Barnes (1999) of performing a large number of iterations with the target χ^2 set to an unreachable value and recording the value of χ^2 that was reached. This was carried out with the night 2 dataset, and we searched $v \sin i$ =66–70 km s^{-1} and v_{rad}=-(26–21) km s^{-1}, with the other parameters held fixed. The minimum on this surface was found at $v \sin i$ = 66 km s^{-1} and v_{rad}=-23.5 km s^{-1}, i.e at the minimum value of $v \sin i$ that was searched. This was the case irrespective of what value was set for the lower search limit of $v \sin i$. In addition, $v \sin i$ = 66 km s^{-1} is well outside the value of $v \sin i = 69 \pm 1$ km s^{-1} determined by Jeffries et al. (1994) and consequently we elected to use the values determined from the initial χ^2 minimisation.

Such a minimisation was not possible for the axial inclination since, as can be seen from Fig. 3.1, neither the spot area or the initial χ^2 shows a minimum that can produce any sort of constraint. In the case of initial χ^2 this is not surprising as a blank image would contain no features to test against the data and the resulting effect of changing the inclination was to alter the ratio of spots in the high and low latitude bands. Consequently we adopted the value of 50° obtained by Jeffries et al. (1994) from photometry and the Barnes-Evans relationship (Barnes, Evans & Moffett 1978). Although no *Hipparcos* parallax was available at the time of Jeffries et al. (1994), the Gliese and Jahreiss parallax (Gliese & Jahreiss 1992) used by Jeffries et al. (1994) to derive the stellar parameters differs only slightly from the *Hipparcos* parallax and are identical within the errorbars. Consequently the effect on the derived parameters is expected to be minimal.

It may be possible to circumvent the time-consuming process of making large numbers of reconstructions to obtain the best value of each parameter by making use of a technique such as *simulated annealing* (Press et al. 1992). With this method it ought to be possible to find the global minimum on the χ^2 hypersurface, corresponding to the correct set of stellar parameters in one step. However the problem of the axial inclination discussed above may mean that such a minimum does not exist or the minimum may yield non-optimal parameters. Another option may be to include the stellar parameters as adjustable pixels and adjust the values along with the surface grid as part of the imaging

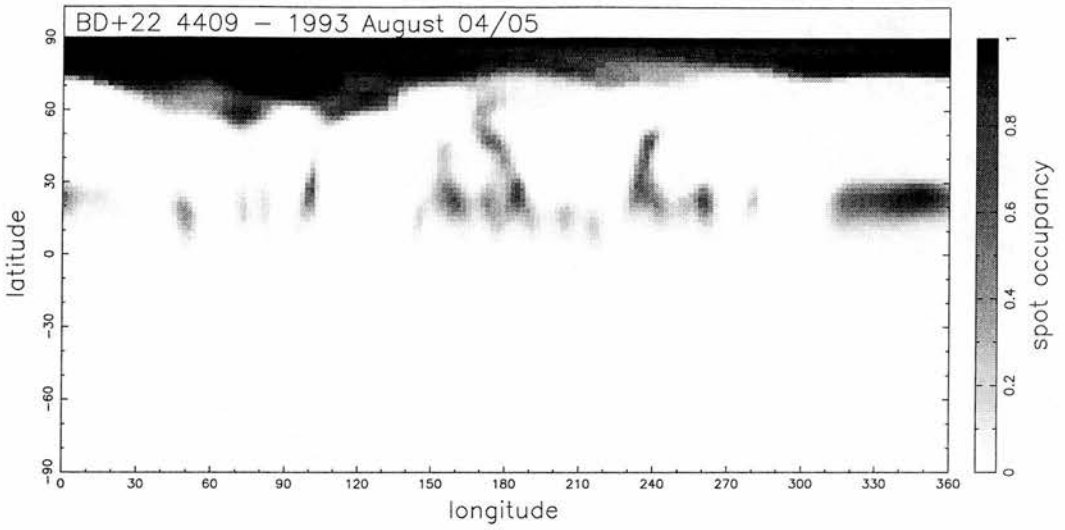

Figure 3.2: Reconstructed image of BD+22° 4409 on night 1.

process, as performed by Hendry & Mochnacki (2000) in their imaging of VW Cep.

3.5.2 Reconstructed images

In Figs. 3.2–3.5 we show the maximum entropy data fits and Mercator projection plots of the reconstructed images for each night. The number of latitudes on the stellar surface grid was set to 90 which provides an improvement in latitude resolution of spot features from 4.5° to 2° over previous investigations (e.g. Collier Cameron & Unruh 1994, Collier Cameron 1995).

Although the maps extend down to −90° latitude, because of the inclination of BD+22° 4409 at 50°, the bottom half of the star below −40° latitude is not visible and the map appears blank.

3.6 Discussion

The images on both nights clearly show two main regions of spot coverage: a high-latitude spot or polar crown with a concentration towards longitude ∼70° and a low-latitude belt at latitude $+25° \pm 10°$ and very little spot coverage at the mid latitudes. The high-latitude spot may not extend polewards into a true polar spot as there is a slight decrease in the spot filling factor at latitudes $\geq 85°$, especially for longitudes ∼ 270°–360°. In addition

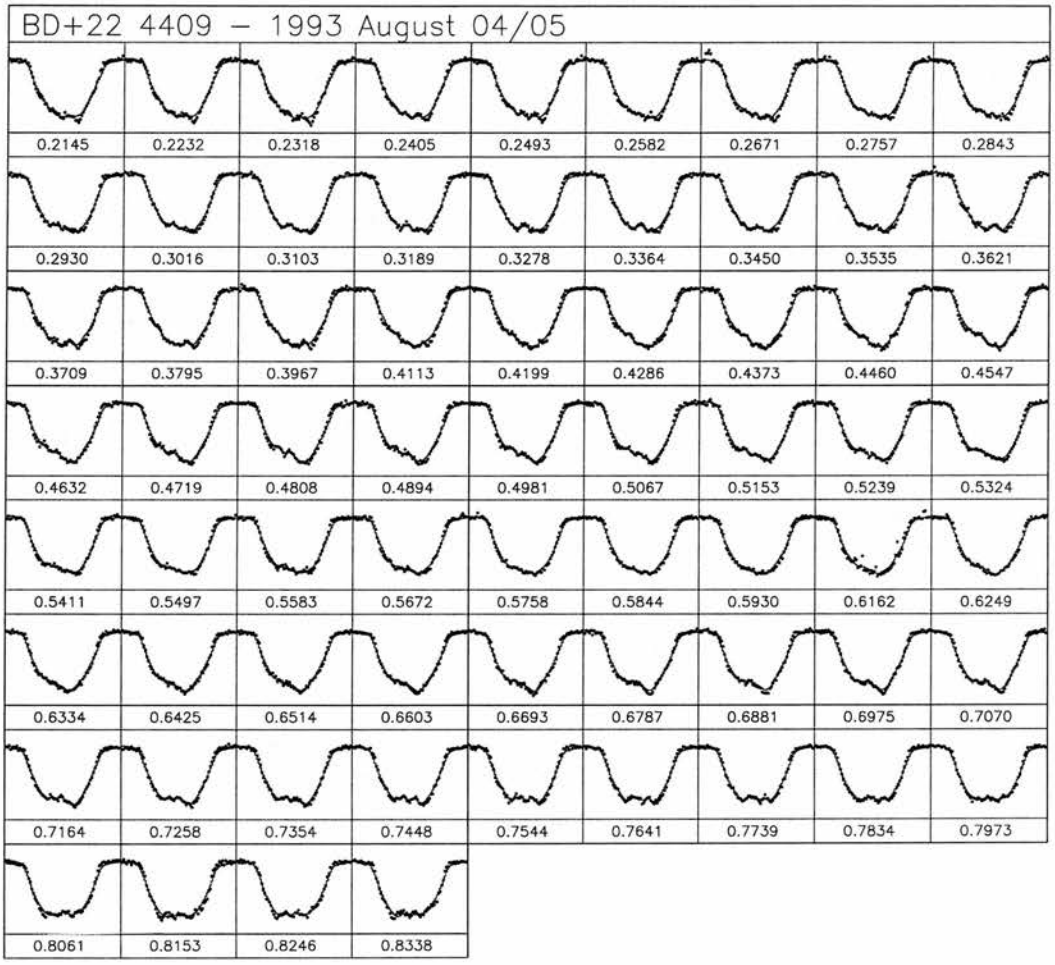

Figure 3.3: Profile fits for BD+22° 4409 on night 1.

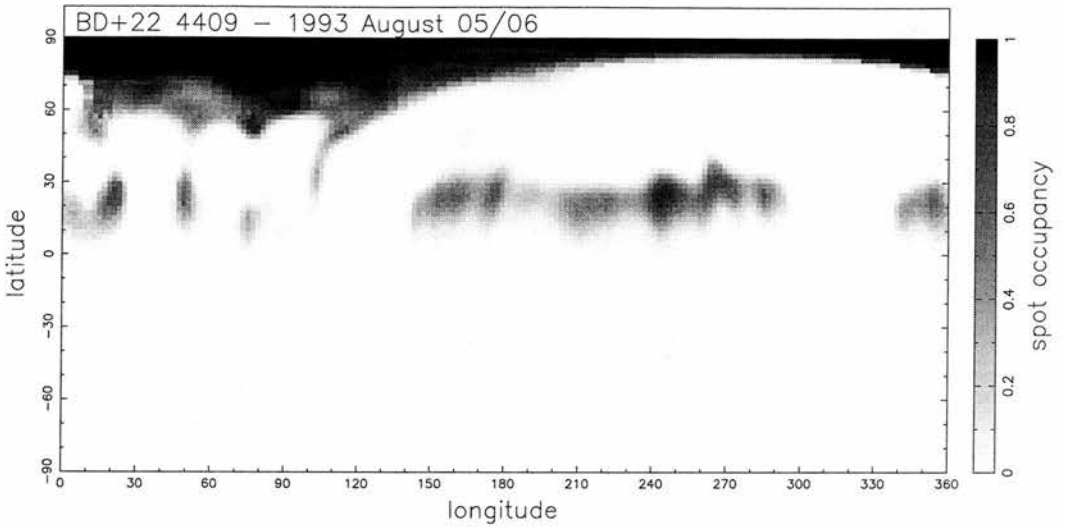

Figure 3.4: Reconstructed image of BD+22° 4409 on night 2.

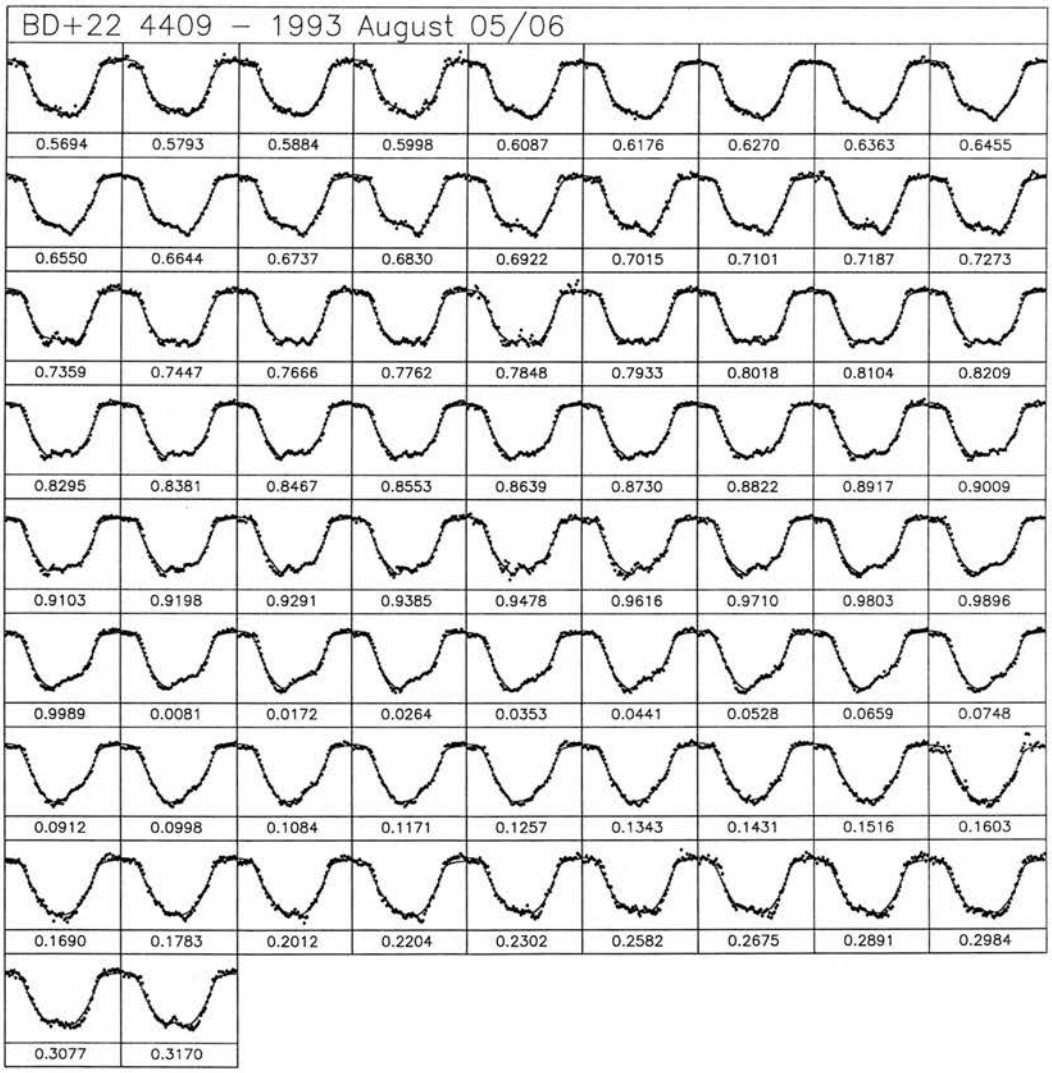

Figure 3.5: Profile fits for BD+22° 4409 on night 2.

although there is distortion of the line profile this is mainly confined to the blue side of the profile and never really turns into the true flat-bottomed profile which is characteristic of a polar spot (see Figs 3.3, 3.5).

Polar spots have been a feature of Doppler image reconstructions from the beginning and there has always been a degree of controversy over whether they are genuine or an artifact of the reconstruction process (see e.g. Strassmeier 1996a; Byrne 1996). Bruls, Solanki & Schüssler (1998) have carried out an investigation into the effects of chromospheric in-filling producing flatter bottoms in 14 of the photospheric lines most commonly used for Doppler imaging. They conclude that chromospheric effects can lead to some in-filling of the profiles but this is a small effect which only affects some of the lines and is unlikely to account for the appearance of a polar spot. The effects of the axial inclination on the appearance of polar spots has been investigated by Hatzes et al. (1996). They tried to reproduce polar spots in simulations by utilizing the effects of gravity darkening, differential rotation and spectral line temperature dependences. It was found that the flat-bottomed line profiles seen in stars with polar spots cannot be entirely reproduced by these effects. Our codes correct for the effect of gravity darkening, which is handled using the standard von Zeipel formula,

$$T_{\rm local} = T_{\rm pole} \left(\frac{g_{\rm local}}{g_{\rm pole}} \right)^{\beta}, \tag{3.1}$$

where $\beta = 0.08$ or 0.25 for convective and radiative envelopes as appropriate. The effects of temperature dependence on the spectral lines, although difficult to quantify in this case, is likely to be much diluted due to the combining of ~2000 lines with a wide variety of line strengths, atomic parameters etc.

These images appear to confirm what is seen on AB Dor and the α Persei G dwarfs and also on a wide variety of other objects from classical T Tauris to FK Com giants (cf. Section 1.3.1, namely the existence of both high-latitude/polar spots and low latitude features. The mounting evidence from a wide variety of rapidly-rotating systems, including single stars, that they possess significant low-latitude features as well as polar spots/crown is proving to be a significant challenge to the rising flux-tube simulations of Schüssler et al. (1996) and DeLuca, Fan & Saar (1997). For a star as young as BD+22° 4409 (age $\geq$ 20-30 Myr Jeffries et al. 1994) and rotating this rapidly the flux tubes should emerge at latitude $\geq 30°$. This is clearly not supported by the reconstructed images which show significant amounts of flux below this latitude and a marked absence of spots in the mid-

latitudes. This would seem to indicate that some mechanism other than the standard one of a dynamo residing in the overshoot layer at the base of the convective zone with flux tubes rising due to buoyancy and Coriolis forces is at work. There is evidence from the maps of radial and azimuthal field on AB Dor (Donati & Collier Cameron 1997) that the toroidal magnetic field is not just confined to the overshoot region but that at least some part must be distributed throughout the convective zone.

One striking difference between these images and those of AB Dor and the α Persei G dwarfs is the almost total absence of mid-latitude features on BD+22° 4409. The reason for this is unclear but BD+22° 4409 is significantly later than AB Dor (K5-K7 compared to K0) and it is possible that the dynamo behaviour changes for stars of later spectral type which have deeper convection zones. Another possibility is that, as seen on the Sun, the latitude of emergence of flux tubes drifts towards the equator as the magnetic cycle progresses. This could reconcile the differences between AB Dor and BD+22° 4409 if BD+22° 4409 was further along in a magnetic cycle and flux tubes were appearing at lower latitudes. It must be stressed that with only one set of images and little photometric study of BD+22° 4409, this is little more than speculation. Further investigations, particularly Zeeman-Doppler Imaging (Donati et al. 1997), would be very valuable to broaden the range of single stars which have been studied in order to try and understand the differences between BD+22° 4409 and other objects and AB Dor in particular.

Several previous Doppler imaging studies have utilized simultaneous broad-band photometry as an additional constraint of the images (Strassmeier et al. 1993; Strassmeier 1996b; Unruh, Collier Cameron & Cutispoto 1995). This has the effect of improving the definition of low-latitude features and reduces the "mirroring" of surface features between hemispheres. Regrettably, BD+22° 4409 has had very few photometric studies and the only ones available are those of Jeffries et al. (1994) and Robb & Cardinal (1995a) which were obtained $\sim$ 10 months prior and $\sim$ 23 months after these data respectively. There is very good evidence from photometry (see e.g. Innis, Coates & Evans 1990, Cutispoto 1998a, Cutispoto 1998b) and from Doppler images (Barnes et al. 1998) of significant evolution of surface features on timescales at least as short as a month. Comparisons with photometry taken so far apart from the spectroscopic data are therefore unlikely to be meaningful.

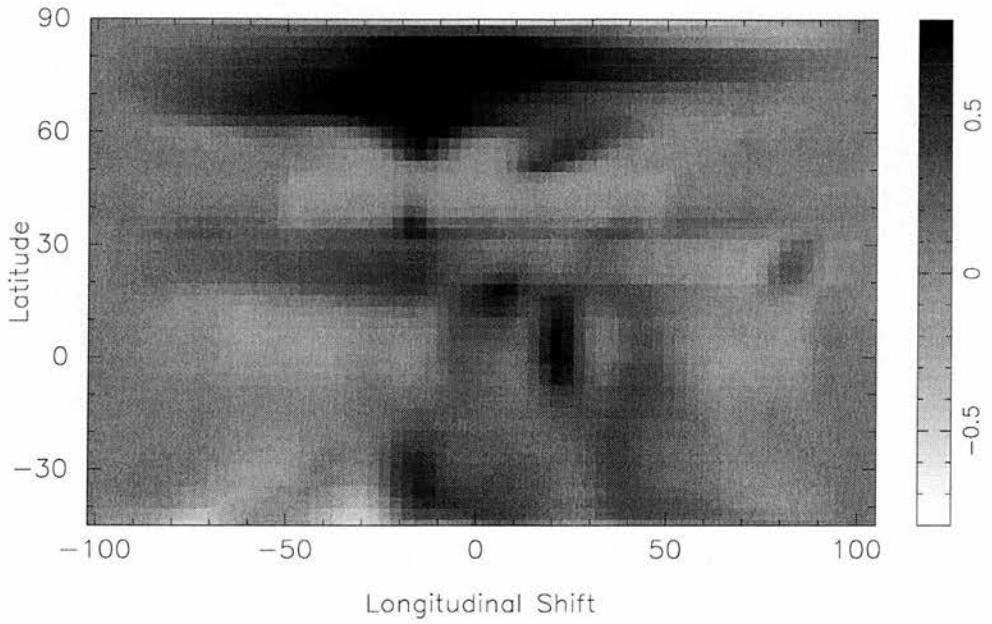

Figure 3.6: Cross-correlation image for BD+22° 4409 from reconstructions using the shorter period of 9.22 h.

3.6.1 Cross-correlation

As discussed in Section 1.3.4, apart from the Sun, there are now three stars to have been reliably shown to exhibit differential rotation. The star most similar to BD+22° 4409 is the K0 dwarf AB Doradus for which Donati & Collier Cameron (1997) and Donati et al. (1999) have determined a lap time of 110 days for the equator to pull one rotation ahead of the pole by cross-correlating slices at each latitude from images taken four to six nights apart. Unfortunately this dataset is not ideal for determining the existence of differential rotation on BD+22° 4409 since we only have two consecutive nights of data and this does not give much time for any of the low-latitude features to pull ahead. In addition, as can been the surface maps in Figures 3.2–3.5, spot are only present at a limited range of latitudes on the stellar surface.

Cross-correlation was carried out using the phase range common to both nights (phases 0.58–0.85). From their photometry Jeffries et al. (1994) were unable to discriminate between two possible rotation periods of 10.17±0.08h and 9.22±0.08h. They preferred the longer period and this is the one we have used in the reconstructions, but they noted that the shorter period is still physically reasonable and produced a light curve with very

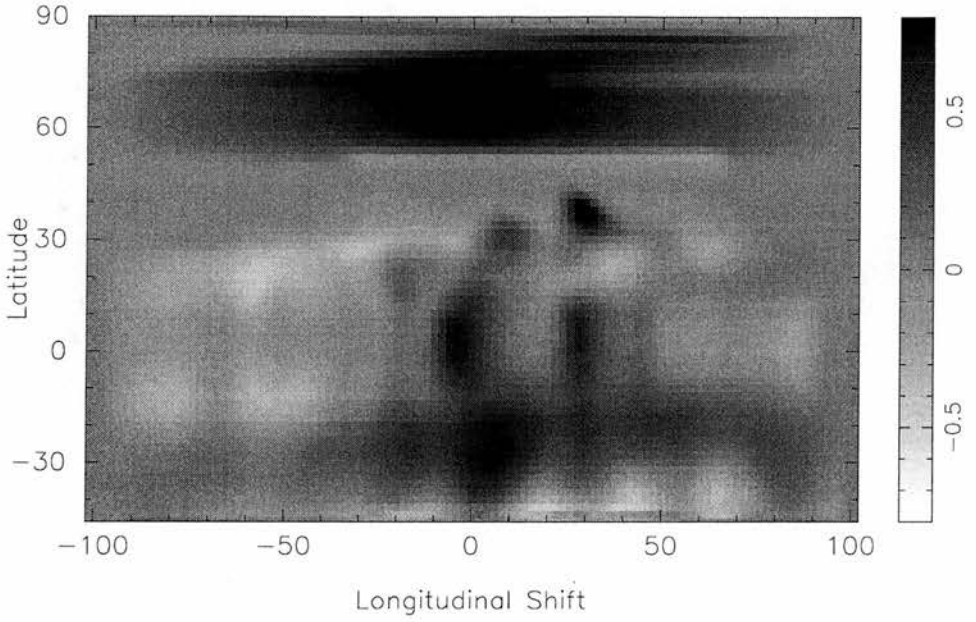

Figure 3.7: Cross-correlation image for BD+22° 4409.

little scatter. Reconstructions were made from both sets of data using the shorter period of 9.22h and the resulting images were cross-correlated in the manner described above. As shown in Fig 3.6 by the lack of correlation and the displacement of the high latitude spot from the line of zero shift, this shorter period is incorrect.

This confirms the result of Robb & Cardinal (1995a) who also rejected the shorter 9.22h period of Jeffries et al. (1994) and determined a new ephemeris of

$$\text{HJD of Maxima} = 2449909.8059(33) + 0.4236(4)E.$$

with the uncertainties in the final digit given in brackets. This period differs from that of Jeffries et al. (1994) by only 13s and is in complete agreement within the bounds of the errors, but improves the precision of the period by a factor of ~ 10. We were unaware of the result of Robb & Cardinal (1995a) at the time the reconstructions were performed and so we have continued to use the period of Jeffries et al. (1994).

Cross-correlating with the correct period produces a quite strong degree of correlation along the line of zero shift and a small hint of the equator lagging slightly in the low-latitude belt. Although the absence of features in the mid-latitude range of the images (Fig. 3.7) makes detection of differential rotation more difficult, the strong correlation

peaks at latitudes 20°-30° and 60°-70° would allow detection of differential rotation given a longer timespan. Above latitude 75° the area of each latitude band diminishes rapidly as the pole is approached and the cross-correlation procedure gives spurious shifts. Below the equator there is some evidence of mirroring between the hemispheres and below -40° there is very little structure because of inclination effects.

Given that only two consecutive nights of data are available, the lack of evidence of differential rotation is unsurprising as there is not enough time between the datasets for the equator to pull any significant distance ahead of the pole. As shown by the lack of correlation in the images of Barnes et al. (1998) which were obtained a month apart, there is a fine line between allowing enough time for differential rotation to become evident and the evolution of the individual spot groups for which the timescale appears to be $\sim$1 week. In the case of future investigations aiming to measure differential rotation, an observing strategy similar to that successfully adopted by Donati & Collier Cameron (1997) of 1-2 night observing runs separated by a gap of several days is more likely to succeed.

3.7 Conclusion

From the use of least squares deconvolution to combine the large numbers of photospheric lines present in a typical echelle spectrum into a single high S:N ratio profile, we have shown that it is possible to obtain good quality Doppler images of stars which are much fainter than those previously possible. This enables many more nearby, single, rapid rotators to be studied than was possible before and opens up the possibility of investigations into the wide variety of spin-down timescales seen in the open clusters without the difficulties of obtaining high quality data on cluster members themselves.

We have applied the method to obtain surface reconstructions of the young, rapidly-rotating member of the Local Assocation, BD+22° 4409. The images from both nights show structure in a low-latitude belt and also in a high-latitude spot or possible polar crown. Unlike the images of the G dwarfs in the α Persei cluster and the K0 dwarf AB Doradus, BD+22° 4409 shows almost no structure in the mid-latitudes where the majority of the flux tubes should appear if the models for rapidly-rotating stars are correct.

Cross-correlation images from the two nights show no evidence of the phase shift that should be caused by differential rotation.

These data have also been used Eibe et al. (1999) to study the H α line profile which is seen in emission on this star which they found to be very asymmetric and extremely variable. They also found evidence for an intense downflow of material and suggested this could be downflows in loop prominences. Cool condensations of material that would indicate prominence structures have been seen on other stars, most notably AB Dor (e.g. Donati et al. 1999), but have not been observed on BD+22° 4409. This is thought to be the result of the inclination of the star which means that the prominences, which tend to form in the equatorial plane of the star, are never seen in projection against the disk and therefore never give rise to absorption transients.

BD+22° 4409 is an important addition to the sample of single stars that have been Doppler imaged as it nearby, young and relatively bright. With a spectral type of K5 V it is also one of the latest single stars to have been imaged (see Section 1.3.1 and Table 1.4) and therefore is important for understanding how the dynamo processes change as the mass decreases and increasing convection zone depths. Further observations and surface maps would help to understand the differences between BD+22° 4409 and other late-type rapid rotators and enable a determination of the differential rotation.

CHAPTER 4

Spectroscopy and eclipse mapping of the eclipsing binary GSC2807-1423

The spectroscopic data presented in this chapter were obtained by J. R. Barnes and D. J. James with the William Herschel Telescope operated on the island of La Palma by the Isaac Newton Group in Spanish Observatorio del Roque de los Muchachos of the Instituto de Astrofisica de Canarias.

4.1 Introduction

GSC2807-1423 (=RX J010124.9+411503) was discovered by the *ROSAT* satellite (Voges et al. 1996) and followed up optically by Robb (1998). He carried out differential R band photometry and showed that GSC2807-1423 is a detached eclipsing system with probable late-type components and a period of 0.67601 days. The light curve showed an obvious asymmetry in the maxima, indicating the presence of starspots on one or both of the components. The system was included in our observing program on short-period RS CVn binaries in order to search for substantive evidence of magnetic activity by means of Doppler imaging and eclipse-mapping.

Normally only full Doppler imaging from high resolution spectroscopic data can give accurate spot locations. The only exception to this rule is the special case where cool spots are present within the region on the inner face of the hotter star that is occulted by the cooler secondary during the course of primary eclipse. Any spots in this region will give rise to distortions in the primary eclipse profile that should be easily detectable in broad-band optical photometry obtained with high precision and sufficient time resolution. The

Table 4.1: Journal of photometric observations of GSC2807-1423 in 1998.

UT Date	HJD - 2450000.0	No. of obs.	Filter	Phase coverage
1998 September 18/19	1075.33 – 1075.51	294	V	430.15 – 430.71
1998 September 21/22	1078.31 – 1078.50	144	V	434.56 – 434.83
1998 October 07/08	1094.37 – 1094.73	265	V	458.32 – 458.85
1998 October 08/09	1095.28 – 1095.48	199	V	459.66 – 459.96
1998 October 11/12	1098.31 – 1098.74	452	V	464.15 – 464.78
1998 October 12/13	1099.42 – 1099.46	36	V	465.78 – 465.85
1998 October 29/30	1116.30 – 1116.74	487	V	490.75 – 491.41
1998 October 30/31	1117.29 – 1117.67	493	V	492.23 – 492.78
1998 October 30/31	1117.67 – 1117.75	121	I	492.79 – 492.91
1998 Oct. 31/Nov. 01	1118.28 – 1118.76	771	I	493.68 – 493.65
1998 November 01/02	1119.29 – 1119.64	673	I	495.18 – 495.70

potential of eclipse-mapping for studying spot locations on eclipsing binaries was examined by Collier Cameron (1997b) and reconstructions using this method were presented by Collier Cameron & Hilditch (1997) for the short-period RS CVn binary XY UMa. Further details of the technique are presented in Section 2.5.

4.2 Observations and Data Reduction

4.2.1 Photometry

The photometric observations of GSC2807-1423 were obtained with the 0.9-m James Gregory Telescope (JGT), at the University Observatory, St. Andrews, and a Wright Instruments CCD camera and associated filter wheel mounted at the Cassegrain focus. The camera uses a GEC CCD02-06 385×578 pixel CCD chip operating in inverted or multipinned phase (MPP) mode to reduce the dark current. The combination of a four-stage Peltier cooler, which cools the chip to around 200 K, and operation of the chip in MPP mode

reduces the dark current to ~ 0.001 electrons pixel^{-1} s^{-1}. The chip is coated with a thin, phosphorescent coating of Lumogen® to enhance the blue response by down-converting blue–UV photons into red photons where the chip's QE is higher.

The pixel size is 22 μm which, when combined with the plate scale of the JGT of 80.22 arcsec^{-1} mm^{-1}, gives a usable field of 11.5×17 arcmin^2. Data were obtained in the V and I filters and exposure times varied from 20–60 s depending on the seeing and the filter in use. The details of the observations are shown in Table 4.1.

The raw data frames were processed using a combination of the Starlink packages FIGARO (Shortridge et al. 1995) and KAPPA (Currie & Berry 1999) to perform bias-subtraction, trimming and flat fielding. Aperture photometry was performed using locally written software, JGTPHOT (Bell, Hilditch & Edwin 1993), and differential magnitudes for Variable–Comparison (V–C) and Check–Comparison (C–K), along with Heliocentric Julian Dates were formed.

The data were initially phased with the ephemeris of Robb (1998):

$$\text{HJD (Min I)} = 2450784.5434(10) + 0.67601(8)E.$$

where the uncertainties in the final digit are given in brackets. However, on phasing the data with this ephemeris we discovered a phase offset of ~ 0.014. We determined several new times of minimum using the bisecting chord code described in Section 5.2.1 and these are shown in Table 4.2. The data were phased with the ephemeris:

$$\text{HJD (Min I)} = 2451116.47385(72) + 0.67601E.$$

where again the uncertainties in the final digit are given in brackets. The light curves are shown in Fig. 4.1 – 4.2.

4.2.2 Spectroscopy

GSC2807-1423 was observed on the nights of 1998 December 6–8 (by J. R. Barnes and D. J. James) with the *Utrecht Echelle Spectrograph* (Walker et al. 1986) on the 4.2 m *William Herschel Telescope*, under conditions of poor seeing ($\sim 2''$– $6''$). The 2048×2048 pixel SiTE CCD detector was used in conjunction with the 31.6 grooves mm^{-1} echelle grating, which was centred at a wavelength of 4916 Å in order 116 of the grating. This

Table 4.2: Times of minima for GSC2807-1423 obtained from the JGT photometry.

Time of minima (HJD - 2400000.0)	Filter	Type of minima
51075.57303	V	Secondary
51094.50169	V	Secondary
51098.55790	V	Secondary
51116.47385	V	Primary
51117.48648	V	Secondary
51118.50150	I	Primary
51119.51476	I	Secondary

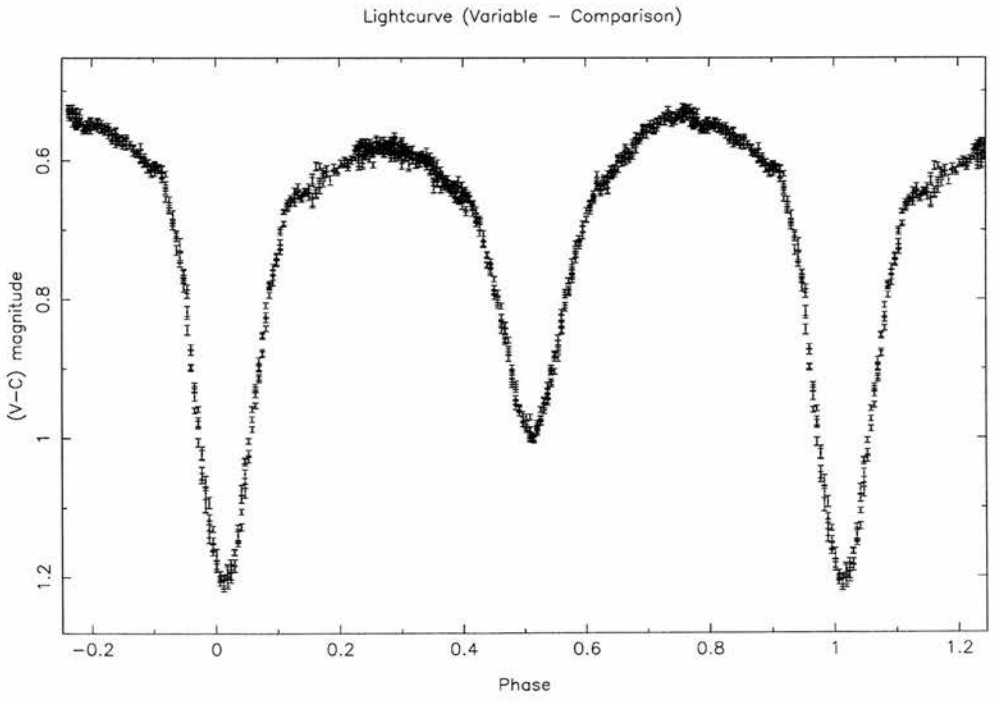

Figure 4.1: V band light curve for GSC2807-1423 taken in 1998 October.

Table 4.3: Journal of spectroscopic observations of GSC2807-1423. The average S:N after deconvolution is also listed for each group of the object spectra.

Object	UT Start	UT End	Exp time	No. of	Comments
	1998 Dec 6/7		[s]	frames	
HD 3901	19:05:56	19:07:56	120	1	B2V telluric std.
HD 1326	19:20:15	19:26:15	360	1	M2V template
HD 222368	19:33:10	19:35:10	120	1	F7V template/RV std.
HD 32963	21:55:02	22:03:22	500	1	G2V template/RV std.
GSC2807-1423	23:28:31	23:33:31	300	1	Mean S:N = 255
GSC2807-1423	23:38:07	00:27:28	450	5	Mean S:N = 210
GSC2807-1423	02:14:41	02:27:11	750	1	Mean S:N = 530
HD 101501	05:04:47	05:08:57	250	1	G8V template
HD 119850	06:55:42	07:10:42	900	1	M1.5V template
HR 3982	07:14:45	07:14:49	4	1	B7V telluric std.
Object	UT Start	UT End	Exp time	No. of	Comments
	1998 Dec 7/8		[s]	frames	
HD 3901	19:37:55	19:39:15	80	1	B2V telluric std.
HD 222368	19:48:20	19:49:20	60	1	F7V template/RV std.
HD 10780	19:54:11	19:57:31	200	1	K0V template
GSC2807-1423	23:21:21	23:28:51	450	1	Mean S:N = 700
GSC2807-1423	00:13:42	00:21:12	450	1	Mean S:N = 635
GSC2807-1423	01:11:07	01:18:37	450	1	Mean S:N = 430
GSC2807-1423	02:29:16	02:41:16	720	1	Mean S:N = 385
HD 126053	07:06:26	07:16:26	600	1	G1V template/RV std.
HD 115617	07:19:53	07:25:17	324	1	G5V template
Object	UT Start	UT End	Exp time	No. of	Comments
	1998 Dec 8/9		[s]	frames	
HD 3901	18:57:58	18:59:18	80	1	B2V telluric std.
HD 693	19:07:07	19:08:27	80	1	F6V template/RV std.
GSC2807-1423	22:03:42	22:11:12	450	1	Mean S:N = 1310
GSC2807-1423	23:23:33	23:31:03	450	1	Mean S:N = 1065
GSC2807-1423	00:28:13	00:35:43	450	1	Mean S:N = 1172
GSC2807-1423	01:53:39	02:05:39	720	1	Mean S:N = 430

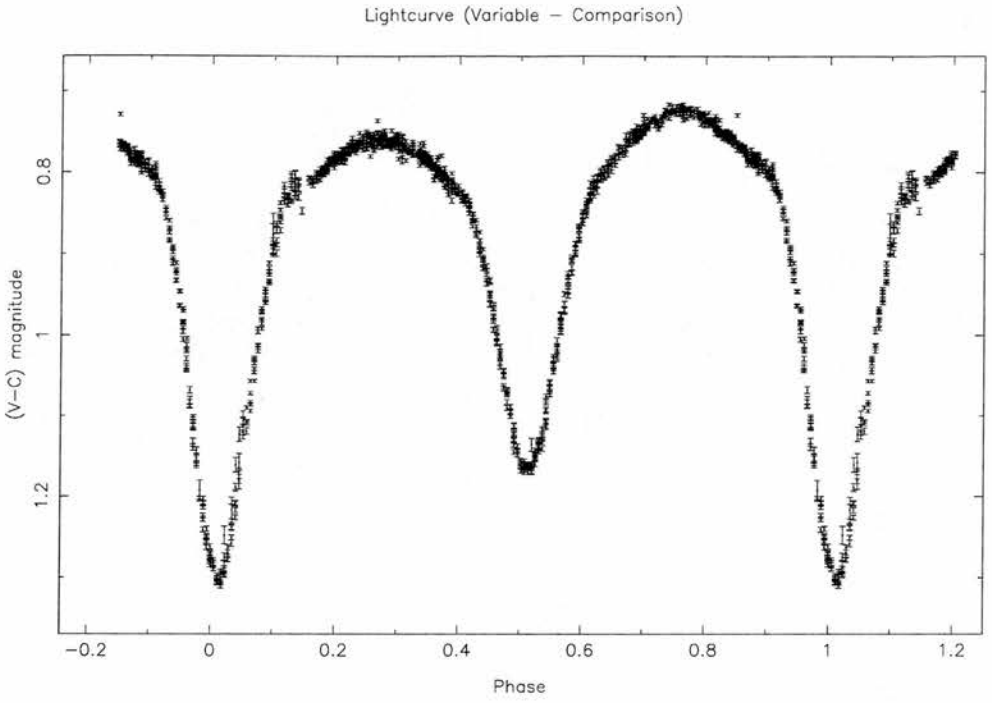

Figure 4.2: I band light curve for GSC2807-1423 taken in 1998 October.

gave a total of 60 extractable orders after the removal of 5 orders at the extreme red and blue ends of the chip which had poor signal. This resulted in a usable wavelength range of 3985 Å – 7025 Å. Observations of radial velocity standards (which doubled as spectral templates) and spectral standards were also obtained along with a few B star observations for use as telluric standards and order tracing in ECHOMOP. Details of the spectroscopic observations are given in Table 4.3.

Bias-subtraction, trimming, rotating and flat-fielding were carried out on the raw CCD frames using the Starlink package FIGARO (Shortridge et al. 1995) prior to extraction.

4.2.2.1 Extraction

The spectra were extracted using ECHOMOP, the echelle reduction package developed by Mills (1994). Pixel to pixel variations were removed using flat-field exposures taken with an internal tungsten reference lamp. Order tracing was performed on frames of late B-type telluric standards.

Cosmic ray rejection was not used during the extraction since it removed relatively few events, whilst slowing the processing down significantly. The deconvolution process

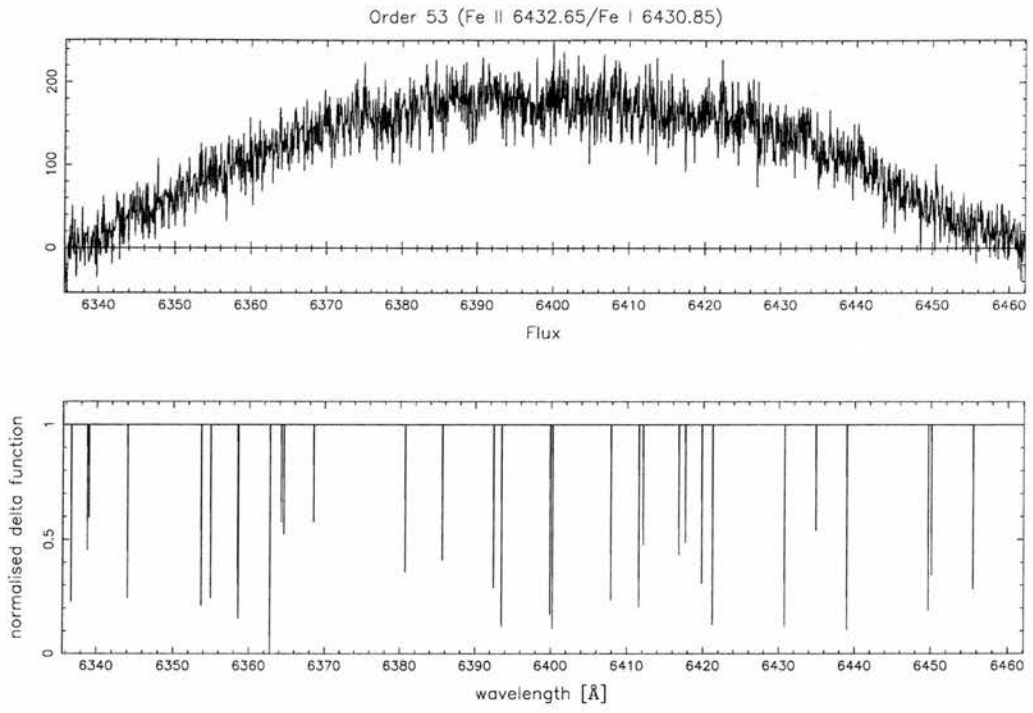

Figure 4.3: An example of one of the extracted spectral order of GSC2807-1423 in the red part of the spectrum. The pattern of delta functions in the lower plot is the linelist used in the deconvolution process.

dealt with any cosmic ray hits within a spectral line sufficiently well that any cleaning of the extracted frames was unnecessary. Orders were extracted using ECHOMOP's implementation of the extraction algorithm developed by Horne (1986) and extended by Marsh (1989). Wavelength calibration was carried out in ECHOMOP using thorium-argon arc-frames, which were treated in a similar manner to the object and standard frames. Error statistics, based on the readout and photon noise, were propagated through the reduction process by ECHOMOP.

4.2.2.2 Continuum fitting

Since the spectral type of GSC2807-1423 is unknown we elected to fit a 7-knot spline function directly to each extracted echelle order to determine the continuum level, rather than fit to a slowly rotating template star as has been done in the past (Collier Cameron & Unruh 1994, Barnes et al. 1998). This minimized any possible continuum tilt in the spectra used for deconvolution. An example of one of the extracted orders in the red part of the spectrum, along with the appropriate section of the line list, is shown in Figure 4.3.

4.2.2.3 Least-squares deconvolution

Since GSC2807-1423 is quite faint ($m_v \sim 10.9$), and the spectra were obtained in very poor conditions, the raw spectra have low S:N which would make determination of radial velocities difficult. To improve the S:N of the spectra we made use of the large wavelength coverage of these data and processed the data using the technique of Least-squares deconvolution.

The technique of Least-squares deconvolution (Donati & Collier Cameron 1997, Barnes et al. 1998, Lister, Collier Cameron & Bartus 1999) is a means of combining the information from all these lines into one high S:N profile. By treating the stellar spectrum as a convolution between a pattern of δ-functions from the linelist and a similar line profile for each line, extracting the average line profile becomes a least-squares solution to a matrix equation. The result of this procedure is a profile with a boosted S:N which in this case enables the determination of radial velocities from fairly poor data. Further details of the method are given in Section 2.4.3.

The linelists used in the procedure were generated by Donati et al. (1997) from a full LTE spectral synthesis based on the ATLAS9 model atmospheres of Kurucz (1993). We used a K1 linelist and removed from it the regions of wavelength range which are badly affected by the telluric lines at the red end of the spectrum. These are usually much stronger than the photospheric lines in this part of the spectrum and would only distort and add noise to the deconvolved profile. The regions around the strong Mg I b lines (5163.50 Å – 5186.86 Å) at the blue end and around the Na I D lines were also excluded. Examples of the deconvolved profiles are shown in Figure 4.4.

4.3 Spectral types and radial velocities

The radial velocities for each component were obtained by least-squares fitting two Gaussian functions to the deconvolved profiles using the ELF routines within DIPSO (Howarth et al. 1997). We were able to fit Gaussians to all the spectral profiles with the exception of the second spectrum obtained on the night of Dec. 6/7 which was too poor to allow fitting. The adopted errors were those produced by the ELF routines from the uncertainty in deriving the value of the line centres. Heliocentric corrections were applied to the derived

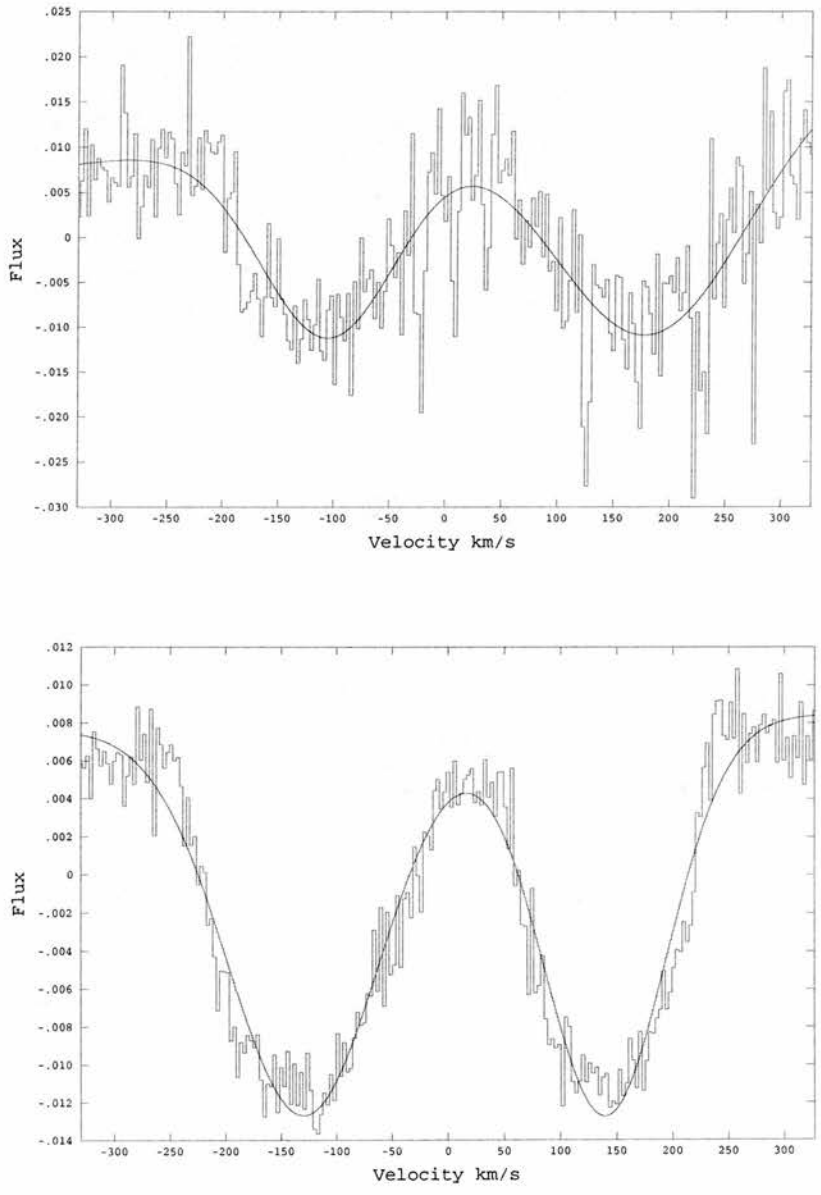

Figure 4.4: Examples of bad and good deconvolved profiles of GSC2807-1423 with the fits from DIPSO.

Table 4.4: Table of heliocentric radial velocities of both components of GSC2807-1423. The quantities marked 'obs' have had heliocentric corrections applied and those marked 'cor' have also had the non-Keplerian corrections (see Section 4.4) applied.

HJD	Phase	V_1 obs	V_1 cor	V_1 err	V_2 obs	V_2 obs	V_2 err
2450000.0+		km s^{-1}	km s^{-1}	km s^{-1}	km s^{-1}	km s^{-1}	km s^{-1}
1154.48341	0.2404	-130.121	-130.81	11.883	167.175	170.73	14.067
1154.49918	0.2638	-121.376	-122.05	4.558	164.251	168.42	11.710
1154.50609	0.2740	-117.808	-118.44	15.883	154.484	158.67	20.245
1154.51298	0.2842	-118.201	-118.78	4.547	144.511	148.47	5.386
1154.52000	0.2946	-113.500	-114.02	5.349	146.699	150.34	6.873
1154.60140	0.4150	-71.583	-71.38	1.883	101.988	96.61	2.206
1155.47924	0.7135	121.353	121.72	1.294	-147.619	-150.45	1.521
1155.51559	0.7678	125.630	126.31	1.588	-153.427	-157.53	1.886
1155.55546	0.8263	119.256	119.75	2.096	-144.655	-146.97	2.548
1155.61129	0.9089	78.662	77.23	5.384	-113.320	-113.53	6.174
1156.42526	0.1129	-78.187	-75.51	1.926	95.191	95.34	2.480
1156.48070	0.1950	-114.621	-115.06	1.237	140.754	142.81	1.788
1156.52561	0.2614	-125.070	-125.75	1.119	154.970	159.09	1.965
1156.58650	0.3515	-106.808	-106.89	1.915	133.720	134.15	2.324

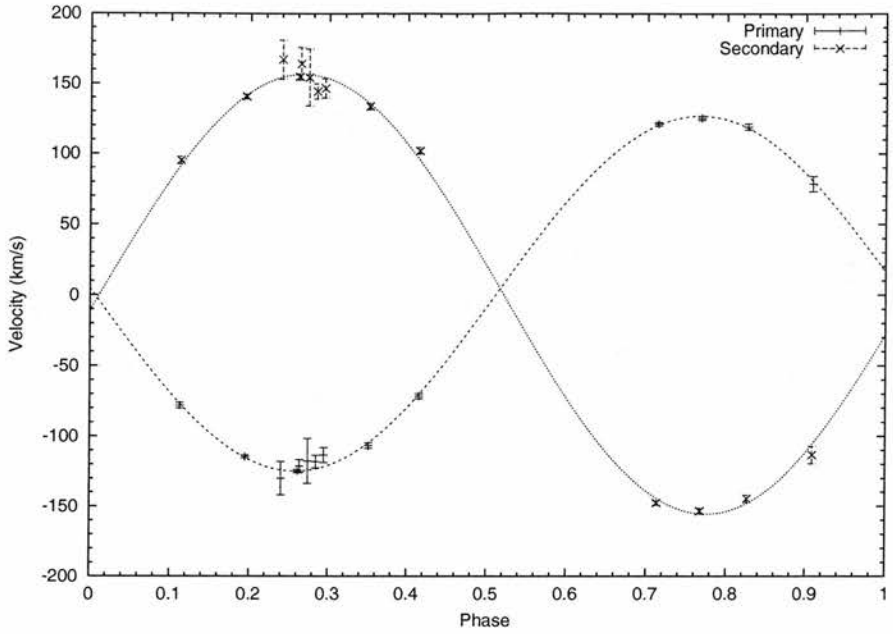

Figure 4.5: Heliocentric radial velocity measurements of GSC2807-1423 plotted against orbital phase, together with the fitted radial velocity curves.

radial velocities and the radial velocities are shown in Table 4.4, together with HJD of observation and orbital phases calculated from the ephemeris above. The data are plotted in Fig. 4.5, along with the results of a sinusoidal fit to each velocity curve. These data are not yet the final values as they need to be have the non-Keplerian corrections applied but this requires a preliminary set of system parameters and so will be discussed in more detail in the next section.

In order to allow a solution to the light curves it is necessary to determine one of the temperatures from a suitable diagnostic such as spectral type or photometric colours. However no previous determination of spectral type is available and our spectra were obtained at high-dispersion in the red. The normal method of obtaining spectral type from line ratios in the blue region of the spectrum (see e.g. Jaschek & Jaschek 1987) is not suitable for these data as the signal is very poor in the blue due to the poor CCD response, the centring of the blaze of the echelle grating around 5000Å and the very poor observing conditions.

Montes & Martin (1998) presented an atlas of high-resolution spectra of F2 V–M8 V stars which were also obtained with the *Utrecht Echelle Spectrograph* and listed several spectral line diagnostics that can be used for spectral and luminosity class typing. Unfortunately the majority of these diagnostics also serve as indicators of chromospheric activity

in magnetically active stars such as GSC2807-1423 so infilling of common diagnostic lines such as the hydrogen Balmer series, the Mg I b lines and the Na I D lines is likely to take place, making them unsuitable for spectral typing.

Robb (1998) did obtain some photometric colour data, but these were taken under non-photometric conditions and our data is purely differential photometry and unsuitable for colour determination. In addition, the presence of cool starspots on the surface will distort the colours of the stars and give an incorrect spectral type. To provide an estimate of the spectral types of the components we deconvolved and measured the equivalent width of the deconvolved profile for a number of template spectra spanning the range F7 V–K0 V. Plotting the equivalent width against spectral type for the standard stars produced a linear relation from which we were able to estimate spectral types of G2.5 V and G5 V ($\pm$0.5 class) for the primary and secondary components. As a further check we also plotted equivalent width against $B - V$ colour for the standard stars and also obtained a linear, although less well-defined, relation. This method gave $B - V = 0.64$ and $B - V = 0.69$ for the two components, corresponding to G3 V and G6 V according to the tables of Gray (1992).

4.4 System parameters

We used the well-known LIGHT2 synthesis code (Hill 1979; Hill & Rucinski 1993) to establish values for the geometrical system parameters, namely the orbital inclination, i, the stellar radii relative to the semi-major axis of the relative orbit r_1, r_2 and the temperature of the secondary star T_2, for a given primary temperature T_1. Since the various methods in the previous section indicated that the primary spectral type was $\sim$ G3 V we used a primary temperature of 5600 K (Gray 1992) as the starting point for the LIGHT2 solutions. The mass ratio was fixed at the value derived from the radial-velocity data.

Since the data were not obtained simultaneously in each filter, we used a least-squares cubic spline code to interpolate the raw V and I data to provide 200 points in each filter at equal intervals in phase.

As can clearly be seen from the light curves the two quadratures differ in brightness by as much as 0.1 mag in V. This effect is also seen in the light curve of Robb (1998) which shows distortions, presumably caused by cool star spots on the surface of one or

both of the components. However Robb (1998) observed that the 2nd quadrature was lower than 1st by roughly the same amount seen here. This is most likely due to a change of active longitude in the system over the $\sim$ 10 month interval, which is discussed in more detail in Section 4.6.

These unequal quadrature heights caused difficulty in producing a set of system parameters that would fit the two quadratures and the eclipse depths. This is due to the assumption of unspotted photospheres used in LIGHT2 when it folds the data around phase 0.5 for the solution. We tried solving 3 sets of data namely:

1. Full set of orbital phases
2. 1st quadrature points removed (phases 0.1–0.4)
3. 1st and 2nd quadrature points removed (phases 0.1–0.4 & 0.6–0.9)

In an attempt to make LIGHT2 fit the higher 2nd quadrature, we removed the points around 1st quadrature to form the second dataset. This produced a semi-detached system with the secondary filling its Roche lobe. We formed the third dataset by removing both quadratures to leave just the primary and secondary eclipses which contain most of the information about the stellar sizes in any event. This also produced a semi-detached system with secondary again filling its Roche lobe as seen from the similarity of the values for r_2/a.

We also carried out a number of trials where we held the inclination fixed and specified a range on the mass ratio, q, of $\pm 3\sigma$. However, due to the lack of total eclipses in this system, there is not enough information in the light curves alone to constrain the mass ratio and these solutions failed to converge. We show these preliminary system parameters along with those of Robb (1998), who carried out a fit to his R band light curve, in Table 4.5.

Close binary systems suffer distortion of the radial velocities from that of a Keplerian orbit. These non-Keplerian corrections include the rotation effect within eclipses (the Rossiter-McLaughlin effect see e.g. Worek 1996) and the changes in velocity caused by the asymmetric geometry and heating effects. The non-Keplerian corrections were calculated using LIGHT2 using the preliminary parameters from the 3rd dataset described above and the corrections are shown in Figure 4.7. The reason for performing the first set of

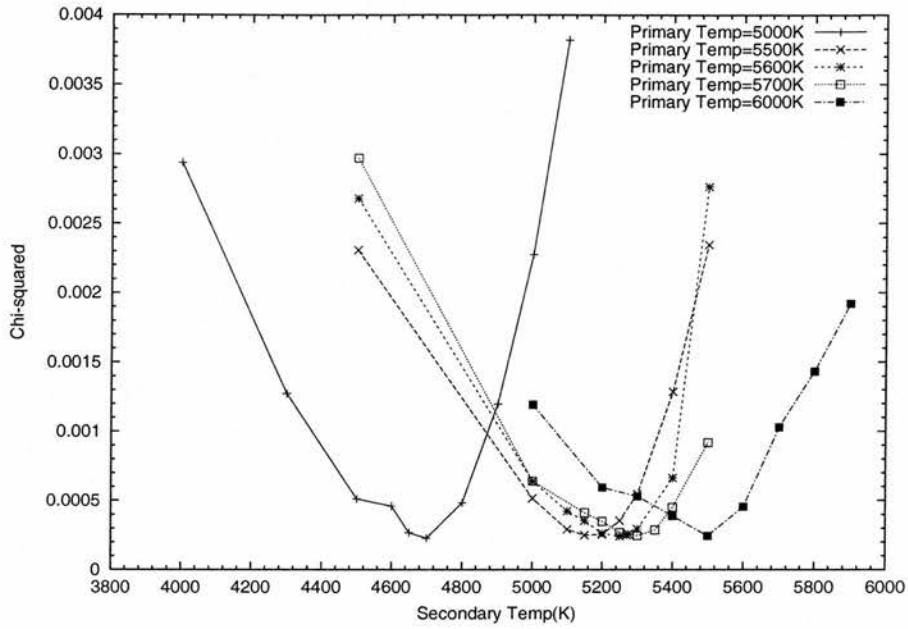

Figure 4.6: Plot of reduced chi-squared against secondary temperature for GSC2807-1423 based on solutions of the third dataset. The three main curves are for primary temperatures in the range 5500–5700 K, while the other two curves illustrate more extreme values of 5000 K and 6000 K.

Table 4.5: Preliminary system parameters for GSC2807-1423.

Parameter	Robb (1998)	LIGHT2 solution (Phases 0.1–0.4 removed)	LIGHT2 solution (Phases 0.1–0.4, 0.6–0.9 removed)
r_1/a (polar)	0.39 ± 0.02	0.3131 ± 0.0034	0.3058 ± 0.0106
r_2/a (polar)	0.37 ± 0.02	0.3341 ± 0.0018	0.3341 ± 0.0034
i	$76\overset{\circ}{.}5 \pm 2°$	$78\overset{\circ}{.}26 \pm 0\overset{\circ}{.}11$	$78\overset{\circ}{.}06 \pm 0\overset{\circ}{.}13$
$q = m_2/m_1$	0.84	0.767 ± 0.015 (fixed)	0.767 ± 0.015
M_1 ($M_\odot$)		0.96 ± 0.03	0.97 ± 0.03
M_2 ($M_\odot$)		0.74 ± 0.02	0.74 ± 0.02
$\langle R_1 \rangle$ ($R_\odot$)		1.26	1.23
$\langle R_2 \rangle$ ($R_\odot$)		1.40	1.40
T_1 (polar)	4775 K	5600 K (fixed)	5600 K (fixed)
T_2 (polar)	4400 K	5250 K	5250 K
Reduced χ^2 of fit	N/A	1.891E-04	2.373E-04

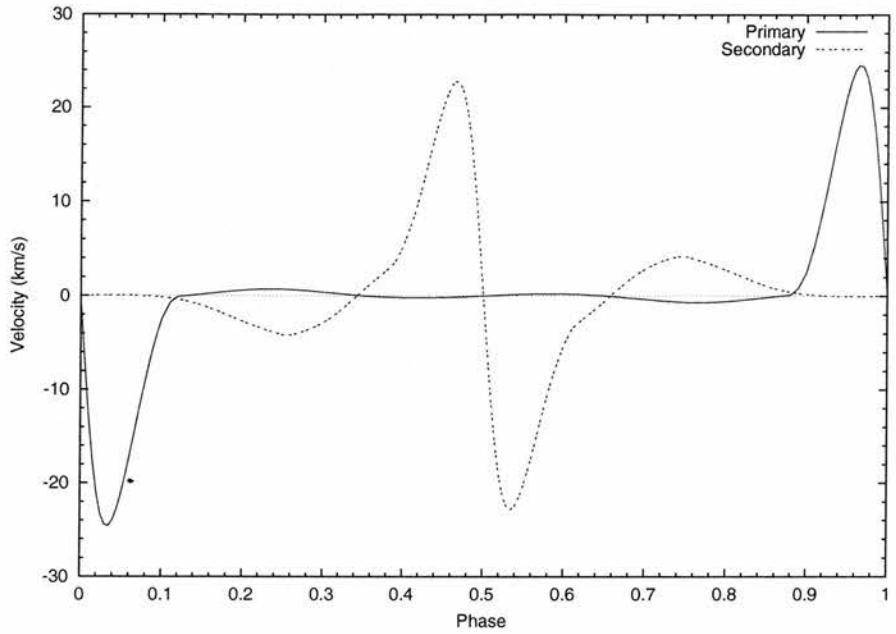

Figure 4.7: Non-Keplerian velocity corrections for both components of GSC2807-1423 plotted against orbital phase.

solutions with LIGHT2 is that the velocity corrections depend on the amount of visible light coming from the binary at each phase, for which the geometric system parameters are obviously required. Although the effect of non-Keplerian rotation does not exceed ~ 5 km s^{-1}, except during eclipses (where there is no radial velocity data anyway), we elected to correct the radial velocities for these effects for the sake of completeness.

We used RVORBIT (Hill 1986) to apply the non-Keplerian corrections to the radial velocities labelled V_1 obs, V_2 obs in Table 4.4 and to solve for a new set of orbital parameters. The corrected radial velocities are also shown in Table 4.4 as V_1 cor, V_2 cor. The orbital parameters changed slightly and the pre- and post-correction parameters are shown in Table 4.6.

With new values for the mass ratio and the velocity semi-amplitudes, we repeated the procedure of deriving system parameters using LIGHT2. The final derived system parameters are shown in Table 4.7 and the light curve fits in Figure 4.8.

The fact that the less massive, lower temperature secondary comes out with a larger radius is puzzling since the mass ratio of 0.751 is much higher than that which is normally seen in semi-detached systems which normally have mass ratios around 0.1–0.3 (see e.g Budding 1986).

Table 4.6: Orbital parameters for GSC2807-1423.

Parameter	Uncorrected	Corrected
Period (days)	0.67601 (*fixed*)	
γ (km s^{-1})	-0.43 ± 2.08	-0.35 ± 1.95
$q = m_1/m_2$	1.303 ± 0.026	1.331 ± 0.025
K_1 (km s^{-1})	123.09 ± 1.63	122.62 ± 1.52
K_2 (km s^{-1})	160.41 ± 2.48	163.17 ± 2.32
$m_1 \sin^3 i$ ($M_\odot$)	0.904 ± 0.024	0.935 ± 0.023
$m_2 \sin^3 i$ ($M_\odot$)	0.694 ± 0.017	0.702 ± 0.016
$a_1 \sin i$ ($R_\odot$)	1.644 ± 0.022	1.638 ± 0.020
$a_2 \sin i$ ($R_\odot$)	2.142 ± 0.033	2.179 ± 0.031
Reduced χ^2 of fit	48.76	42.86

Given the period of the system and the absence of evidence of mass transfer it seems unlikely that this solution is physically realistic. In addition, the spectral types derived from the colours and equivalent widths in Section 4.3 indicated G to early K-type dwarf stars rather than the usual earlier than mid-F type of Algol systems. Another reason why a semi-detached configuration is unlikely to be correct is the mass and luminosity ratios which are much closer to 1 in GSC2807-1423 than is usual for Algol systems.

4.5 Eclipse Mapping with DOTS

Surface images of the binary components were recovered using the DOTS code for Doppler tomography of stellar surfaces (Collier Cameron 1997b). The general operation of this code is identical to that of its predecessor SSSIP (Collier Cameron 1992; Collier Cameron, Jeffery & Unruh 1992; Unruh, Collier Cameron & Cutispoto 1995), in terms of its treatment of the stellar surface as having two distinct temperature components. However DOTS can handle the surface geometry and radial velocity variations of tidally distorted close binary components. Its potential as an eclipse-mapping tool was examined in detail by Collier Cameron (1997b) and is discussed in Section 2.5.

We used DOTS to refine the system parameters generated by LIGHT2 by running a grid of models where we varied $r_1 \times 0.88 \ldots 1.10$ and $r_2 \times 0.94 \ldots 1.10$ in steps of 0.02, for

Table 4.7: Final system parameters for GSC2807-1423.

Parameter	Robb (1998)	LIGHT2 solution (Phases 0.1–0.4 removed)	LIGHT2 solution (Phases 0.1–0.4, 0.6–0.9 removed)
r_1/a (polar)	0.39 ± 0.02	0.3218 ± 0.0053	0.2983 ± 0.0107
r_2/a (polar)	0.37 ± 0.02	0.3311 ± 0.0023	0.3324 ± 0.0035
i	$76\overset{\circ}{.}5 \pm 2°$	$78\overset{\circ}{.}34 \pm 0\overset{\circ}{.}11$	$78\overset{\circ}{.}06 \pm 0\overset{\circ}{.}13$
$q = m_2/m_1$	0.84	0.751 ± 0.014 (fixed)	0.751 ± 0.014
M_1 $(M_\odot)$		1.00 ± 0.03	1.00 ± 0.03
M_2 $(M_\odot)$		0.75 ± 0.02	0.75 ± 0.02
$\langle R_1 \rangle$ $(R_\odot)$		1.31 ± 0.03	1.20 ± 0.04
$\langle R_2 \rangle$ $(R_\odot)$		1.40 ± 0.02	1.41 ± 0.02
T_1 (polar)	4775 K	5600 K (fixed)	5600 K (fixed)
T_2 (polar)	4400 K	5250 K	5250 K
Reduced χ^2 of fit	N/A	1.874E-04	2.413E-04

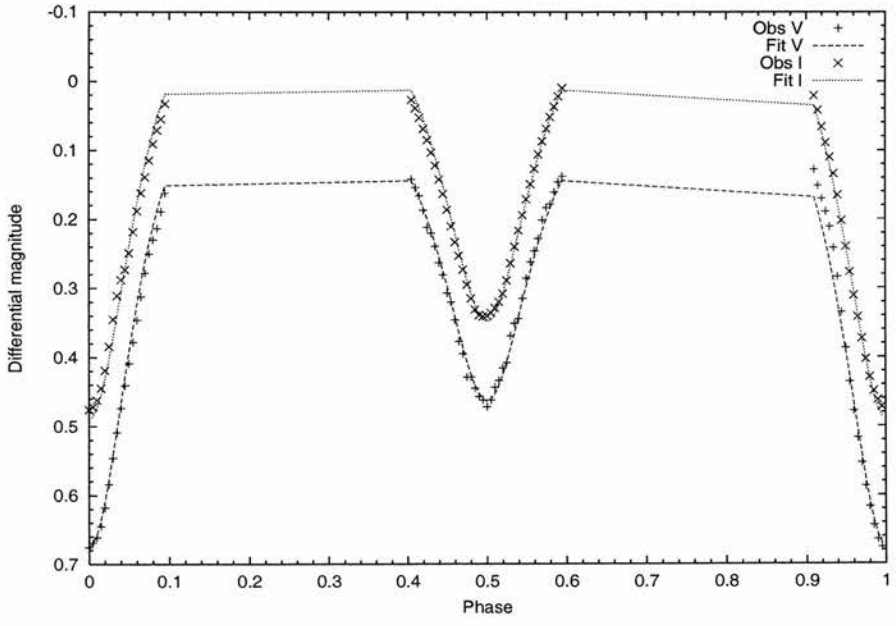

Figure 4.8: V (bottom) and I (top) band light curves for GSC2807-1423 formed from the normal points, along with the LIGHT2 model fits. The I band light curve and fit have been shifted by -0.1 mag for clarity.

Table 4.8: Parameters of the DOTS models for GSC2807-1423.

Model No.	T_1(phot)	T_1(spot)	T_2(phot)	T_2(spot)	Radii
1	5700 K	3750 K	5250 K	3750 K	$r_1 \times 1.0, r_2 \times 1.0$
2	5700 K	3750 K	5250 K	3750 K	$r_1 \times 0.96, r_2 \times 1.0$
3	5700 K	4000 K	5300 K	3600 K	$r_1 \times 1.0, r_2 \times 1.0$
4	5800 K	4100 K	5250 K	3550 K	$r_1 \times 1.0, r_2 \times 1.0$
5	5600 K	3900 K	5400 K	3700 K	$r_1 \times 0.96, r_2 \times 1.0$

a total of 108 models. The second LIGHT2 model with phases 0.1–0.4 and 0.6–0.9 removed was used as the starting point for the parameters (cf. Table 4.7. For each trial, the values of the initial χ^2 produced by DOTS upon loading partly converged stellar images, and the fractional spot area after iterating were recorded. The minimum value on this χ^2 surface was found at $r_1 \times 0.96$, $r_2 \times 1.00$, indicating that the values derived by LIGHT2 are very close to the true values, despite the assumption of unspotted photospheres and the poorer atmospheres used.

Once we had the set of system parameters which gave the best fit we also tried varying the primary and secondary temperatures. As can be seen from Figure 4.6 in the previous section, the temperatures of the two stars are correlated. This is because the quantity that is solved for by LIGHT2 is the light ratio which depends on the ratio of the two temperatures. Although this ratio is well determined by the light curves in two colours, without additional information it is impossible to break the degeneracy. With eclipse mapping the problem is further compounded because we have two further unknowns in the form of the spot temperatures on the two components. In GSC2807-1423 the problem is made worse by the fact that the two stars are very similar in temperature, unlike the situation in other RS CVn systems where the light from the secondary is negligible.

Preliminary investigations indicated that the best fit, in the sense of the lowest obtainable χ^2 after a fixed number of iterations could be found for $T_1 = 5700$ K and $T_2 = 5250$ K. These are also very close to the values derived with LIGHT2 and, as can be seen from Figure 4.6, the curves for $T_1 = 5600$ K and $T_1 = 5700$ K are very similar. Spot temperatures were initially set at 1500 K below the photospheric value for each star.

In order to illustrate the effect of the different temperatures on the spot maps we

constructed 5 sets of models and produced surface maps and synthetic light curves with DOTS. The first pair of models use a absolute value for the spot temperature which is similar to the value found in sunspot umbra and has been used by other investigators for stars of similar photospheric temperature (Barnes et al. 1998). The other three use a fixed temperature difference of 1700 K between the spots and the photosphere, similar to what is observed on the Sun, but with a range of photospheric temperatures. In addition we have performed some reconstructions using the parameters produced by LIGHT2 and some with the primary radius adjusted to match the best value found in the grid search discussed above. The parameters of the models are summarized in Table 4.8.

In an attempt to secure a better fit to the data around 2nd quadrature, we also tried placing hot spots at a variety of temperatures ($T_s = 6500, 7000, 7500, 8000$ K) on the surface of the secondary and keeping the cool spots on the primary. We found that while the hot spots improved the fit slightly around the quadratures, it caused a greater mismatch in the eclipse depths, particularly secondary eclipse. It therefore seems unlikely that active mass-transfer is occuring in this system. This is also supported by the (mostly) undistorted light curve after secondary eclipse compared to that of V361 Lyr (Hilditch et al. 1997) which exhibits strong asymmetries in the light curve and has been shown to have a $T \sim 10000$ K hotspot on the secondary from the impact of the accretion stream.

4.6 Discussion

The fitted light curves produced by DOTS and the Mercator projections of the surface of both components are shown in Figs. 4.9– 4.13. The greyscales for the surface maps have been chosen to allow inter-comparison with other maps of BD+22° 4409 (Chapter 3) and XY UMa (Chapter 5) and the pixel values range from 1.0 (total spot occupancy) to 0.0 (zero spot occupancy) for the primary. For the cooler secondary star, the maps range from 0.5 to 0.0 and the weaker features indicate that, except in extreme cases such as model 5, the majority of the spot activity is confined to the primary. One major feature is that, although the strengths of the spots depend on the particular set of parameters chosen, the locations remain quite constant. This indicates that the eclipse mapping process is being constrained by the data and is not introducing spurious structure.

The primary map only shows evidence for one significant spot at $\sim 270°$ longitude

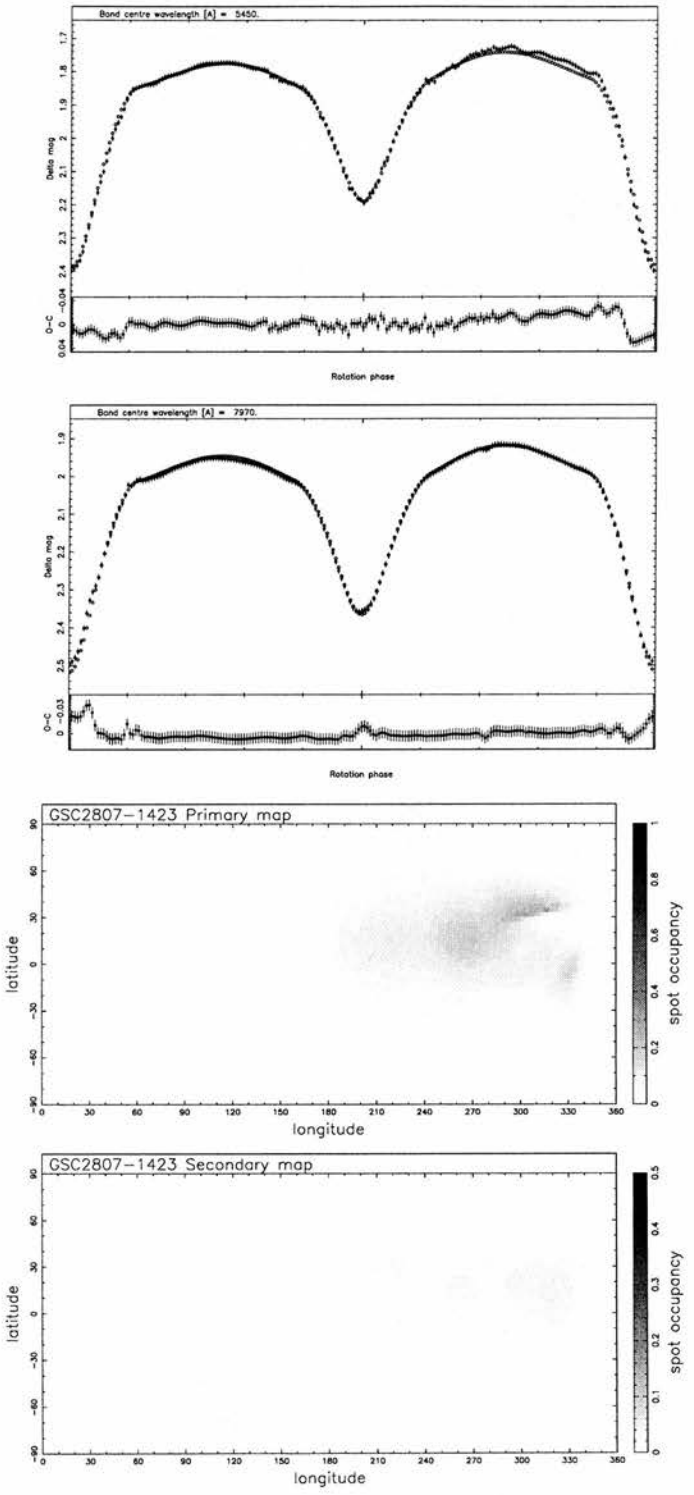

Figure 4.9: Light curves of GSC2807-1423 along with the fit from DOTS using model 1 in (top) V and (bottom) I bands. The bottom two plots are the images of the primary and secondary components of GSC2807-1423. The lower panel of the light curves show the residuals from the computed light curves derived from the reconstructed images.

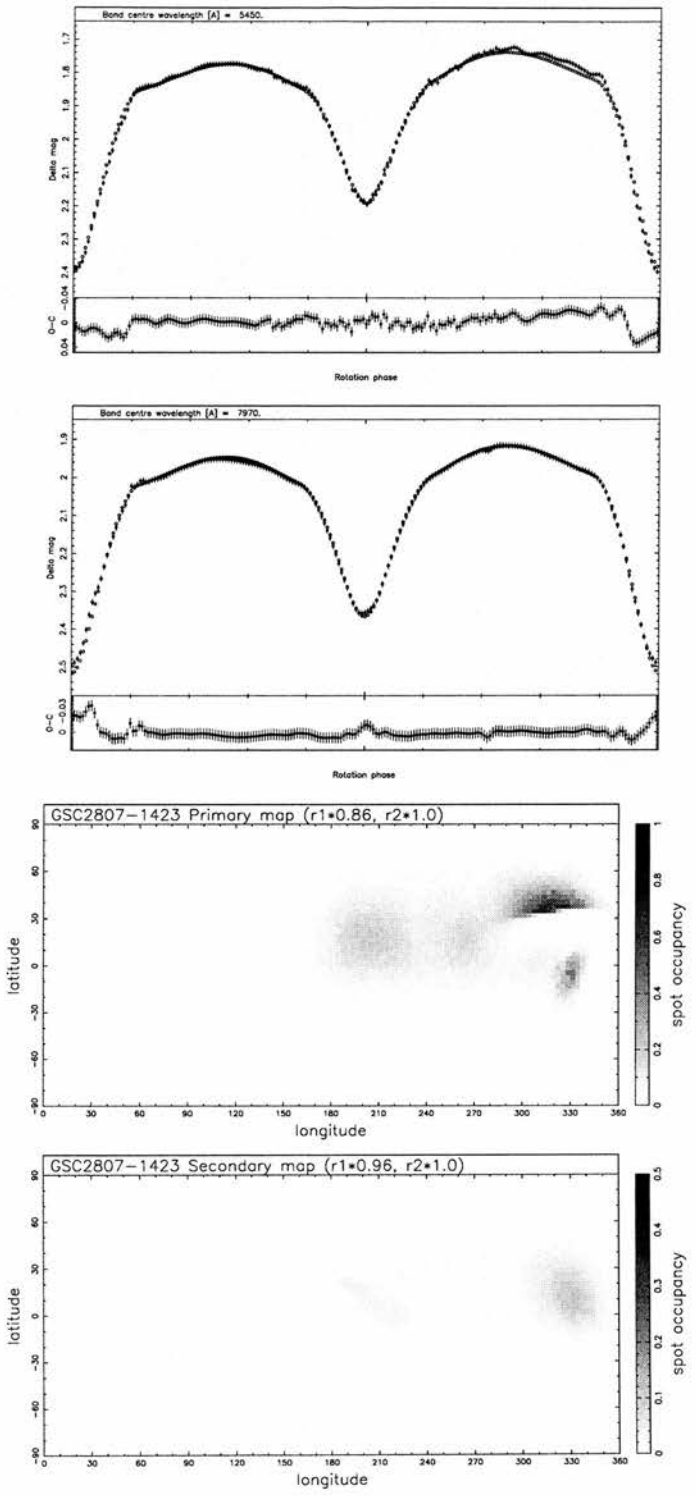

Figure 4.10: Light curves of GSC2807-1423 along with the fit from DOTS using model 2 in (top) V and (bottom) I bands. The bottom two plots are the images of the primary and secondary components of GSC2807-1423. The lower panel of the light curves show the residuals from the computed light curves derived from the reconstructed images.

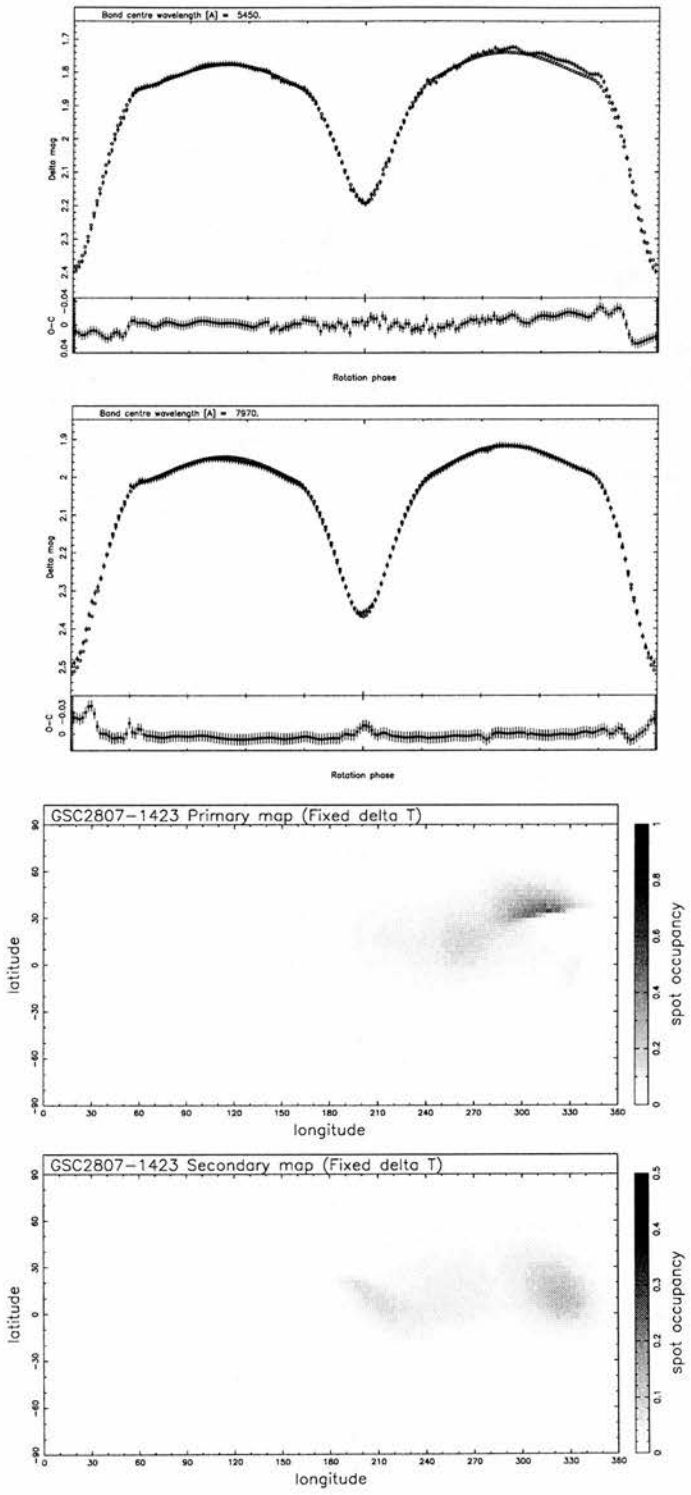

Figure 4.11: Light curves of GSC2807-1423 along with the fit from DOTS using model 3 in (top) V and (bottom) I bands. The bottom two plots are the images of the primary and secondary components of GSC2807-1423. The lower panel of the light curves show the residuals from the computed light curves derived from the reconstructed images.

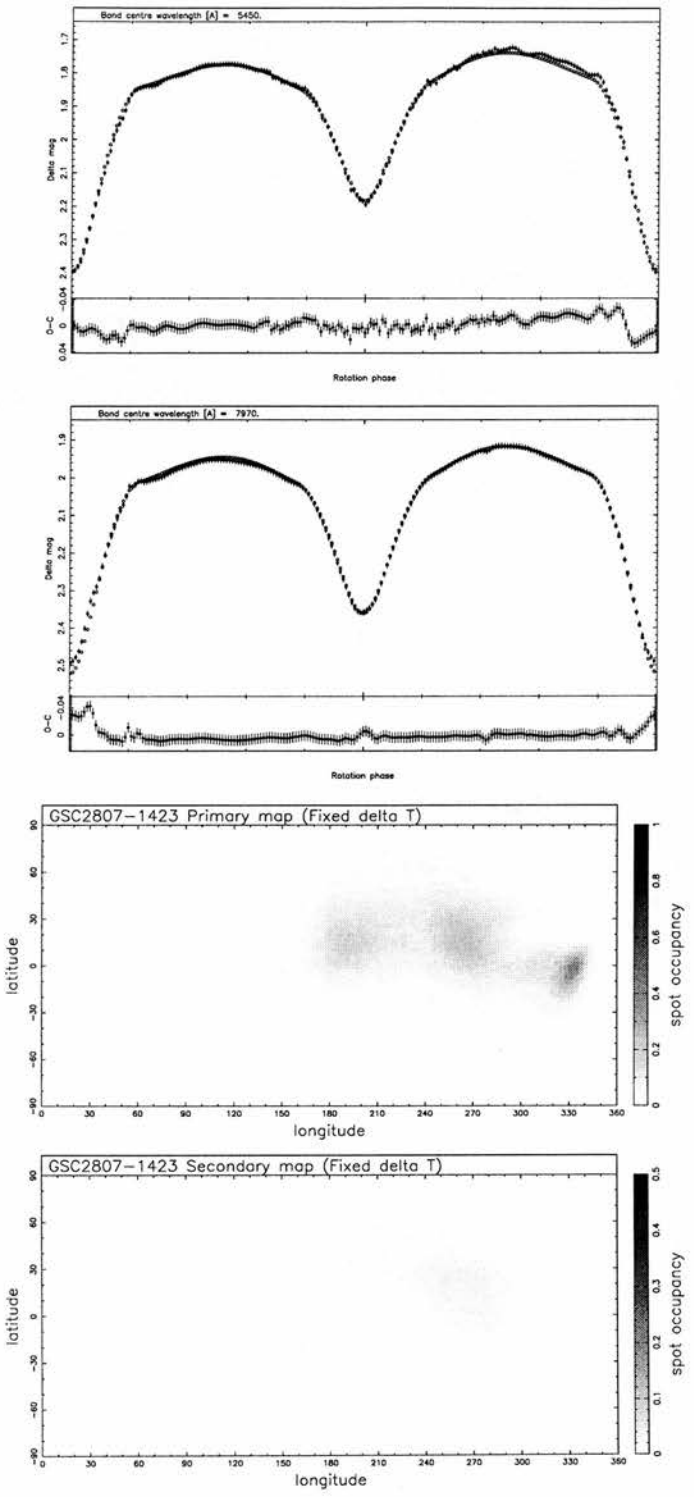

Figure 4.12: Light curves of GSC2807-1423 along with the fit from DOTS using model 4 in (top) V and (bottom) I bands. The bottom two plots are the images of the primary and secondary components of GSC2807-1423. The lower panel of the light curves show the residuals from the computed light curves derived from the reconstructed images.

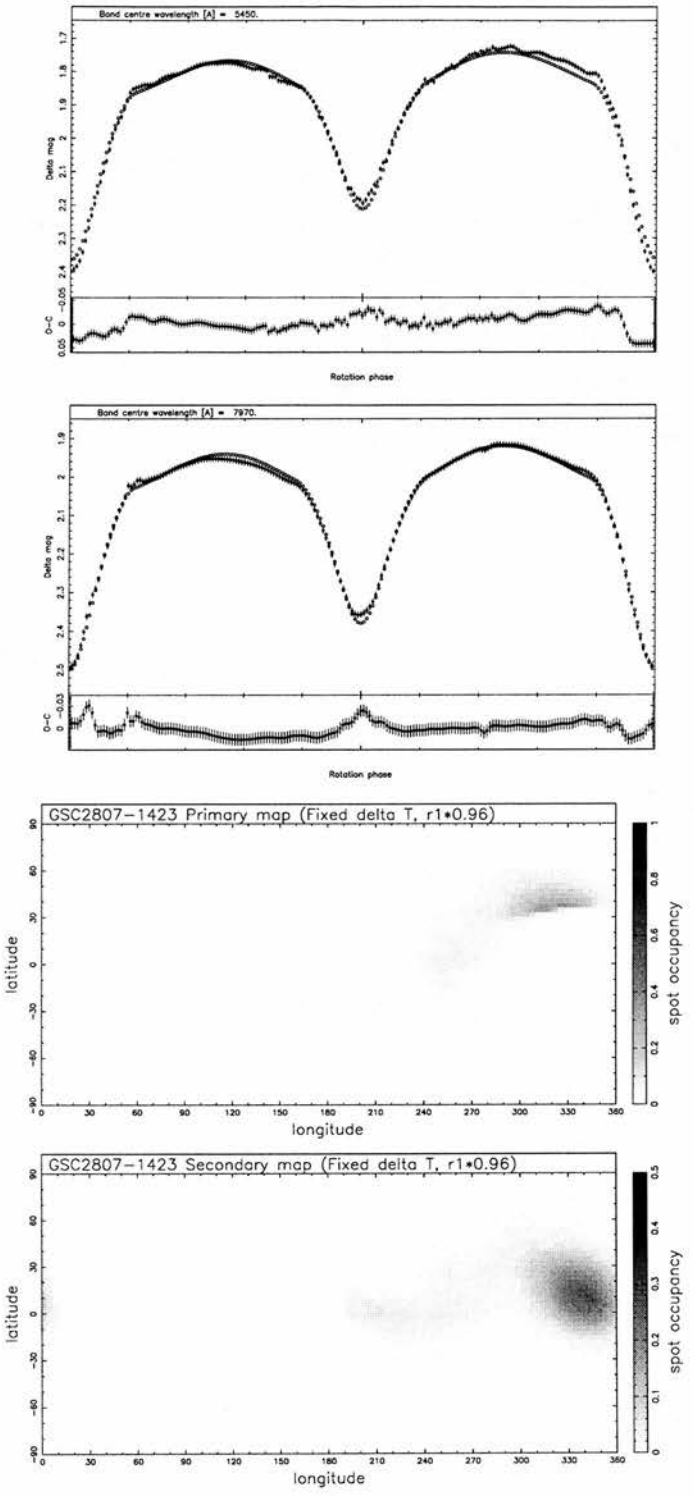

Figure 4.13: Light curves of GSC2807-1423 along with the fit from DOTS using model 5 in (top) V and (bottom) I bands. The bottom two plots are the images of the primary and secondary components of GSC2807-1423. The lower panel of the light curves show the residuals from the computed light curves derived from the reconstructed images.

which is responsible for the asymmetry in the heights of the quadratures and the distortions visible in the light curves (Figs. 4.9–4.13) in the phase range 0.7–0.9. In most cases, the absence of any strong spots around secondary eclipse on either star is evidence that the temperatures of the components are close to the true values and that DOTS is not trying to adjust the lightlevels by the introduction of spurious structure.

The residuals displayed in the lower part of each plot in Figures 4.9–4.13 are mostly flat, indicating a good fit, with the exception of the 2nd quadrature in V. The light curve in V shows more distortion than the I curve that was obtained after it. However both the V and I band light curves were obtained over a continuous run of 4 nights and so it is unlikely that there would have been significant spot re-arrangement in this short time. Further light curves should be obtained in order to confirm the system parameters and results presented here and to investigate the time evolution of spot features.

The fact that the asymmetry in the heights of the quadratures has reversed in the $\sim$ 10 months between our photometric observations and those of Robb (1998) is evidence for spot evolution on this system and also for the swapping of active longitudes seen on XY UMa and other systems (cf. Sections 5.3.2, 5.4.1; Berdyugina & Tuominen 1998).

In order to explain the discrepancy between the primary and secondary radii and masses we searched for evidence of the Li I line at 6708 Å that would indicate a pre-main sequence evolutionary state. This would explain why the lower mass secondary has a larger radius than the more massive primary, if the secondary has not finished its contraction towards the main sequence.

We found no evidence of lithium in these data, but a positive detection of lithium is difficult given the poor quality of these data, and the large amount of broadening caused by the high rotational velocities. Further observations at high resolution and with better S:N would be very valuable in order to confirm or deny a young evolutionary state for this object.

We have added the observed time of minima from Robb (1998) to those in Table 4.2 and computed O-C residuals using the ephemeris determined in Section 4.2.1. The results are given in Table 4.6 and are plotted in Figure 4.14, along with a linear least-squares fit to the data. We also computed a quadratic fit to the data but the result was a very slightly worse fit in terms of the rms of the residuals and the small number of minima

Table 4.9: Published times of primary minimum for GSC2807-1423 and residuals calculated from the ephemeris given in Section 4.2.1.

HJD − 2400000.0	Cycle No.	Computed	O-C residuals(days)	Reference
50784.54340	-491.0	50784.55294	-0.009540	Robb (1998)
51075.57303	-61.5	51075.57524	-0.002215	this work
51094.50169	-33.5	51094.50353	-0.001835	this work
51098.55790	-27.5	51098.55959	-0.001685	this work
51116.47385	0.0	51116.47385	0.000000	this work
51117.48648	1.5	51117.48787	-0.001385	this work
51118.50150	3.0	51118.50188	-0.000380	this work
51119.51476	4.5	51119.51590	-0.001135	this work

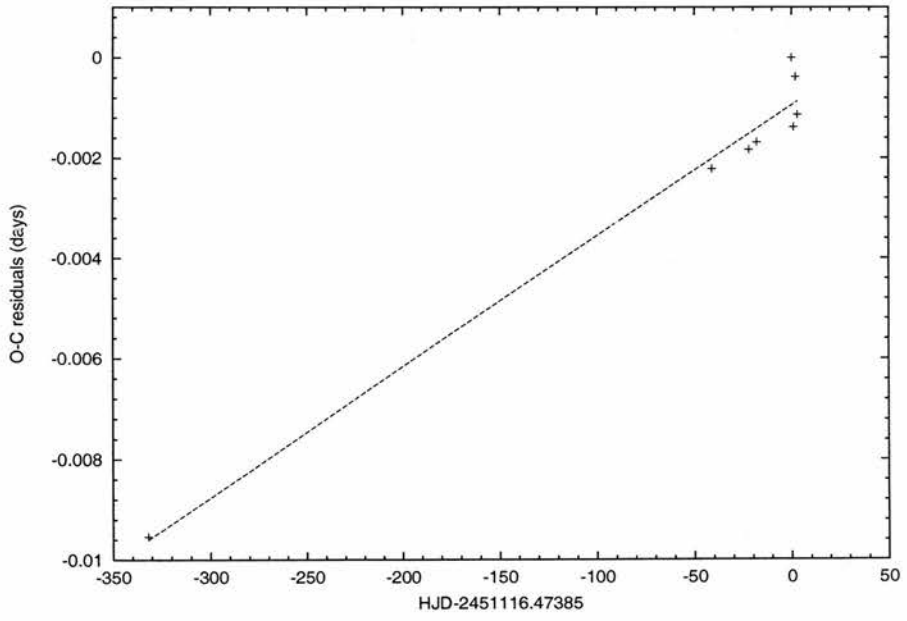

Figure 4.14: O-C residuals diagram for GSC2807-1423. The straight line is a linear fit to the data.

times does not warrant higher terms in a fit.

There is evidence of a period decrease but the derived decrease depends somewhat critically on the data point of Robb (1998) and a discussion of the period evolution of GSC2807-1423 should be postponed until further observations of minima have been obtained and the timebase extended.

4.7 Conclusion

We have obtained the first spectroscopic observations of GSC2807-1423 along with complete V and I band light curves which have enabled us to determine the system parameters of this binary. From the light curves and system maps we find clear evidence for spot activity on the surface of the primary component of the system, probably making GSC2807-1423 the 11th known RS CVn system with period ≤ 1 day.

The system is unusual in that our light curve modelling indicates that the secondary is oversized for its mass. Further photometric and spectroscopic observations are required to determine whether this is a consequence of the highly distorted nature of the light curves and to make a more definite search for the presence of lithium which would indicate a pre-MS evolutionary state for this binary.

Another possibility is a post-mass transfer state which could be more likely, given the short timescales involved during the pre-MS stage. Although there is no evidence in the light curves for the kind of asymmetries produced by the accretion stream that are seen in V361 Lyr, the system could be undergoing more sedate mass transfer. The theory of Thermal Relaxation Oscillations (TRO) (cf. Lucy 1976; Vilhu 1982; Rucinski 1986; Eggleton 1996) which states that close binary systems should oscillate about shallow contact with states of broken contact leading to a semi-detached configuration, is also unable to provide an explanation for what is seen in GSC2807-1423. This is because in all the phases of the theory, it is always the more massive primary star which fills its Roche lobe first irrespective of whether the lower mass secondary subsequently also fills its Roche lobe.

The question of the evolutionary status of GSC2807-1423 cannot be readily answered with the existing data, and determining between the two scenarios of a young, pre-MS

binary which has not completed its contraction or an evolved post-mass transfer system will require further observations.

CHAPTER 5

Starspot distributions on XY UMa in 1997–2000 from eclipse mapping

5.1 Introduction

The short-period eclipsing RS CVn binary XY UMa (=SAO 27143, G2V + K5V, $m_v \sim 10.2$) has been the subject of numerous photometric studies in recent years. Its light curve shows substantial variability in shape and in overall brightness both within and outside eclipse. This variability has normally been attributed to the presence of cool, dark starspots on the G2V primary. The system is a strong X-ray source, as would be expected for a system consisting of a pair of tidally-locked late-type stars in a 0.48-day orbit. Indeed, the mutual eclipses have been used by Bedford et al. (1990) and Jeffries (1998) to study the structures of the two stars' coronae from X-ray data.

To produce the long-term changes in the light curve level and shape that have been observed on this system, Hilditch & Bell (1994) showed that there must be spots at a wide range of latitudes. Single or two spot modelling techniques that have been used in the past to study rotational modulation from photometric data cannot constrain spot locations since either the spot latitude or spot area has to be taken as a free parameter.

Normally only full Doppler imaging from high resolution spectroscopic data can give accurate spot locations. The only exception to this rule is the special case where cool spots are present within the region on the inner face of the hotter star that is occulted by the cooler secondary during the course of primary eclipse. Any spots in this region will give rise to distortions in the primary eclipse profile that should be easily detectable in broad-band optical photometry with high precision and sufficient time resolution.

Although the technique of Doppler imaging has been used for several years, the extension to eclipsing binary systems was first examined by Vincent, Piskunov & Tuominen (1993). They found in particular that information derived from spectral line-profile variations during eclipse can resolve the mirroring of features between hemispheres that causes problems in Doppler imaging of high-inclination objects, and gives better latitude resolution near the stellar equator than normal Doppler imaging. This technique has been employed by Piskunov (1996) to produce temperature maps of the eclipsing RS CVn system ER Vul which show clear evidence of the reflection effect due to mutual heating of the components' inner faces.

It was first noted by Hall (1991a) that photometry of eclipsing spotted stars during secondary eclipse would be a powerful tool for determining spot latitudes. The potential of eclipse-mapping for studying spot locations on eclipsing binaries was examined by Collier Cameron (1997b). Reconstructions of the spot distribution on XY UMa in 1992 and 1995 were presented by Collier Cameron & Hilditch (1997) using the eclipse-mapping method. Further details on the eclipse mapping technique are given in Section 2.5.

We present further observations and surface maps secured in the years 1997–2000. The observations are described in Section 5.2. In Section 5.3.2 we present eclipse maps derived from the narrowband light curves of XY UMa. We discuss possible long-term trends in the system brightness and O-C residuals in Section 5.4.1.

5.2 Observations

The photometric observations of XY UMa were obtained with the 0.9-m James Gregory Telescope (JGT), at the University Observatory, St. Andrews, and a Wright Instruments CCD camera mounted at the Cassegrain focus. More details of the equipment and the photometric reduction procedures employed are given in Section 4.2.1 and in Bell, Hilditch & Edwin (1993). Data were obtained in a narrowband filter of bandwidth 11.3 nm centred on 640 nm in order to reduce the brightness of XY UMa, while still providing data of high S:N. Exposure times varied from 120 s to 45 s, depending on the conditions and the seeing. With the exception of the different filter in use, the observational setup and the reduction of the photometric data was the same as that of Hilditch & Bell (1994) and Collier Cameron & Hilditch (1997). The details of the observations are shown in Table 5.1.

Table 5.1: Journal of observations of XY UMa, 1997–2000. See Section 5.2.1 for details of the ephemerides used.

UT Date	HJD - 2400000.0	No. of obs.	Phase coverage
1997 January 29/30	50478.49 – 50478.79	250	$\overline{0}$.48 – 0.14
1997 January 30/31	50479.26 – 50479.46	150	1.13 – 1.55
1997 February 13/14	50493.38 – 50493.78	287	30.62 – 31.44
1997 February 15/16	50494.60 – 50494.78	146	33.15 – 33.53
1997 Feb. 28/March 1	50508.35 – 50508.60	170	61.86 – 62.37
1997 March 19/20	50527.33 – 50527.53	123	101.49 – 101.91
1997 March 20/21	50528.41 – 50528.68	165	103.74 – 104.31
1998 January 19/20	50833.33 – 50833.80	252	740.32 – 741.30
1998 February 27/28	50872.38 – 50872.76	220	821.84 – 822.65
1998 March 4/5	50877.59 – 50877.76	103	832.72 – 833.08
1998 March 5/6	50878.29 – 50878.39	60	834.18 – 834.39
1998 March 8/9	50881.30 – 50881.60	180	840.46 – 841.11
1998 March 18/19	50891.45 – 50891.60	143	861.67 – 862.17
1999 February 1/2	51211.30 – 51211.69	262	$\overline{0}$.10 – 0.72
1999 February 5/6	51215.31 – 51215.58	150	8.27 – 8.84
2000 January 15/16	51559.33 – 51559.82	349	$\overline{0}$.02 – 1.01
2000 January 16/17	51560.48 – 51560.09	81	2.38 – 2.62
2000 March 17/18	51621.43 – 51621.72	230	129.64 – 130.25
2000 March 22/23	51626.51 – 51626.68	111	140.24 – 140.61
2000 March 24/25	51628.37 – 51628.63	212	144.13 – 144.66

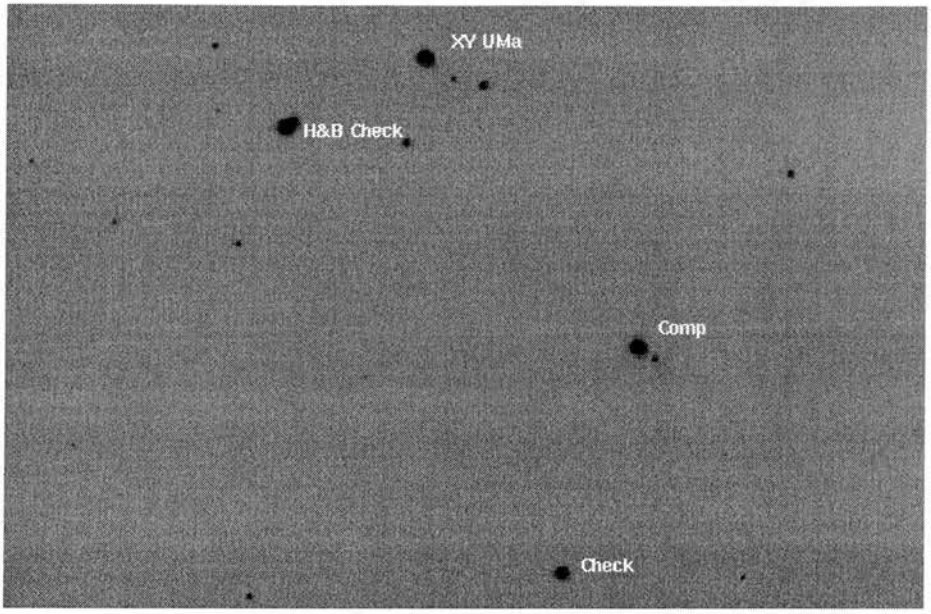

Figure 5.1: Finder chart for XY UMa, showing the comparison (SAO 27139) and check (comparison star for Hilditch & Bell 1994) stars. Also shown is the check star used by Hilditch & Bell (1994) which is actually a blend of two stars.

As can be seen from the light curve given in Hilditch & Bell (1994), where the level of the light-curve around secondary eclipse changed by about 0.01 magnitude between data sets only 10 days apart, data sets more than a week apart were not combined.

Since the original comparison star used by Hilditch & Bell (1994) (star C in their finding chart) was sometimes rather close to the edge of the CCD frame, we used the comparison star of Geyer (1976) (SAO 27139) and relegated the original comparison to use as a check (see the finder chart in Figure 5.1). We found the magnitude difference between these constant comparison stars to be $\Delta V = 1.106 \pm 0.004$ mag for the 4 datasets in 1997, and $\Delta V = 1.109 \pm 0.004$ mag for the 3 in 1998, in most excellent agreement with the values reported by Hilditch & Collier Cameron (1995) and Collier Cameron & Hilditch (1997).

5.2.1 Determination of new ephemerides

The ten light curves are presented in Fig. 5.2, and illustrate the continuing photometric variability of this binary system. The data were originally phased according to the

ephemeris given by Hilditch & Bell (1994):

$$\text{HJD (Min I)} = 2448919.58162 + 0.47899493E.$$

However on phasing these data with this ephemeris we found an obvious phase drift from the first set of data. We determined a new ephemeris using a computer code to perform bisection of the primary eclipse profile. This works by constructing an index table and using this to sort the HJD, magnitude and magnitude errors. The odd and even numbered pairs of values are scanned to find values of the magnitude that are close with HJDs far enough part, so that the pair of points lie on opposite side of the primary eclipse. The midpoint of the pair of dates is computed and several of these are used to compute the time of primary minimum with an estimate of the errors calculated from the scatter of the midpoints, although this error is a overestimate. The method works reliably for these data and should, in theory, work for any primary eclipse profile which is sampled well enough. This method was used for the observations in 1997–98 for deriving the times of primary minima only.

When we modified our code for computing O-C residuals (see Section 5.4.1) to handle seondary minima as well, we changed our method of determining the times of minimum since our bisection code was unable to handle the much shallower secondary eclipses. For these later data we fitted a parabola to the data within ± 0.02 days of an estimated time of minimum. This method of least-squares fitting worked much better for the shallower secondary eclipses and provides an error in the times of minima which more accurately reflects the uncertainty in determining the time of minimum light. We tested the two methods of determining times of minima and found they gave identical times to within the errors ($\sim \pm 0.00050$ using the bisection code and $\sim \pm 0.00010$ for fitted parabolas). The complete list of minima times determined from the 4 years of light curves are given in Table A.1. Typical errors in the primary minima are ± 0.00010 and ± 0.00030 for the secondary minima.

We derived a new of ephemeris from 1997 January data of:

$$\text{HJD (Min I)} = 2450478.71867 + 0.47899493E.$$

The start of each new batch of light curves each year also showed a phase drift and so new ephemerides were determined at the start of the 1999 and 2000 seasons. The data

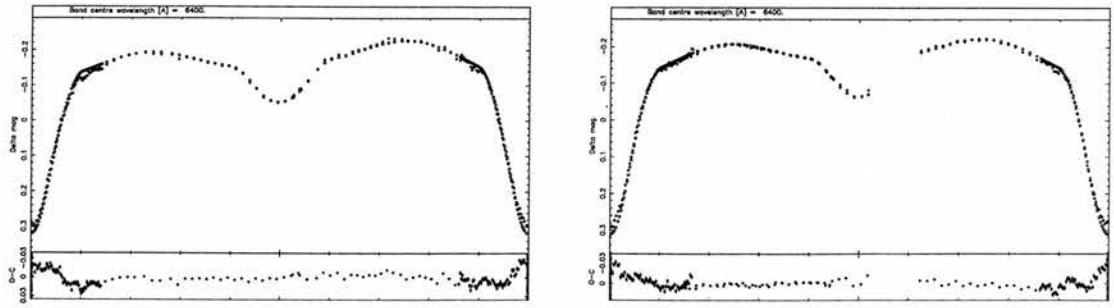

(a) 1997 Jan

(b) 1997 Feb

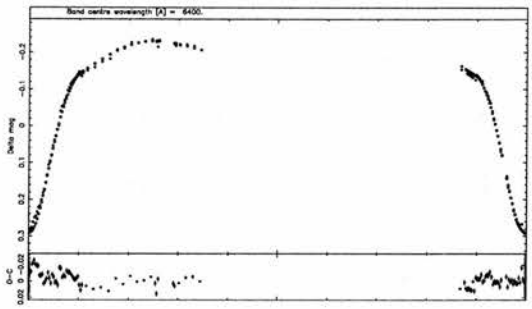

(c) 1997 Feb–Mar

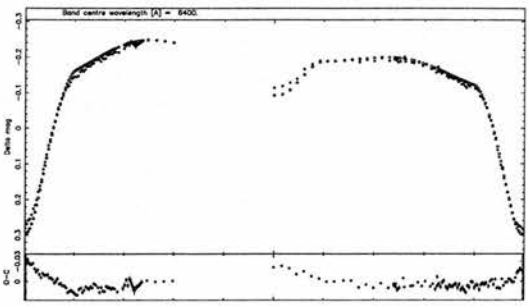

(d) 1997 Mar

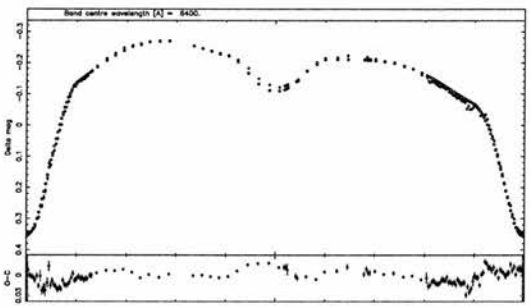

(e) 1998 Jan

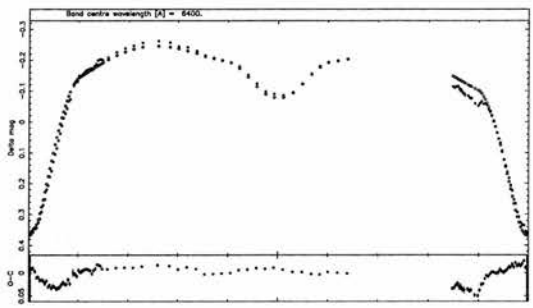

(f) 1998 Feb

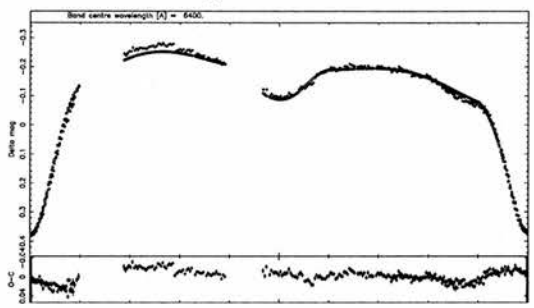

(g) 1998 Mar

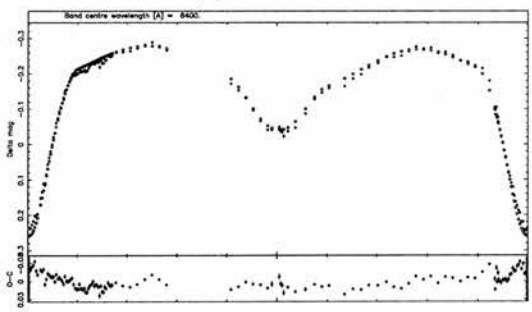

(h) 1999 Feb

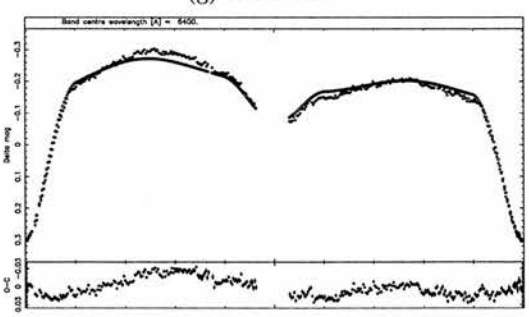

(i) 2000 Jan

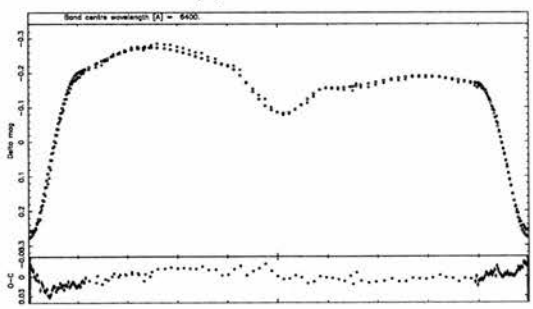

(j) 2000 Mar

Figure 5.2: Light curves of XY UMa secured during 1997–2000. The lower panel shows the residuals from the computed light curves derived from the reconstructed images.

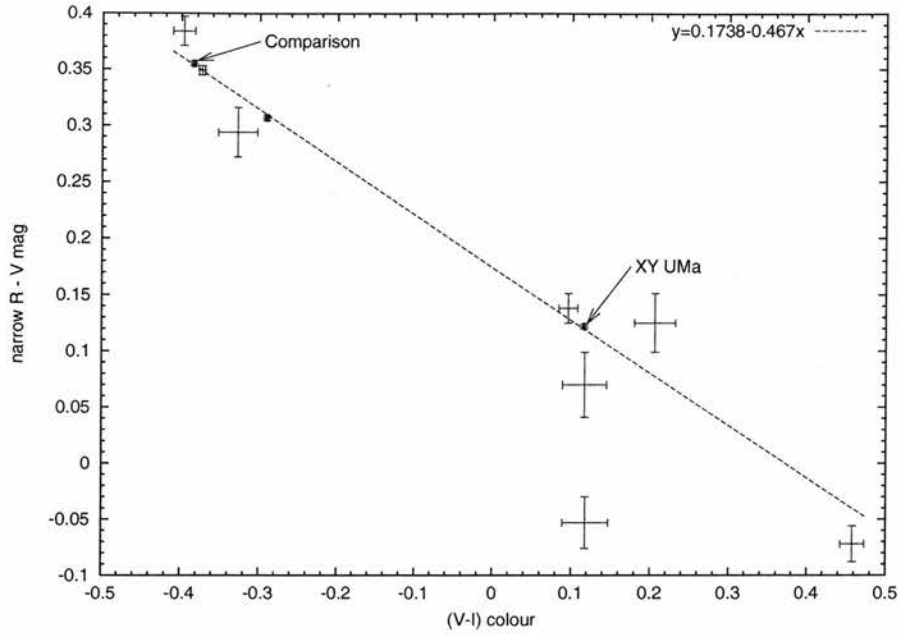

Figure 5.3: Narrowband $R - V$ magnitude against $(V - I)$ colour for the stars in the field of XY UMa. XY UMa and the comparison star (SAO 27139) used in this study are marked.

from 1999 were phased with:

$$\text{HJD (Min I)} = 2451211.34858 + 0.47899493E.$$

and those from 2000 with:

$$\text{HJD (Min I)} = 2451559.33552 + 0.47899493E.$$

During the 1998 March observing run, we also obtained broad band Johnson V and Cousins I images of the XY UMa field, with the aim of determining the colour transformation between the narrowband R filter used for these observations and the Johnson V filter that has been used previously. From stars that were visible in all three filters, we determine the following colour equation:

$$V = \text{narrow } R + 0.467\,(V - I) - 0.1738$$

Using this result along with the relation between XY UMa–SAO 27139 of $(V - I) = 0.116 - (-0.384) = 0.5$ enables us to transform these narrowband R data to Johnson V with reasonable accuracy in order to investigate possible long-term trends in brightness. This topic is discussed in more detail in Section 5.4.1.

Table 5.2: Datasets used for surface reconstructions of XY UMa.

Dataset	No. of obs.	After re-binning
1997 January	390	169
1997 February	428	143
1997 March	168	100
1997 March B	276	155
1998 January	252	134
1998 February	220	112
1998 March	344	340
1999 February	293	132
2000 January	334	332
2000 March	440	156

5.3 Eclipse mapping with DOTS

Surface images of the binary components were recovered using our code for Doppler tomography of stellar surfaces DOTS. The general operation of this code is identical to that of its predecessor SSSIP (Collier Cameron 1992; Collier Cameron, Jeffery & Unruh 1992; Unruh, Collier Cameron & Cutispoto 1995), in terms of its treatment of the stellar surface as having two distinct temperature components. However DOTS can handle the surface geometry, mutual irradiation and radial velocity variations of tidally distorted close binary components. Its potential as an eclipse-mapping tool was examined in detail by Collier Cameron (1997b). We found a problem with DOTS's equal weighting of data points with phase, which stems from its origin as a spectroscopic surface reconstruction package. In eclipse-mapping only the phases around primary eclipse actually carry any useful information about the spot distribution. With large numbers of photometric data points and the short duration of the primary eclipse on XY UMa, the effects of the primary eclipse were being diluted by the large number of points outside the eclipse.

We chose to re-bin the data outside primary eclipse by taking the weighted mean of

5 data points and leaving the data inside primary eclipse untouched. The original number of observations and the number used as input for DOTS are shown in Table 5.2.

We performed tests of the reconstructions with both binned and unbinned data and found no difference in the reconstructed spot distribution. However the memory use of the reconstruction code scales as $\mathcal{O}(n_{vpu} \times n_{vpv} \times n_{phot})$ where n_{vpu} and n_{vpv} are the sizes of the 2D viewplane grid and n_{phot} is the number of photometric data points. The sizes of n_{vpu} and n_{vpv} are set by the need for the grid to be fine enough. This 2D grid relates the stellar intensities at *each observation phase* of the 3D star to the courser output image of DOTS and must be fine enough to ensure that pixelation due to undersampling doesn't occur in the output image. We use relatively high resolution final images, and given the large number of phase points, the memory use approaches several GB. We therefore bin the data in regions of the lightcurve which give the least amount of information to the final image.

5.3.1 System parameters

As with Doppler imaging, the success of the reconstruction depends on the accuracy with which the system parameters are known. Collier Cameron (1997b) found that the details of surface brightness variations in the eclipsed region of the hotter star are recovered consistently by the eclipse-mapping process, provided the mass ratio q, the polar radii r_1 and r_2, the axial inclination i and the unspotted polar temperatures $T_{\rm eff,1}$ and $T_{\rm eff,2}$ are known with reasonable precision. The details of the reconstructed images are not strongly sensitive to small perturbations to the values of these parameters.

For a heavily spotted system such as XY UMa, the very process of determining the system parameters is complicated to a certain extent by the systematic errors introduced by the variable light curve distortion. Hilditch & Bell (1994), however, took careful account of these effects in determining the parameter set that was subsequently used by Collier Cameron (1997b) to explore the effects of errors in the system parameters on the reconstructed image.

Collier Cameron & Hilditch (1997) carried out an investigation of the system parameters of XY UMa using grids of models and varying the secondary temperature, secondary radius and the inclination, with the parameters of Hilditch & Bell (1994) as a starting

Table 5.3: System parameters for XY UMa.

Parameter	Hilditch & Bell (1994)	Collier Cameron & Hilditch (1997)
r_1/a (polar)	0.363 ± 0.002	0.363 ± 0.002 (unchanged)
r_2/a (polar)	0.211 ± 0.002	0.216 ± 0.002
i	$82\overset{\circ}{.}0 \pm 0.3$	$81\overset{\circ}{.}0$
m_2/m_1	0.60 (fixed)	0.60 (fixed)
T_1 (polar)	5780 K	5780 K
T_2 (polar)	4100 K	3850 K

point. The optimal set of parameters were found by minimising the spot area reported by DOTS. The two sets of system parameters are shown in Table 5.3. Since the parameters of Collier Cameron & Hilditch (1997) have been obtained through use of DOTS, we used these for our reconstructions. The spot temperatures were set at 1500 K below $T_{\rm eff,1}$ for the primary component (in analogy with the solar case) and at 3500 K for the secondary component. The issue of spot temperature for the secondary is much less critical since it contributes a very small fraction of the total light of the system.

The use of DOTS, which does take into account the spot effects, to refine the system parameters produced by a traditional light curve solver such as LIGHT2 (Hill 1979; Hill & Rucinski 1993) which does not include spot effects, can lead to more reliable parameters for active systems. A possible refinement of this two-step process would be to adopt the technique used by Hendry & Mochnacki (2000) in their surface mapping of VW Cep and incorporate the determination of the binary system parameters as additional pixels to be solved for, along with the spot distribution.

5.3.2 Eclipse maps of XY UMa

The images show the continued evolution in the surface spot distribution on XY UMa which is hinted at by the changing shape of the light curves. In particular the second, third and fourth surface maps taken in 1997 with gaps of $\sim$ 2 weeks between each map show a fair amount of evolution between each map. This change in the active regions is taking place on timescales of about a week and possibly as short as a few days. The

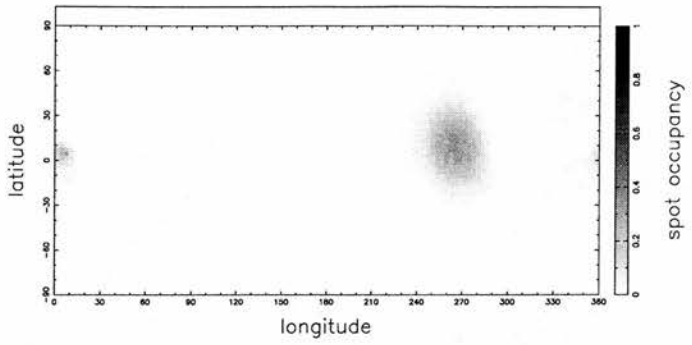

(a) 1997 Jan

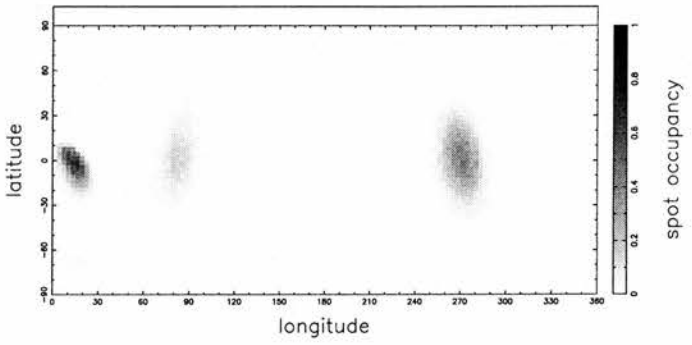

(b) 1997 Feb

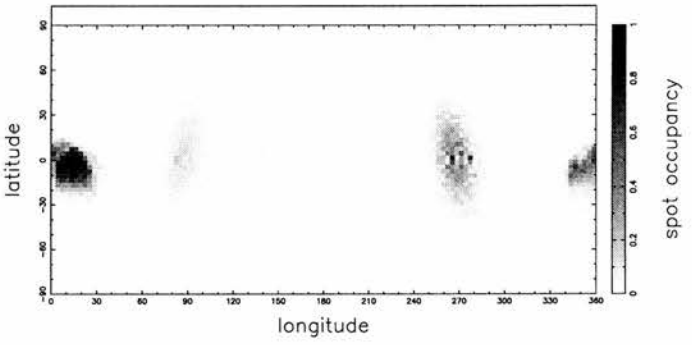

(c) 1997 Feb–Mar

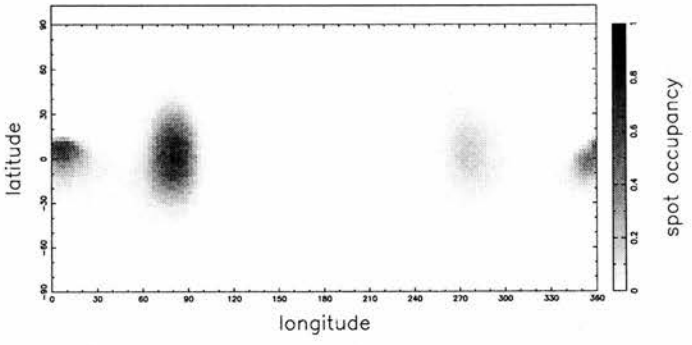

(d) 1997 Mar

Figure 5.4: Images of the XY UMa primary reconstructed from the light curves secured on (a) 1997 Jan 29 – 31; (b) 1997 Feb 13 – 16; (c) 1997 Feb 28 – Mar 1; (d) 1997 Mar 19 – 20;

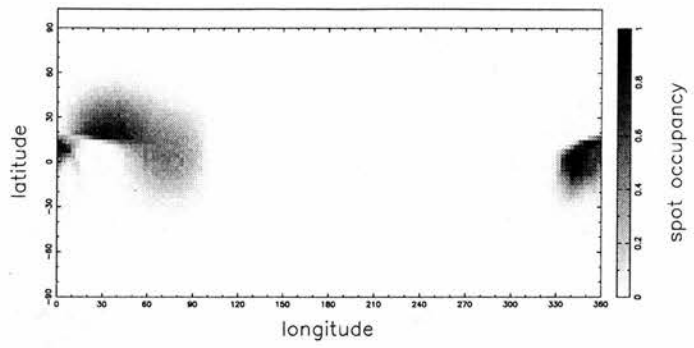

(e) 1998 Jan

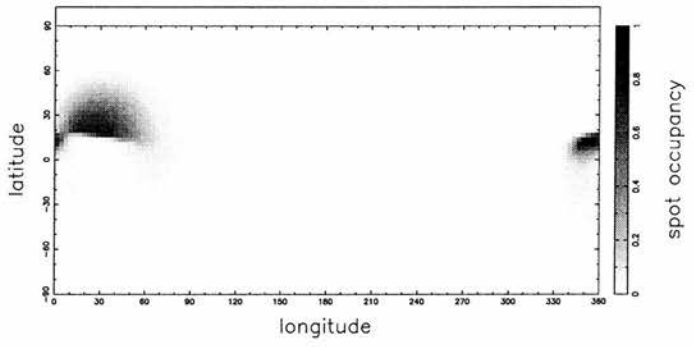

(f) 1998 Feb

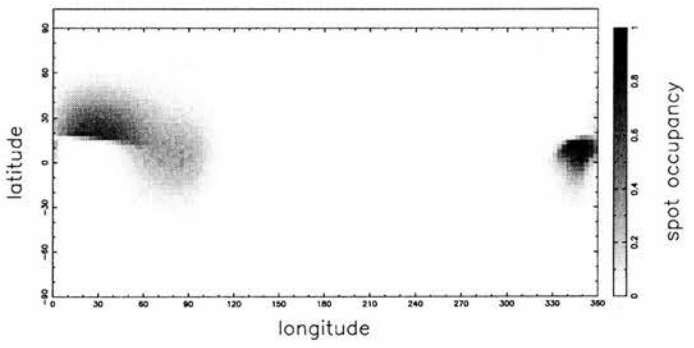

(g) 1998 Mar

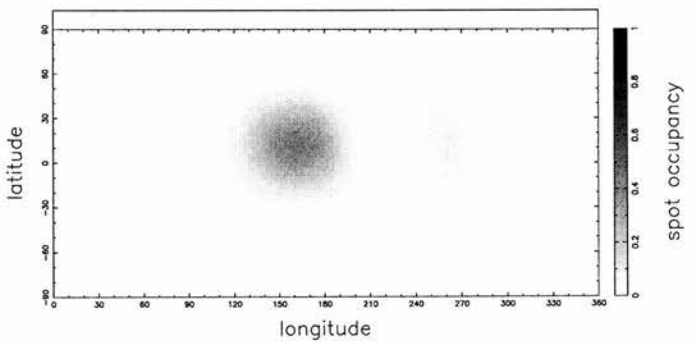

(h) 1999 Feb

Figure 5.4: (continued) (e) 1998 Jan 19 – 20; (f) 1998 Feb 27 – 28; (g) 1998 Mar 4 – 9; (h) 1999 Feb 1 – 6;

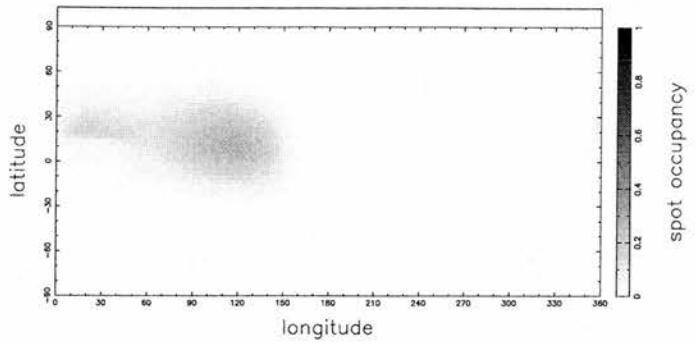

(i) 2000 Jan

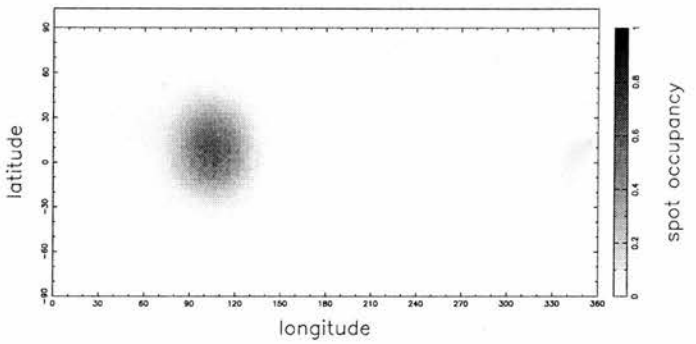

(j) 2000 Mar

Figure 5.4: (continued) (i) 2000 Jan 15 – 17; (j) 2000 Mar 17 – 25.

spots in the uneclipsed region of the primary are smeared in latitude as the photometric information alone is insufficient to constrain their precise locations.

All of the images obtained in 1997 and 1998 show much less spot coverage than the images presented by Collier Cameron & Hilditch (1997) from data obtained in 1992 and 1995. The images obtained in 1997 show spots confined to the eclipsed region of the primary at almost mid-eclipse and to two active longitude zones at $\sim 90°$ and $\sim 270°$ longitude. These two longitude zones show continued evolution through all the 1997 images with the region at 90° growing in strength from 1997 January up to the last map in 1997 March 19/20. The region at 270° declines in strength over the four maps in 1997 to a small compact spot with low filling factor in the 1997 late March image. The large broken-up nature of this spot group in 1997 March (Fig. 5.4(c)) is due to the incompleteness of that light curve around 2nd quadrature and the start of primary eclipse. As discussed by Collier Cameron & Hilditch (1997) and Collier Cameron (1997b) this illustrates the need for good phase coverage, especially around primary eclipse, for the success of the reconstruction process.

The area around 340° – 20° longitude, which is well observed in all the light curves,

shows a spot at or near the sub-stellar point on the primary star which grows in strength up to a maximum around 1998 January. In the 1998 February and 1998 March maps this has begun to decline again, but is still at a stronger level than seen in the 1997 maps. The 1998 maps show the existence of a large dark spot near the eclipsed region but above the stellar equator, covering the latitude range $\sim 30^\circ - 60^\circ$. This spot group appears to have merged with the persistent group at 90° in the 1998 January and 1998 March maps, although this could be due to a lack of resolution in our surface maps. In the later maps obtained in 1999 and 2000 this spot seems to have disappeared again, although there is a hint in the 2000 January map.

The active longitude region at $\sim 270^\circ$ longitude seems to have decreased in strength throughout the time of observations from its initial strong level in 1997 January. This decline is confirmed by the lightcurves around 1st quadrature which gradually become less depressed and distorted during the 3 year of maps indicating a return to predominately unspotted photosphere on the part of the star. The reason for this decline in activity in this longitude region which was a feature of all the 1997 maps is unclear, although it may be linked with the possible changes in the course of a magnetic cycle which is discussed in the next section.

The growth and the decline of the active regions at different longitudes over the 4 years of the surface maps is illustrated in Figure 5.5. This plot is obtained by collapsing each surface map in latitude and converting the pixel grid to longitude. The active region at longitude 270° is seen to increase in strength until the 1997 March B dataset and then activity switches to the longitudes 50°–100° with a lot of activity around the sub-stellar point in 1998. In the two images obtained in 2000, the activity in the sub-stellar point declines and in the final map in 2000 March the spots are concentrated around longitude 90°–100°. The situation is quite complicated and it is not simply the case of one fixed longitude or another dominating and more maps will be needed in the coming years to fully resolve the picture.

The possible existence of a "flip-flop" mechanism of active longitudes, as seen on other RS CVn stars, is given more support by the growth of activity around $\sim 90^\circ$ longitude and the increasing distortion of the light curve around 2nd quadrature seen in 1997 February to 1998 March and again in the maps obtained in 2000. There is some evidence for an activity minimum at some point in 1999 from the undistorted light curve and sur-

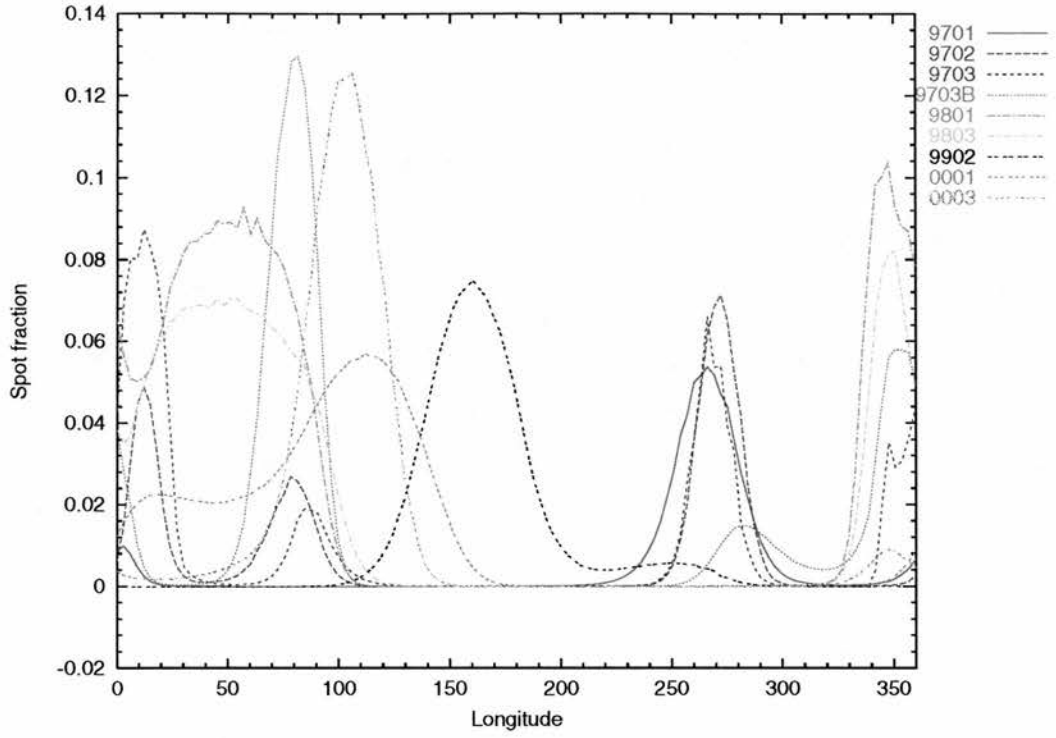

Figure 5.5: The evolution of the spot features on XY UMa over time as a function of longitude.

face map obtained during that year. As discussed further in Section 5.4.1, XY UMa was at its brightest level for many years during 1999 and the surface map for this year (Figure 5.4(h)) shows only a diffuse spot of low filling factor around secondary eclipse which could indicate a slight discrepancy in the secondary temperature and the absence of any substantial spot activity.

5.4 Discussion

5.4.1 Long-term trends

XY UMa has been observed by several investigators since its discovery in 1955. Studies of O-C diagrams have been performed several authors including Pojmanski & Geyer (1990), Erdem & Güdür (1998) and Chochol et al. (1998). In order to search for any long-term trends in the system such as could be caused by the effects of spots, we have searched the literature for photometric observations of XY UMa which include times of primary or secondary eclipse. Only those observations that were obtained by photoelectric or

electronic methods were used; visual and photographic observations were discarded. The ephemeris of Hilditch & Bell (1994) was used as the reference ephemeris and times of minimum and O-C residuals were computed relative to this. A circular orbit was assumed so that secondary eclipses occur at phase 0.5. This is reasonable as the published velocity curves (Rainger, Hilditch & Edwin 1991; Arévalo & Lázaro 1999) show no evidence for any orbital eccentricity. The times of minimum and the O-C residuals are shown in Table A.1.

As can be seen from the plot in Fig. 5.6, there seems to be some evidence of a periodicity in the timing information, although the sampling is far from ideal. The recent peak corresponds to the second 1997 March dataset and the four times of primary in 1998 have shown a decrease in the residuals, although this is difficult to see in Fig. 5.6 due to the long timebase of observations. It is possible that this peak in O-C residuals corresponds to the prediction of Hilditch & Collier Cameron (1995) that XY UMa should be entering a phase of greater magnetic activity. This seems to be supported by the surface reconstructions which indicate a greater amount of spot activity on the primary in 1998, compared to 1997.

We have seperated the times of primary and secondary minima in Fig. 5.6, in order to investigate the possibility of spots distorting the times of minima. If spots were causing distortion of the minima times we would expect to see opposite effects for primary and secondary minima, since the spot would be on the opposite limb of the primary component in the two cases. As can be seen from the figure, this is not the case and both primary and secondary minima lie along the same trends which makes this scenario an unlikely cause of the O-C variations.

An alternative explanation is that the periodicity is caused by a unseen third body, with an orbital period equal to the ~25 year period seen in Fig. 5.6. Using period-finding code written by the author we obtain a peak in the Lomb-Scargle statistic at a period of 9699.6±1765 days. From this and the maximum deviation in the the O-C diagram of $\simeq$ 0.015 days, we obtain a minimum mass for the third body of 0.17 $M_{\odot}$ and a radial velocity variation of $\Delta v = 2.89$ km s^{-1} in the centre of mass of the close binary. This assumes a total mass of the close binary of 1.0+0.6 $M_{\odot}$ from the G2V spectral type of the primary and the mass ratio given in Table 5.3. This third body mass translates to a spectral class of about M6 with $M_V \sim 13.5$ (Lang 1992). At the distance of XY UMa ($\sim$ 120 pc) it is highly unlikely that this third component would be detectable in the spectra, but

the change in radial velocity of the close pair may be observable with sufficient spectral resolution and spectrograph stability.

Table 5.4: Differential V magnitudes (XY UMa – SAO 27139) at four orbital phases.

Date (yr)	Pri. Min V	Max 1 V	Sec. Min V	Max 2 V	Reference
1955.30	0.58	0.05	0.30	0.13	Lee (1985)
1958.20	0.75	0.27	0.49	0.28	Lee (1985)
1959.10	0.73	0.23	0.48	0.27	Lee (1985)
1961.20	0.85	0.19	0.48	0.46	Lee (1985)
1968.10	0.62	0.18	0.31	0.15	Lee (1985)
1976.10	0.62	0.19	0.20	0.10	Geyer (1980)
1976.20	0.76	0.12	0.30	0.10	Geyer (1980)
1977.10	0.68	0.02	0.32	0.15	Geyer (1980)
1977.96	0.73	0.22	0.36	0.18	Geyer (1980)
1979.02	0.75	0.20	0.42	0.28	Geyer (1980)
1979.25	0.73	0.28	0.51	0.27	Jassur (1986)
1982.10	0.41	-0.05	0.13	-0.06	Zeilik et al. (1983)
1986.20	0.38	-0.15	0.00	-0.27	Bedford et al. (1990)
1986.20	0.38	-0.05	0.00	-0.17	Bedford et al. (1990)
1987.20	0.55	0.00	0.20	0.00	Heckert & Zeilik (1988)
1988.25	0.48	-0.07	0.17	-0.07	Zeilik et al. (1988a)
1989.20	0.42	-0.12	0.00	-0.12	Li, Zhang & Zhang (1989)
1989.30	0.45	-0.12	0.00	-0.10	Li, Zhang & Zhang (1989)
1989.25	0.58	0.00	0.13	0.00	Lee (1993)
1990.25	0.38	-0.13	0.05	-0.13	Zeilik et al. (1990b)
1992.80	0.49	-0.09	0.01	-0.04	Hilditch & Bell (1994)
1993.17	0.39	-0.22	-0.04	-0.21	Jeffries et al. (1995)
1995.22	0.34	-0.08	0.11	-0.16	Jeffries et al. (1995)
1995.85	0.43	-0.07	0.19	-0.01	Cameron & Hilditch (1997)
1997.08	0.35	-0.13	0.00	-0.17	this work
1997.12	0.35	-0.15	0.00	-0.16	this work

continued on next page

continued from previous page

Date (yr)	Pri. Min V	Max 1 V	Sec. Min V	Max 2 V	Reference
1997.21	0.34	-0.19	-0.06	-0.13	this work
1998.05	0.40	-0.21	-0.06	-0.14	this work
1998.18	0.44	-0.22	-0.04	-0.13	this work
1999.09	0.30	-0.23	0.03	-0.20	this work
2000.04	0.35	-0.24	-0.02	-0.14	this work
2000.22	0.32	-0.22	-0.03	-0.12	this work

Hilditch & Collier Cameron (1995) tabulated differential B and V (in the sense XY UMa - SAO 27139) magnitudes at four orbital phases from lightcurves in the literature which are sufficiently complete stretching back to 1976. The four orbital phases selected were mid-primary eclipse, maximum brightness between phases 0.0 and 0.5, mid-secondary eclipse, and maximum brightness between phases 0.5 and 0.0. We have repeated this in Table 5.4 for the V data only and have corrected the values tabulated by Hilditch & Collier Cameron (1995) for printing errors in the original work of Geyer (1980), as pointed out by Chochol et al. (1998).

To these values we have added seven sets of data points from the literature, two sets from V data obtained at St. Andrews in 1995 and an additional seven from the narrow-band R data obtained in 1997–2000, and the results are shown in Fig. 5.7. As can be seen the brightness at all four of the phase points increases from the late 1970s through to the late 1990s, and perhaps has started to decrease again by 1999–2000. If this very recent fading is due to an increase in the amount of spot coverage, then this provides further evidence for an increase in magnetic activity on the primary, possibly heralding the start of a new magnetic cycle. In addition, the fact that the primary minimum ΔV tracks the changes in ΔV (Max 1) and ΔV (Max 2) indicates that there is uniform spot coverage at all latitudes, as suggested by Hilditch & Bell (1994).

Additional evidence of a possible link between the orbital period variations and the overall light level can be seen in Figs. 5.6 and 5.7, especially 1979–80. Here a peak in the O-C residuals corresponds quite well to the system being faint at all 4 phase points. There is also weaker evidence for a correspondances in 1993 and 1968–69 between a minimum in

the O-C residuals and a local maximum in the system brightness, although the sampling of the O-C curve in the latter case at this point is somewhat sparse. Continued monitoring of the system in the coming years is essential to firm up this link between the O-C variations and the overall light level of the system.

5.5 Conclusions

We have used eclipse-mapping technique based on the maximum entropy method to recover images of the visual surface brightness distribution on the primary component of the eclipsing binary XY UMa.

The reconstructed images show the presence of time-variable starspot activity in the eclipsed region of the primary. In particular, the results indicate that eclipse mapping can give better definition of low-latitude features than is possible with conventional spectroscopic Doppler imaging techniques, which tend to have poor latitude resolution in the equatorial regions of the star. The images obtained in 1997 and 1998 show significant differences, with a greater spot coverage on the primary in 1998. In 1997 the bulk of the activity was confined to near the sub-stellar point and two active longitude zones at $\sim 90^\circ$ and $\sim 270^\circ$ longitude. In contrast, the 1998 images showed no activity at $\sim 270^\circ$ longitude and a large spot spanning 30° in latitude appeared above the stellar equator at longitude $\sim 35^\circ$.

In 1999 there is some evidence for a activity minimum with an undistorted light curve and only a diffuse, low filling factor spot in the surface map. Unfortunately the year was marred by generally poor weather conditions and no other lightcurves of sufficient phase coverage were obtained without unacceptably large gaps between the individual nights. During 2000 the activity picked up again with an increasingly large distortion around 2nd quadrature visible in the light curves and a growth in the corresponding spot at $\sim 90^\circ$ longitude.

There is some evidence from the spot maps and the historical differential magnitudes that XY UMa reached a peak brightness (corresponding to a minimum amount of spots) at sometime in 1999 and magnetic activity seems to be increasing again. Further observations in the coming years will help confirm whether this is the start of another magnetic cycle. There is also marginal evidence from the O C residuals that a peak was reached around

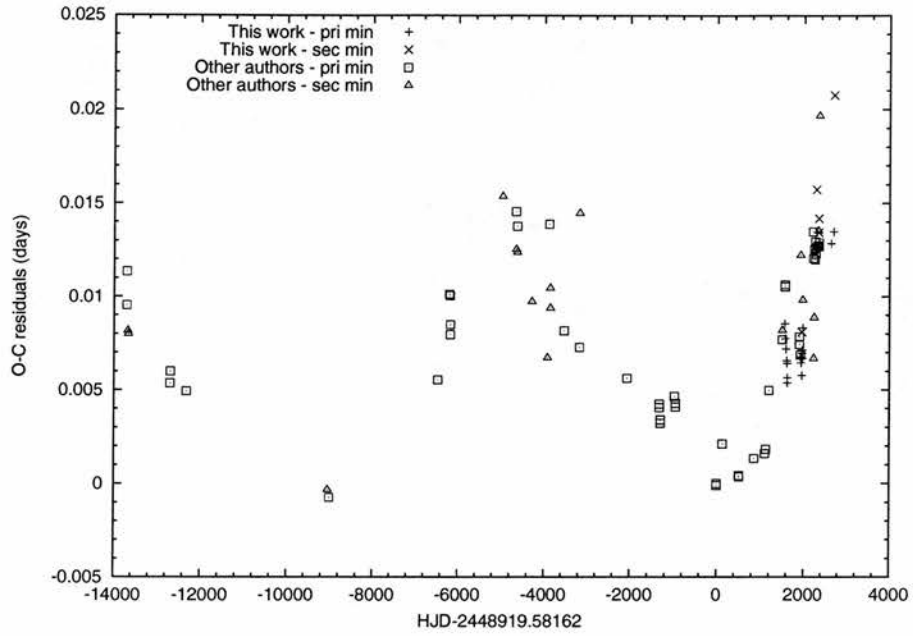

Figure 5.6: O-C residuals diagram for XY UMa. The primary and secondary minima have been plotted seperately.

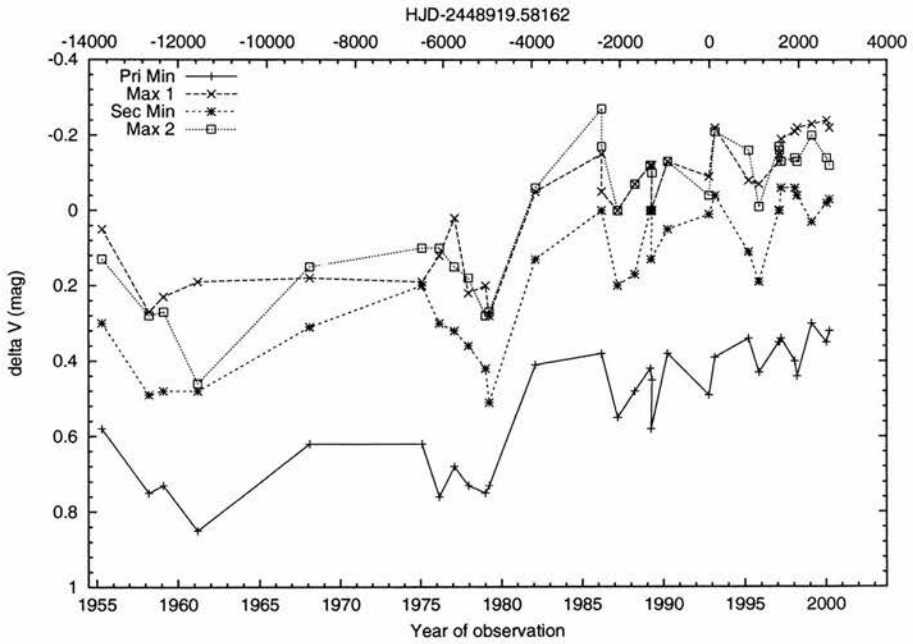

Figure 5.7: Differential magnitudes (XY UMa - SAO 27139) at four orbital phases as a function of time. The scale is the same as the above figure.

this time and this could correspond to the possible magnetic activity up-turn.

Although these light curves were secured in the red, where more flux is expected from the spots, it will be desirable to secure true simultaneous light curves in more than one colour – preferably V and I – in order to obtain tighter constraints on the relative temperatures of the binary components' photospheres and the primary's spots.

Although faint, XY UMa would be in range of Doppler imaging using the Least-squares deconvolution technique (see Section 2.4.3; Donati & Collier Cameron 1997; Barnes et al. 1998), which would provide information about the higher latitude spot structure to which eclipse-mapping is insensitive. With appropriate observations separated by a few days, it should be possible to repeat the differential rotation measurements that have now been obtained on several systems (see Section 1.3.4) and obtain the first comprehensive differential rotation measurement for a binary system.

It would also be valuable if the spectra needed for a Doppler imaging study covered the TiO bandheads at 7055 Å and 8860 Å which would allow an independent determination of the spot temperatures and the value of the spot filling factor as discussed by Neff, O'Neal & Saar (1995) and O'Neal, Saar & Neff (1996).

CHAPTER 6

Photometric study of the contact binaries V523 Cas and TY UMa

The work in this chapter is published in Monthly Notices of the Royal Astronomical Society, "A photometric study of the contact binaries V523 Cas and TY UMa" *MNRAS (2000) 317, 111* . Some of the data on V523 Cas were obtained with R. M. McDermid as part of his Senior Honours Astrophysics Project.

6.1 Introduction

The W UMa group of short period eclipsing binaries are important testbeds for theories of stellar evolution and magnetic dynamo processes. The evolution towards shorter orbital periods and into contact is thought to occur by means of angular momentum loss via magnetic braking (see for example Rucinski 1994; Sarna & Fedorova 1989). After contact has been established, the systems are expected to oscillate about shallow contact via thermal relaxation oscillations (the TRO theory cf. Lucy 1976; Vilhu 1982; Rucinski 1986; Eggleton 1996). Many of the W UMa systems show evidence for period changes but on timescales that are several orders of magnitudes shorter than that predicted by TRO theory.

A possible explanation for these shorter-period variations has been proposed by Applegate (1992). This mechanism explains these orbital modulations as gravitational coupling of the orbit to variations in the shape of a magnetically active star during the course of a magnetic cycle. Whilst this mechanism has the potential to explain the short term period behaviour of W UMa systems, there is a lack of the necessary high quality observational data for many systems and too short a timebase of available accurate timings of eclipse minima to make a serious test of the Applegate mechanism.

In their review of the subject area, Maceroni & van't Veer (1996) noted that only about 15% of the 561 stars listed as W UMa type binaries in the 4^{th} General Catalogue of Variable Stars have relatively complete studies. Of these 78 systems, less than half have spectroscopic mass ratios derived with modern techniques. Although there has been some significant improvement recently (Lu & Rucinski 1999; Rucinski & Lu 1999; Rucinski, Lu & Mochnacki 2000), there is clearly a great deal of scope for improvement. As part of a program investigating magnetic activity on detached and contact binaries with high precision photometry, we have examined the contact systems V523 Cas and TY UMa.

V523 Cas (m_V=10.6–11.4, Sp. type K5V) was discovered to be variable by Weber (1958). It has been studied photometrically by several groups (Bradstreet 1981; Hoffman 1981a; Samec, van Hamme & Bookmyer 1989) and radial velocity measurements were made by Milone, Hrivnak & Fisher (1985). Samec, van Hamme & Bookmyer (1989) found a discrepancy between the mass ratio derived from spectroscopy and that derived from photometric solutions.

TY UMa (= SVS 366, m_V=11.5–12.1) was found to be a W UMa-type variable by Beljawsky (1933) and has only been the subject of very few further studies (Broglia & Conconi 1981; Hoffman 1981b; Broglia & Conconi 1983) in the years following discovery. Broglia & Conconi (1983) found evidence for asymmetries in the light curve and slight inequalities in the heights of the two maxima indicating the likely presence of starspots in the system.

6.2 Observations and data reduction

6.2.1 Photometry

The photometric observations of V523 Cas and TY UMa were obtained with the 0.9-m James Gregory Telescope (JGT), at the University Observatory, St. Andrews, and a Wright Instruments CCD camera mounted at the Cassegrain focus. More details of the equipment and the photometric reduction procedures employed are given in Section 4.2.1 and in Bell, Hilditch & Edwin (1993). Data were obtained in the V and I filters and exposure times varied from 20–60 s depending on the seeing and the filter in use. Typical photometric errors reported by JGTPHOT for V–C differential magnitudes were $\pm$0.004

Table 6.1: Journal of photometric observations of V523 Cas in 1998–2000.

UT Date	HJD - 2450000.0	No. of obs.	Filter	Phase coverage
1998 Nov 24/25[1]	1142.25 – 1142.44	122	V	$\overline{18}.54 - \overline{17}.74$
1998 Nov 28/29[1]	1146.38 – 1146.64	227	V	$\overline{0}.87 - 0.23$
1998 Dec 14/15[1]	1162.29 – 1162.53	366	I	67.19 – 68.24
1998 Dec 23/24	1170.24 – 1170.41	237	I	105.51 – 106.23
1999 Jan 25/26	1204.31 – 1204.42	139	I	247.02 – 247.47
2000 Jan 17/18	1561.32 – 1561.56	276	V	$\overline{0}.31 - 0.69$
2000 Jan 24	1568.27 – 1568.47	315	I	29.45 – 30.28
2000 Jan 25/26	1569.27 – 1569.56	446	I	33.70 – 34.76

[1] *Obtained with R. M. McDermid*

mag. in both filters. The details of the observations are shown in Tables 6.1 and 6.2.

The data for V523 Cas were initially phased with the ephemeris of Samec, van Hamme & Bookmyer (1989):

$$\text{HJD (Min I)} = 2446708.7712 + 0.23369145E.$$

For TY UMa the only available ephemeris is that of Broglia & Conconi (1983):

$$\text{HJD (Min I)} = 2439532.4965 + 0.354538609E.$$

These gave phase offsets of ~ 0.08 and ~ 0.1 respectively on phasing our data with these ephemerides. We determined several new times of minimum using the bisecting chord code described in Section 5.2.1 and these are given, along with others taken from the literature, in Tables A.2 and A.3. The data were phased with the following ephemerides:

$$\text{HJD (Min I)} = 2451146.58560 + 0.23369145E \quad \text{(V523 Cas)},$$

and

$$\text{HJD (Min I)} = 2451262.37684 + 0.354538609E \quad \text{(TY UMa)},$$

and the light curves are shown in Fig. 6.1–6.2.

Table 6.2: Journal of photometric observations of TY UMa in 1999-2000.

UT Date	HJD - 2450000.0	No. of obs.	Filter	Phase coverage
1999 Mar 24/25	1262.31 – 1262.71	342	V	$\overline{0}.18$ – 0.94
1999 Mar 27/28	1265.32 – 1265.71	621	I	8.36 – 9.40
1999 Dec 18/19	1531.42 – 1531.57	114	V	758.85 – 759.26
2000 Jan 18	1561.56 – 1561.81	251	V	$\overline{121}.15$ – $\overline{120}.45$
2000 Jan 20/21	1564.45 – 1564.81	379	V	$\overline{113}.01$ – $\overline{111}.99$
2000 Jan 26	1569.53 – 1569.81	448	I	$\overline{98}.69$ – $\overline{97}.90$
2000 Feb 29/Mar 1	1604.39 – 1604.59	201	V	$\overline{0}.36$ – 0.22
2000 Mar 2/3	1606.37 – 1606.56	194	V	5.23 – 5.76
2000 Mar 19/20	1623.32 – 1623.62	309	V	53.05 – 53.89
2000 Mar 20/21	1624.32 – 1624.51	207	V	55.85 – 56.40
2000 Mar 22/23	1626.31 – 1626.51	205	I	61.48 – 62.02
2000 Mar 24/25	1628.63 – 1628.71	151	I	68.02 – 68.25
2000 Apr 03/04	1638.34 – 1638.69	450	I	95.41 – 96.40
2000 Apr 04/05	1639.39 – 1639.69	302	I	98.36 – 99.20

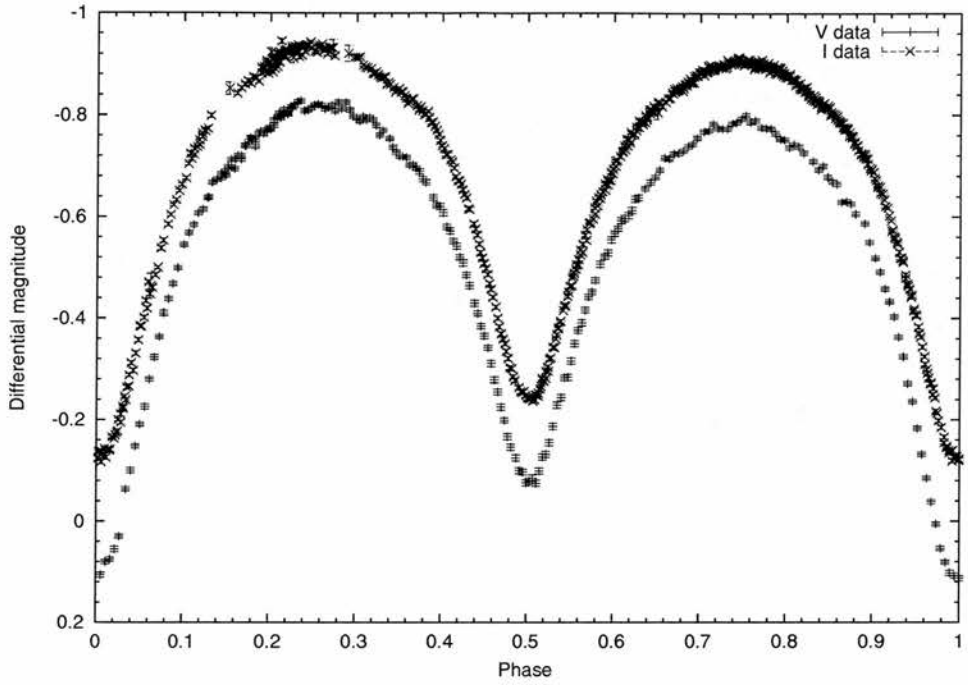

Figure 6.1: V (bottom) and I (top) band light curves for V523 Cas taken in 1998 November–December. The I band light curve has been shifted by 0.2 mag for clarity.

In order to investigate the long-term changes of the two systems with a view towards establishing the nature of any cyclic behaviour, V523 Cas and TY UMa were re-observed in 2000. We again found phase offsets, although they were not as serious as those seen in 1999. The data taken in 2000 were phased with the following ephemerides:

$$\text{HJD (Min I)} = 2451561.39289 + 0.23369145E \quad \text{(V523 Cas)},$$

and

$$\text{HJD (Min I)} = 2451604.51556 + 0.354538609E \quad \text{(TY UMa)},$$

and the light curves are shown in Fig. 6.3–6.4.

In some cases, sections of the light curves have been observed on more than one night giving rise to complex features. Our check–comparison differential magnitudes are stable to ≤ 0.01 magnitudes and so these features are likely to be intrinsic to the stars and could possibly be caused by re-arrangement of spots on the stellar surface.

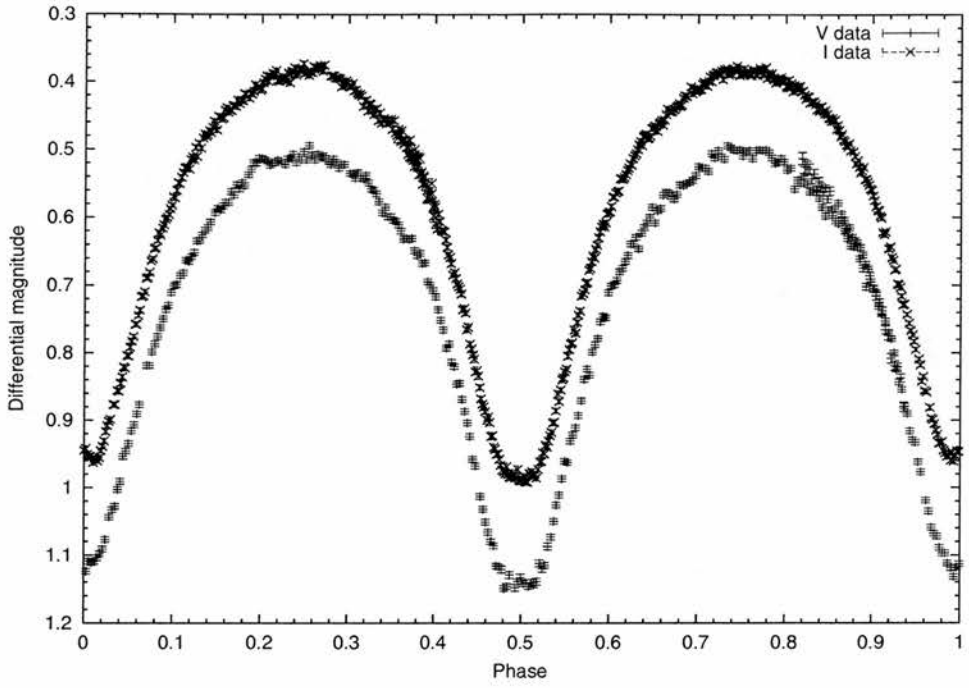

Figure 6.2: V (bottom) and I (top) band light curves for TY UMa taken in 1999 March. The I band light curve has been shifted by -0.6 mag for clarity.

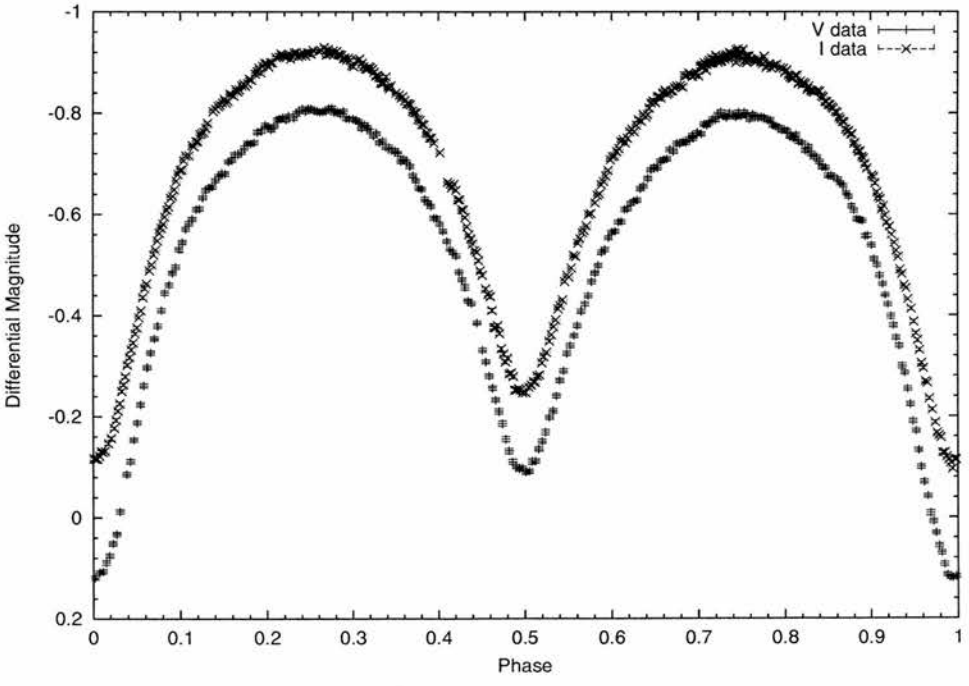

Figure 6.3: V (bottom) and I (top) band light curves for V523 Cas taken in 2000 January. The I band light curve has been shifted by 0.2 mag for clarity.

Table 6.3: Times of minima for V523 Cas and TY UMa

Time of minima (HJD - 2400000.0)	Object	Filter	Type of minima
51142.26200	V523 Cas	*V*	Secondary
51146.46946	V523 Cas	*V*	Secondary
51146.58551	V523 Cas	*V*	Primary
51162.36093	V523 Cas	*I*	Secondary
51162.47682	V523 Cas	*I*	Primary
51171.35786	V523 Cas	*I*	Primary
51561.39289	V523 Cas	*V*	Primary
51561.51100	V523 Cas	*V*	Secondary
51568.28731	V523 Cas	*I*	Secondary
51568.40265	V523 Cas	*I*	Primary
51262.37684	TY UMa	*V*	Primary
51262.55370	TY UMa	*V*	Secondary
51265.39007	TY UMa	*I*	Secondary
51265.56764	TY UMa	*I*	Primary
51531.47882	TY UMa	*V*	Primary
51561.61504	TY UMa	*V*	Primary
51561.79173	TY UMa	*V*	Secondary
51564.62856	TY UMa	*V*	Secondary
51569.59186	TY UMa	*I*	Secondary
51569.77004	TY UMa	*I*	Primary
51604.51556	TY UMa	*V*	Primary
51606.46517	TY UMa	*V*	Secondary
51623.48351	TY UMa	*V*	Secondary
51624.37021	TY UMa	*V*	Primary
51638.37443	TY UMa	*I*	Secondary
51639.61570	TY UMa	*I*	Primary

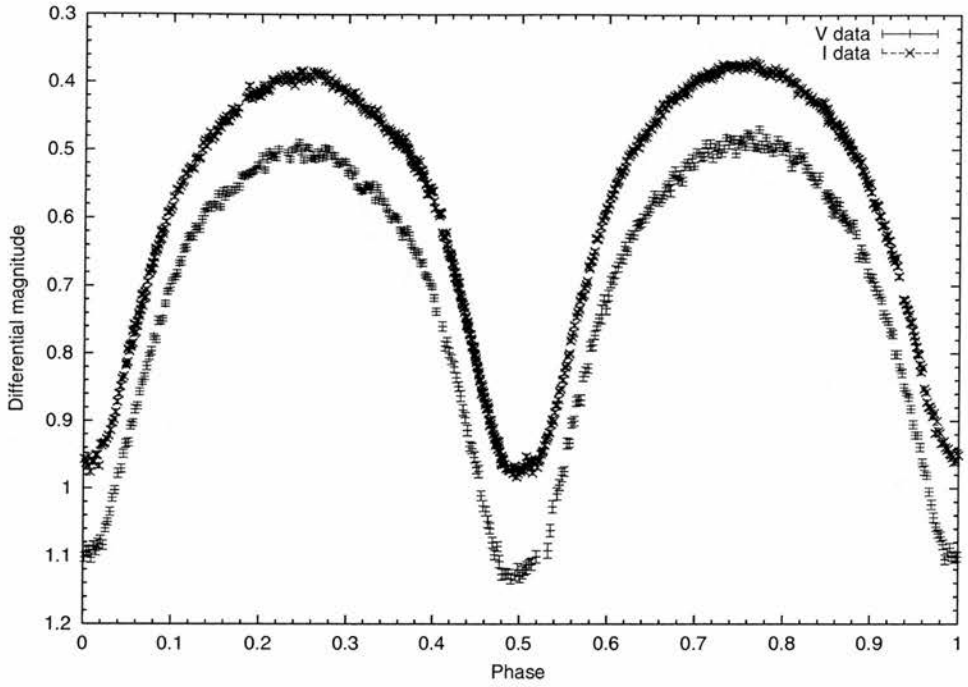

Figure 6.4: V (bottom) and I (top) band light curves for TY UMa taken in 2000 March–April. The I band light curve has been shifted by -0.6 mag for clarity.

6.2.2 Astrometry

As the position listed by SIMBAD for V523 Cas was only accurate to arcminutes in declination, we elected to perform astrometry on our CCD frames using the STARLINK packages PISA (Draper & Eaton 1998) for object detection and ASTROM (Wallace 1998) to compute the astrometric solution. This proceeded in two steps.

The first step was to obtain a *Digitized Sky Survey*[1] image of the V523 Cas field with a size that was double the 11.5 × 17 arcmin^2 field of the JGT. PISA was used to detect all the object which had reasonable brightness in the DSS image. A list of reference stars for this field was then obtained by retrieving the equatorial (Right Ascension and Declination) co-ordinates of all stars within 30 arcmin of the field centre from the *Guide Star Catalogue Version 1.2*[2].

A total of 18 GSC stars were then identified in the DSS image and their rectangular co-ordinates determined by PISA were matched with their equatorial co-ordinates for use as reference stars. The rest of the stars detected by PISA were entered as unknowns and

[1] http://stdatu.stsci.edu/dss/

[2] http://www-gsss.stsci.edu/gsc/gsc12/description.html

ASTROM was used to compute a 6 coefficient plate solution and new equatorial co-ordinates for all the detected stars. Reference star with large residuals in their computed positions were removed from the solution and a new plate solution computed.

This procedure is necessary because the GSC co-ordinates have a quite poor ($\sim 1.0''$) absolute global accuracy due to limitations in the modelling of deformations in the original Schmidt plates and other effects such as field rotation and radial distortion. These increase significantly towards the edges of the Schmidt plates which form the basis of the GSC and limit the overall accuracy of the catalogue. However a local plate solution of a much smaller field than the $6.^{\circ}5 \times 6.^{\circ}5$ field of a Schmidt plate can reach a higher accuracy than the overall global accuracy.

The next step was to identify those stars that appeared in both the DSS image and the JGT CCD frames for use as reference stars for computing a plate solution for the JGT frames and a position for V523 Cas. PISA was again used to detect the objects in the JGT CCD frames and to derive (x, y) co-ordinates for suitable reference stars which were matched with the equatorial co-ordinates determined in the previous step.

A new 6 coefficient plate solution for the JGT CCD frames was then determined with ASTROM and iterated, discarding the reference star with the largest residuals each time. This procedure continued until no reference stars with significant deviations in position remained and the resulting position for V523 Cas is RA (2000.0) = $00^{\mathrm{h}}\ 40^{\mathrm{m}}\ 06.^{\mathrm{s}}21$, Dec. (2000.0) = $+50^{\circ}\ 14'\ 15.''6$, with RMS errors adopted from the plate solution for the reference stars in the DSS image of 0.08^{s} in RA and $0.48''$ in Dec. This accuracy will be a fair assesment of the likely errors on the position overall.

6.3 System parameters

We used the well-known LIGHT2 synthesis code (Hill 1979; Hill & Rucinski 1993) to establish values for the geometrical system parameters, namely the orbital inclination, i, the stellar radii relative to the semi-major axis of the relative orbit r_1, r_2 and the temperature ratio of the two stars, T_1/T_2 (yielding component temperatures when combined with an estimate of T_1 derived from a spectral type for example). Also in the case of contact systems, we have the 'fillout factor', which is the fraction of the potential between the inner (L_1) and outer (L_2) Lagrangian surfaces and given by Rucinski (1976)

as $f = (\Omega - \Omega_{outer})/(\Omega_{inner} - \Omega_{outer})$. Here Ω_{inner} and Ω_{outer} are the potentials corresponding to the inner and outer Lagrangian surfaces. In Tables 6.4– 6.6 of this Chapter we expressed this fillout as $1 - f$, expressed as a percentage.

Since the data were not obtained simultaneously in each filter and the LIGHT2 code is unable to handle data with non-simultaneous phases, we used a least-squares cubic spline code to interpolate the raw V and I data to provide 200 points in each filter at equal intervals in phase. These interpolated V and I curves were solved simultaneously by LIGHT2 for each system.

Although the filter set used at the JGT has been shown to closely match the Cousins VRI set, our data have not been transformed to a standard system. Consequently we could not use our V and I data alone to estimate spectral types or temperatures. As a starting point we used the temperatures derived by previous investigators of each system i.e. Samec, van Hamme & Bookmyer (1989) (V523 Cas) and Broglia & Conconi (1983) (TY UMa) and adjusted the primary temperature and the secondary temperature difference to obtain the best fit.

In addition since the eclipses are not total in either system, it is not possible to solve for the mass ratio and the inclination simultaneously and so an initial value of q had to be adopted. For V523 Cas the mass ratio was initially fixed at the value derived by Samec, van Hamme & Bookmyer (1989), namely $q = 0.571$.

With V523 Cas we experienced problems obtaining a satisfactory fit to both quadratures simultaneously, due to the unequal maxima (O'Connell effect) and LIGHT2's standard assumption of immaculate photospheres. To solve this problem we performed two sets of fits, namely:

1. 2nd quadrature points removed (phases 0.6–0.9)
2. 1st quadrature points removed (phases 0.1–0.4)

We found much better fits, in terms of lower values of chi-squared, when the 1st quadrature points were removed and the resulting system parameters are shown in Table 6.4 along with those of Samec, van Hamme & Bookmyer (1989). There is the possibility of an arrangement of spots that could produce a symmetric distortion which would invalidate our assumption of having one undistorted quadrature and could give incorrect

Table 6.4: System parameters for V523 Cas obtained from the data in 1998 November–December, along with the simultaneous fit (Model 3) of Samec et al. (1989).

Parameter	Samec et al. (1989)	LIGHT2 solution (1)	LIGHT2 solution (2)
r_1/a (polar)	0.406 ± 0.001	0.4335 ± 0.015	0.4184 ± 0.015
r_2/a (polar)	0.324 ± 0.001	0.3296 ± 0.012	0.3136 ± 0.012
i	$83\overset{\circ}{.}7 \pm 0\overset{\circ}{.}1$	$83\overset{\circ}{.}97 \pm 0\overset{\circ}{.}04$	$83\overset{\circ}{.}67 \pm 0\overset{\circ}{.}04$
$q = m_2/m_1$	0.571 ± 0.005	0.53 ± 0.02	0.53 ± 0.02
fillout	13%	29.5%	11.4%
T_1 (polar)	4200 K	4434 K	4434 K
T_2 (polar)	4407 K	4711 K	4720 K
Reduced χ^2 of fit	N/A	3.915E-04	2.876E-04

system parameters. However due to the non-uniqueness of spot solutions, especially from photometric data alone, we have elected to proceed under the assumption that the 2nd quadrature is cleaner and will produce system parameters that more accurately reflect the true parameters. The derived parameters agree quite well with those of Samec, van Hamme & Bookmyer (1989) with the main differences being slightly larger radii and a slightly lower mass ratio. As noted by Samec, van Hamme & Bookmyer (1989) the mass ratio derived from photometry is discrepant with that derived spectroscopically by Milone, Hrivnak & Fisher (1985) and we also find evidence for a higher mass ratio of $q = 0.53$, in broad agreement with the results of Samec, van Hamme & Bookmyer (1989).

The data obtained in 2000 January were also solved for system parameters with LIGHT2 and the results are shown in Table 6.5. As with the data obtained in 1998 November–December we did find an improvement in the fit, in terms of a lower chi-squared, when the first quadrature was removed but the effect was not as marked as in 1998 November–December. As discussed in more detail in Section 6.4, the 2000 data appear to be "cleaner" and less affected by the presence of spots, allowing a better fit with the unspotted model used in LIGHT2. For this reason we have plotted the full dataset and fits in Fig. 6.7. The system parameters agree well between the different sets of data, with the differences being mainly down to the slightly different mass ratio and corresponding change in fillout factor.

The discrepancy between mass ratios determined photometrically and spectroscopi-

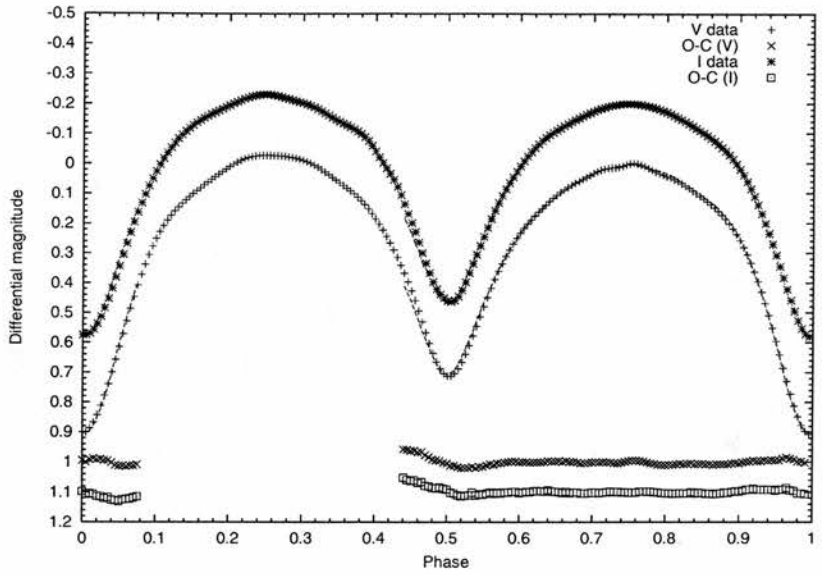

Figure 6.5: V (bottom) and I (top) band light curves for V523 Cas formed from the normal points, along with the LIGHT2 model fits. The I band light curve and fit have been shifted by -0.2 mag for clarity. The (observed-model) curves have been shifted by 1.0 and 1.1 magnitudes for V and I respectively.

Table 6.5: System parameters for V523 Cas obtained from the data in 2000 January.

Parameter	LIGHT2 solution (i) (All data)	LIGHT2 solution (ii) (No phases 0.6–0.9)	LIGHT2 solution (iii) (No phases 0.1–0.4)
r_1/a (polar)	0.4225 ± 0.015	0.4262 ± 0.015	0.4208 ± 0.015
r_2/a (polar)	0.3211 ± 0.015	0.3249 ± 0.012	0.3192 ± 0.012
i	$83\overset{\circ}{.}72 \pm 0\overset{\circ}{.}02$	$83\overset{\circ}{.}78 \pm 0\overset{\circ}{.}03$	$83\overset{\circ}{.}65 \pm 0\overset{\circ}{.}02$
$q = m_2/m_1$	0.54 ± 0.02	0.54 ± 0.02	0.54 ± 0.02
fillout	18.4%	22.9%	16.3%
T_1 (polar)	4435 K	4435 K	4435 K
T_2 (polar)	4744 K	4742 K	4745 K
Reduced χ^2 of fit	1.213E-04	1.408E-04	7.947E-05

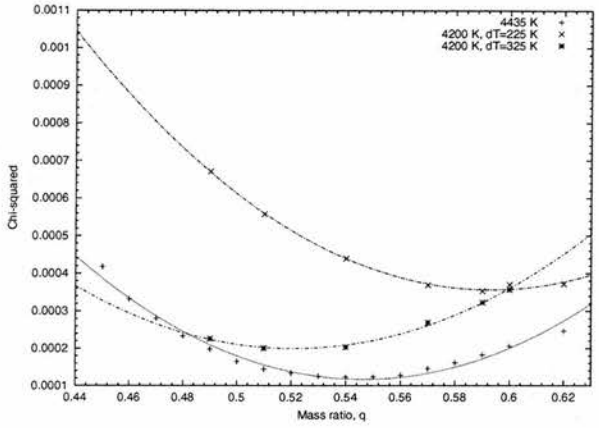

Figure 6.6: Plot of reduced chi-squared against mass ratio, q, for V523 Cas in 2000. The indicated temperatures are polar temperatures and the results were obtained with the full set of data (solution (i) in Table 6.5).

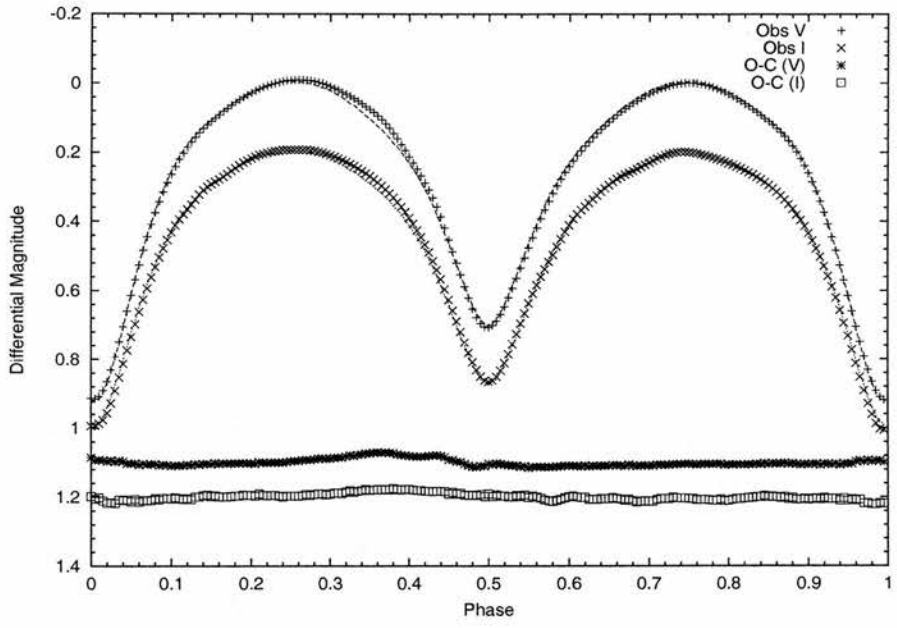

Figure 6.7: V (bottom) and I (top) band light curves for V523 Cas in 2000 formed from the normal points, along with the LIGHT2 model fits. The I band light curve and fit have been shifted by -0.2 mag for clarity. The (observed-model) curves have been shifted by 1.1 and 1.2 magnitudes for V and I respectively.

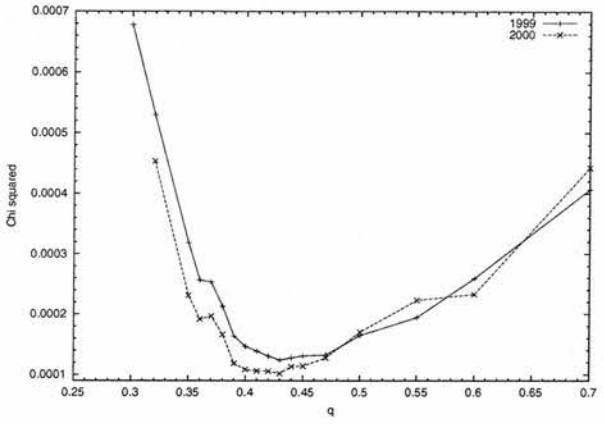

Figure 6.8: Plot of reduced chi-squared against mass ratio, q, for TY UMa.

Table 6.6: System parameters for TY UMa.

Parameter	Broglia & Conconi (1983)	LIGHT2 solution 1999 March	LIGHT2 solution 2000 March–April
r_1/a (polar)		0.4499	0.4486
r_2/a (polar)		0.3127	0.3113
i	$83\overset{\circ}{.}3 \pm 1\overset{\circ}{.}0$	$80\overset{\circ}{.}38 \pm 0\overset{\circ}{.}02$	$80\overset{\circ}{.}30 \pm 0\overset{\circ}{.}03$
$q = m_2/m_1$	0.40 ± 0.02	0.43 ± 0.05	0.43 ± 0.05
fillout	12%	$27.5 \pm 0.5\%$	$26.1 \pm 0.6\%$
T_1 (polar)	5550 K	5650 K	5625 K
T_2 (polar)	5545,5672,5849 K	5892 K	5848 K
Reduced χ^2 of fit	N/A	7.593E-05	1.184E-04

cally has been seen in several systems and was investigated to some extent by van Hamme & Wilson (1985). They found that neglect of the eclipse and proximity effects can significantly alter the radial velocities and derived mass ratio. We note here that the spectra of Milone, Hrivnak & Fisher (1985) were obtained at relatively low dispersion on photographic plates and no correction for the proximity and eclipse effects were reported. As V523 Cas has the second shortest period of all the W UMa contact binaries, this system warrants a new spectroscopic investigation with modern equipment to try and resolve this discrepancy.

In the case of TY UMa there are no radial-velocity data available and only one photometrically determined mass ratio (Broglia & Conconi 1983) and we elected to perform a grid of solutions with a range of q of 0.1–0.7 for both datasets and the results are shown

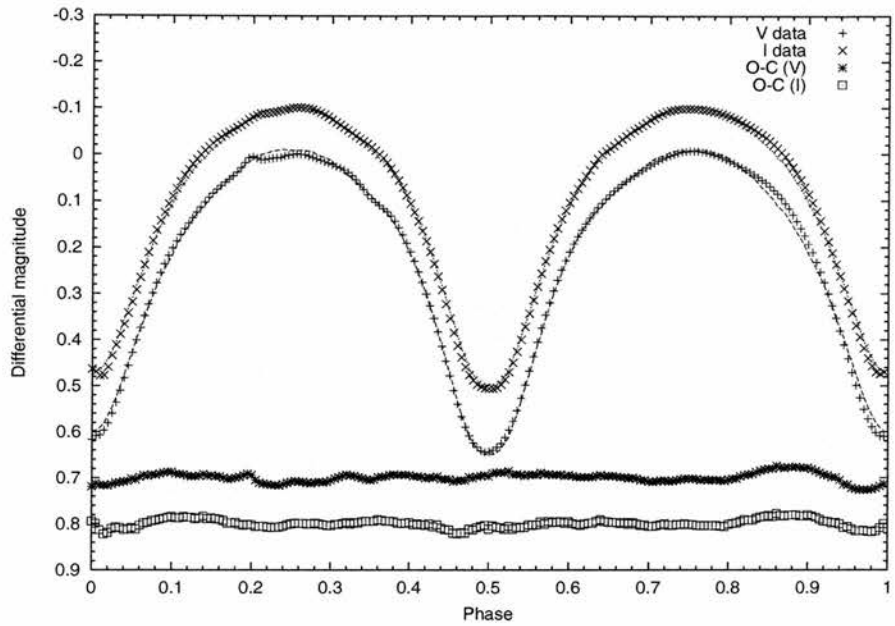

Figure 6.9: V (bottom) and I (top) band light curves for TY UMa formed from the normal points, along with the LIGHT2 model fits. The I band light curve and fit have been shifted by -0.1 mag for clarity. The (observed-model) curves have been shifted by 0.7 and 0.8 magnitudes for V and I respectively.

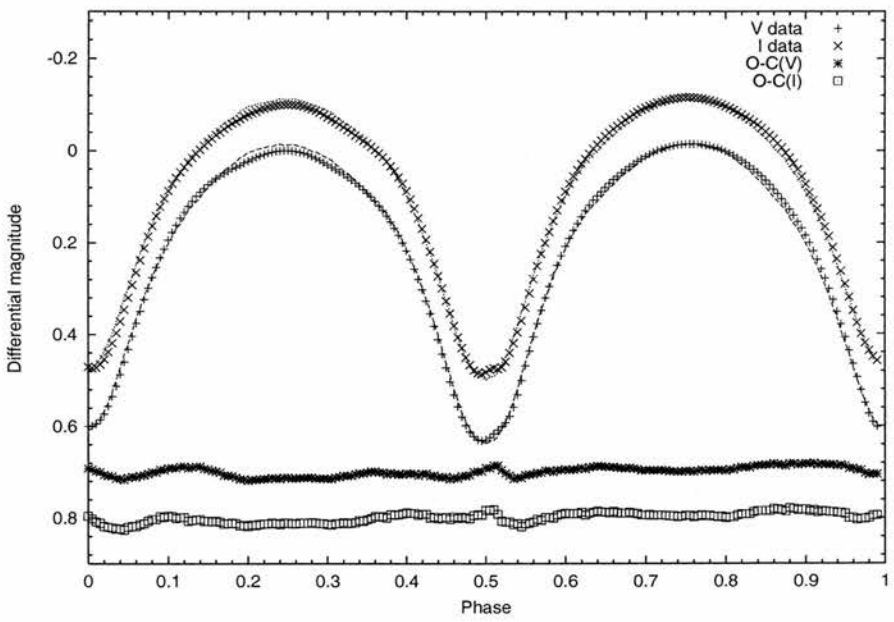

Figure 6.10: V (bottom) and I (top) band light curves for TY UMa in 2000 formed from the normal points, along with the LIGHT2 model fits. The I band light curve and fit have been shifted by -0.1 mag for clarity. The (observed-model) curves have been shifted by 0.7 and 0.8 magnitudes for V and I respectively.

in Figure 6.8.

We show the derived system parameters for TY UMa from the 1999 March and 2000 March–April datasets along with those of Broglia & Conconi (1983), who carried out a fit to their B and V band data (although they did not derive radii for the stars), in Table 6.6.

We found a minimum chi-squared for TY UMa at a mass ratio of $q = 0.43 \pm 0.01$ in both datasets which is not too discrepant from that found by Broglia & Conconi (1983) of $q = 0.40 \pm 0.02$. However we find the degree of overcontact, defined to be $(\Omega_{inner} - \Omega)/(\Omega_{inner} - \Omega_{outer})$, to be significantly different at 27.5 (1999 March) and 26.1 (2000 March–April) per cent compared to their value of just 12 per cent. The reasons for this large apparent change in the degree of contact in the 18 years separating the two investigations is unclear and the system obviously merits further study.

The normal points used to solve for the system parameters, along with the LIGHT2 fits and O-C light curve residuals are shown for both systems in Figs. 6.5–6.7 and 6.9–6.10.

6.4 Long-term trends

We have collected all the times of minima based on photoelectric or CCD data that are available in the literature for V523 Cas and TY UMa. The ephemeris of Lavrov & Zhukov (1976), HJD (Min I) = 2441220.3036 + 0.2336905E., was used as the reference ephemeris for V523 Cas. For TY UMa we used that given by Broglia & Conconi (1983), HJD (Min I) = 2439532.4965 + 0.354538609E., and times of minima and O-C residuals were computed relative to this ephemeris. The times of minima and the O-C residuals are shown in Tables A.2–A.3 and are plotted in Figs. 6.11–6.12, along with least-squares quadratic fits to the data.

Both O-C diagrams clearly show evidence of period change, with the period increasing in the case of V523 Cas and decreasing in the case of TY UMa. Although TY UMa has suffered from a lack of study, one noticeable feature is the large apparent jump of ~ 0.02 days in the ~ 1000 days between the results of Agerer & Huebscher (1998) and our results. Agerer & Huebscher (1997) also list times of minima for TY UMa, which differ from the later results of Agerer & Huebscher (1998) by ~ 0.001 day. However no indication is given

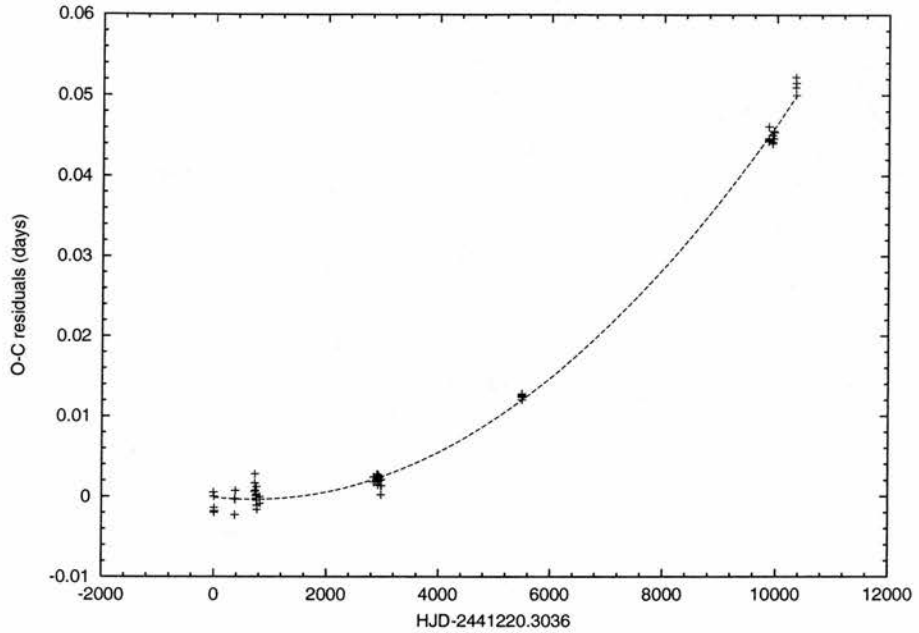

Figure 6.11: O-C residuals diagram for V523 Cas along with a quadratic fit to the data.

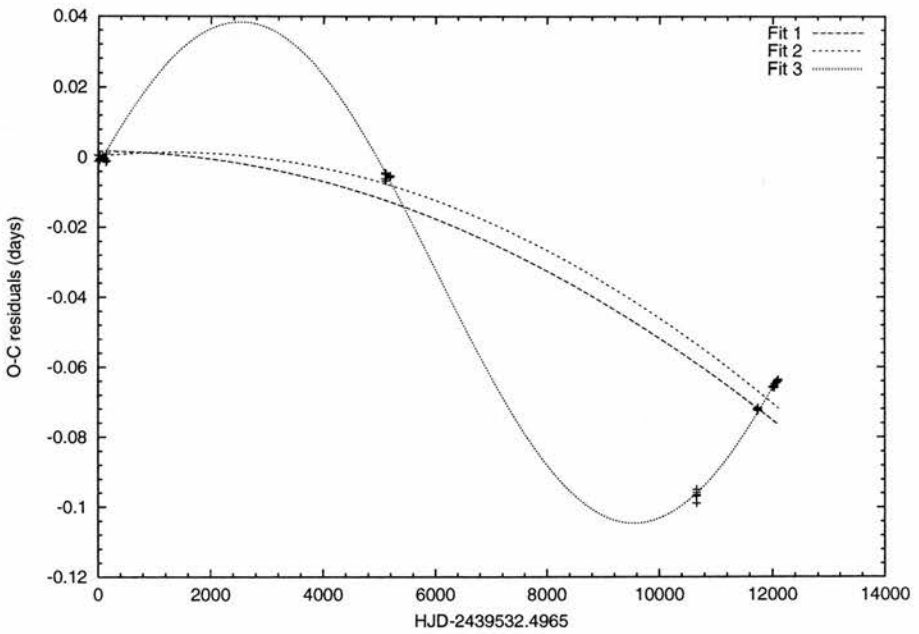

Figure 6.12: O-C residuals diagram for TY UMa along with various fits to the data. Fit 1 has all the data weighted equally, Fit 2 is with the data of Agerer & Huebscher (1998) given half weight. Fit 3 is a sine fit with all the data weighted equally.

as to whether the times of minima of Agerer & Huebscher (1998) are corrections of the earlier ones. We have used the values in Agerer & Huebscher (1998) as these gave the smaller O-C residuals. We carried out two quadratic fits to the TY UMa residuals, one with all the data weighted equally and one with the data of Agerer & Huebscher (1998) given half weight and these are also shown in Figure 6.12. In addition we performed a sine fit to all the data under the assumption that the points of Agerer & Huebscher (1998) were part of a long-term periodic trend. The derived period was $P = 14066.4 \pm 38.8$ days (~ 38.5 years) but as only one cycle has been observed this result should be treated with caution. Another problem is that the sparse sampling will allow shorter period sine curves to be fitted to the same data with equally good results. The times of minima obtained in 1999 December, 2000 January and 2000 March fit better with the other minima times obtained in this work, but clearly additional eclipse timings would be very valuable in determining whether the abrupt period increase is real or whether there is a long-term periodic trend.

Using a quadratic ephemeris of the form $c_0 + c_1\epsilon + c_2\epsilon^2$ and the relation $\dot{P} = 2c_2/P_{le}$, where $\dot{P}$ is the rate of change of orbital period with time and P_{le} is the reference epoch, we obtain $c_2 = (5.399 \pm 0.142) \times 10^{-10}$ and $c_2 = (-5.33 \pm 1.46) \times 10^{-10}$ for V523 Cas and TY UMa (from the fit with all data weighted equally) respectively. This corresponds to a period increase for V523 Cas of $\dot{P}/P = (1.977 \pm 0.052) \times 10^{-8}$ d^{-1} and a period decrease of $\dot{P}/P = -(0.848 \pm 0.233) \times 10^{-8}$ d^{-1} for TY UMa.

Since we have not derived absolute values of the masses of the two components for either system a calculation of the mass transfer rate is not possible. We also note that the available timescales of about 12000 days (~ 30 yrs) of accurate times of minima and the absence of any indication of cyclical behaviour, means that at present there is not enough data for a discriminating test of the Applegate mechanism.

Another alternative for tracing long-term activity cycles is to study the variation of brightness of the system over time. Since close binaries appear to have preferred longitudes of $\sim 90°$ and $\sim 270°$, then a measurement of the height difference between the maxima in light curves, $\delta n = (m_1 - m_2)$ will give a rough measurement of the amount of spot activity at the time. This O'Connell effect (O'Connell 1951), defined here as the difference between m_1, the magnitude of the system at phase 0.25, and m_2, the magnitude at phase 0.75, was stated by Zhukov (1985) to undergo a ten to twelve year cyclic variation on V523 Cas. We

Table 6.7: Heights of maxima for V523 Cas in V.

Max I	Max II	δn	Reference	Year
N/A	N/A	$0\overset{m}{.}015$	Zhukov (1985)	1971.74
N/A	N/A	$0\overset{m}{.}010$	Zhukov (1985)	1973.84
N/A	N/A	$-0\overset{m}{.}003$	Zhukov (1985)	1976.01
N/A	N/A	$0\overset{m}{.}016$	Hoffman (1981a)	1979.88
N/A	N/A	$-0\overset{m}{.}003$	Zhukov (1985)	1980.97
N/A	N/A	$0\overset{m}{.}033$	Zhukov (1985)	1981.70
N/A	N/A	$0\overset{m}{.}025$	Zhukov (1985)	1981.74
N/A	N/A	$0\overset{m}{.}015$	Zhukov (1985)	1981.79
$0\overset{m}{.}358$	$0\overset{m}{.}340$	$0\overset{m}{.}018$	Samec & Bookmyer (1987)	1986.76
$-0\overset{m}{.}817$	$-0\overset{m}{.}797$	$-0\overset{m}{.}020$	this work	1998.90
$-0\overset{m}{.}808$	$-0\overset{m}{.}794$	$-0\overset{m}{.}014$	this work	2000.05

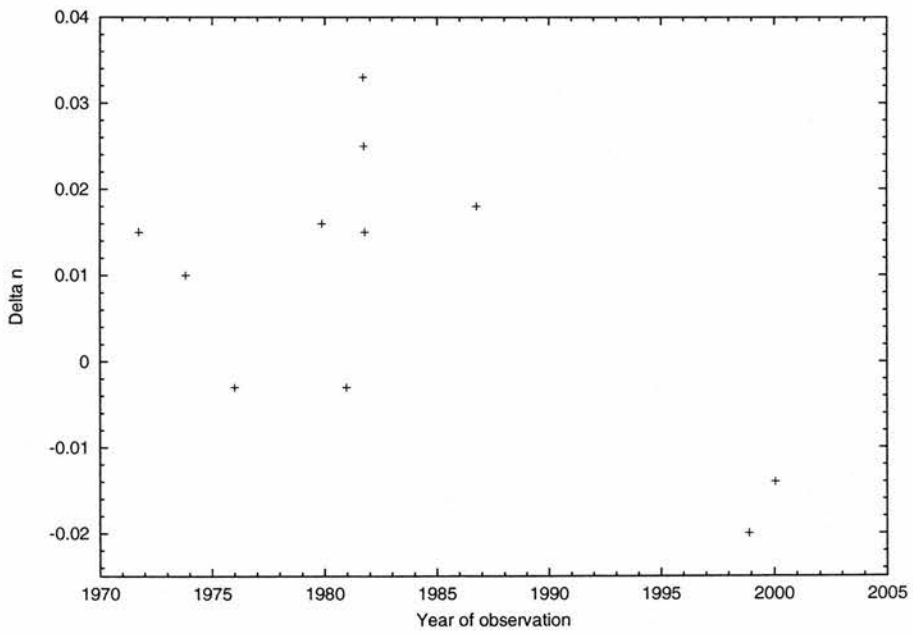

Figure 6.13: Difference in heights of maxima for V523 Cas.

Table 6.8: Heights of maxima for TY UMa in V.

Max I	Max II	δn	Reference	Year
$11\overset{m}{.}528$	$11\overset{m}{.}475$	$0\overset{m}{.}053$	Broglia & Conconi (1983)	1967.32
$11\overset{m}{.}496$	$11\overset{m}{.}513$	$-0\overset{m}{.}017$	Broglia & Conconi (1983)	1981.09
$11\overset{m}{.}487$	$11\overset{m}{.}506$	$-0\overset{m}{.}019$	Broglia & Conconi (1983)	1981.33
$0\overset{m}{.}508$	$0\overset{m}{.}501$	$0\overset{m}{.}007$	this work	1999.22
$0\overset{m}{.}486$	$0\overset{m}{.}469$	$0\overset{m}{.}017$	this work	2000.05
$0\overset{m}{.}500$	$0\overset{m}{.}486$	$0\overset{m}{.}014$	this work	2000.30

have added our determinations of δn to those listed by Samec & Bookmyer (1987) and these are shown in Table 6.7 and plotted in Figure 6.13. There is some evidence of a cycle with a minimum in 1979–80 and possible maxima in 1971 and 1981–82, but this is very difficult to substantiate with the $\sim$ 17 year gap with virtually no observations between 1982 and our observations presented here. Further observations in the coming years would obviously be very valuable to determine if the present downward trend in δn continues and the active longitude flips.

In the case of TY UMa, the number of available light curves is much smaller and too widely separated for this approach to be of great value. However, Broglia & Conconi (1983) did note slight inequalities in the heights of the maxima which are also present in these data, with this effect increasing in 2000. Consequently we have tabulated the 3 sets of maxima listed by Broglia & Conconi (1983) and added those from our own lightcurves and these are shown in Table 6.8 and plotted in Figure 6.14. The data of Broglia & Conconi (1983) was obtained throughout 1967 and in two batches in 1981. In the absence of other information as to the dates of observation, we took the mid-point between the HJD of the first and last observation that was tabulated for each batch and used this to determine the decimal year given in Table 6.8. Studies at more regular intervals would be needed to determine the existence of the expected brightness cycle.

Unfortunately, the sampling rate of complete light curves is too sparse to make any definite statements about the behaviour of the system and any possible magnetic cycle. However it does seem that from the recent light curves of V523 Cas that the data obtained in 2000 January with the JGT show less disturbance in the light curve and a smaller value of δn. This would be the case if magnetic activity in the system was declining again, but

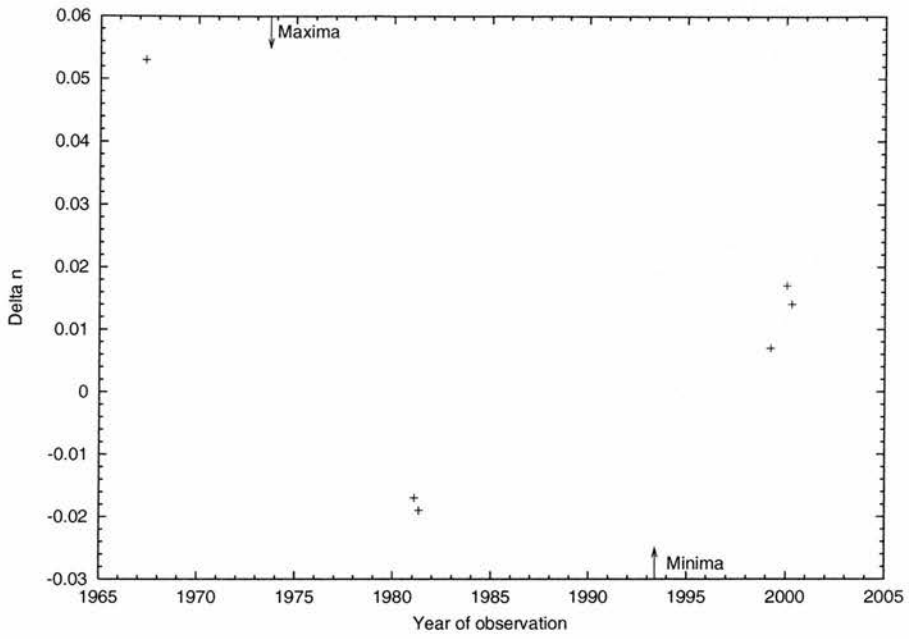

Figure 6.14: Difference in heights of maxima for TY UMa. Also marked are the maxima and minima of the sine curve fit to the O-C residuals (see Figure 6.12).

more data would be needed to substantiate this.

6.5 Discussion

We have obtained complete high precision V and I band light curves for two W UMa systems and derived system parameters. For V523 Cas we find that the mass ratio obtained is compatible with that derived from other photometric studies, but discrepant with the only spectroscopic study that has been carried out to date. In addition we have derived a new, more accurate astrometric position for this object.

In the case of TY UMa, these data are only the second set of light curves and the first set of complete system parameters to be published. We find a mass ratio for this system which is close to that derived by Broglia & Conconi (1983) but find a large difference in the derived fillout factors. Further analysis of the astrophysical parameters of this object and investigation into this discrepancy will require spectroscopic data to enable a more accurate mass ratio to be determined.

Both systems show evidence for spot activity and unequal heights of the maxima,

with V523 Cas being the more active system, as could be naively expected from its later spectral type and shorter period. The O-C residual diagrams show evidence for period changes in both systems with a period increase in the case of V523 Cas and a decrease for TY UMa. The timescales of these changes are many orders of magnitudes too short for these changes to be explained by TRO or angular momentum loss (AML) theories but a possible explanation in terms of the Applegate mechanism is not yet feasible due to the short baselines of the observations.

V523 Cas shows evidence for variation in its O'Connell effect, which may indicate the presence of a magnetic cycle but the sampling is too coarse to make any definite statements about any cyclic behaviour. In the case of TY UMa there are only a few light curves available which have sufficient time resolution and accuracy for use in this sort of analysis.

CHAPTER 7

Summary and Conclusions

In order to investigate the distribution of starspots on the surfaces of late-type stars we have obtained high resolution surface images through entropy-regularized fits to a variety of data. In order to search for any long-term variability which could be cyclic, these have been combined with other diagnostics which have a longer timebase and we have attempted to produce links between these different diagnostics and the surface images.

7.1 Eclipse mapping

We have used the technique of eclipse mapping, first presented by Collier Cameron (1997b) and applied by Collier Cameron & Hilditch (1997), to obtain surface images from high precision differential photometry. The results, in terms of resolution of the surface maps, are comparable with what can be achieved using conventional Doppler imaging from high resolution spectroscopy, but with a much smaller telescope ($\sim$1-metre rather than a 4-metre) and cheaper, simpler instrumentation (a CCD imager or photoelectric photometer rather than an echelle spectrograph). However the advantages of eclipse mapping over spectroscopic Doppler imaging will be eroded slightly by the use of least-squares deconvolution, which can increase the S:N ratio of spectroscopic data significantly, and the development of new higher throughput echelle spectrographs (e.g. FEROS (Kaufer & Pasquini 1998)).

The method is applicable to any eclipsing binary system where complete phase coverage of high precision (a few millimags) photometry can be obtained within the likely time of significant spot re-arrangement. This makes the practical limit on orbital periods $\lesssim 7$ days.

In Chapters 4 and 5 we present results for two short-period eclipsing RS CVn binaries with surface images derived using the eclipse mapping technique. For GSC2807-1423 (Chapter 4) we only have images at one epoch so it is not possible to make any significant conclusions about any long-term evolution. However the image does show spots at longitude $\sim 270°$, corresponding to the lower, more distorted quadrature seen in the light curves, and this is the opposite quadrature to that seen by Robb (1998) in his data obtained 10 months earlier.

For XY UMa (Chapter 5) we have presented an additional 4 year series of high precision light curves and surface maps to add to those obtained by Collier Cameron & Hilditch (1997) in 1992 and 1995/96. With the increase in CPU speed and memory capacity of our Doppler imaging workstations, we have been able to boost the number of latitudes and consequently the latitude resolution of our surface grids used in the reconstructions. For XY UMa, the grid has increased from 40 latitudes (4.5° resolution) to 60 latitudes (3° resolution), and further increases, although possible from a computational point of view, are not justified by the data as they cause the map to break up and become "pixelated".

The results show evolution from one map to the next within timescale of a month or less, as well as long-term evolution. Sensible agreement is found between these maps and the light curves used to generate them, with spots on the surface maps occurring at longitudes corresponding to the depressed and distorted quadratures.

There is the potential to extend the eclipse mapping procedure to contact and over-contact geometries and to incorporate the parameters of the orbit as additional adjustable pixels in the regularized fits, as was done by Hendry & Mochnacki (2000) in their Doppler imaging of the contact system VW Cephei. The highly distorted shapes of the stars in these systems may force an abandonment of the traditional rectangular pixel grid for the surface map in favour of a different technique such as the interlocking triangular grid used by Hendry & Mochnacki (2000), with consequent modifications to the definitions of the imaging parameter and entropy.

7.2 Activity cycles

From the summary of Doppler imaging results presented in Section 1.3 it can be seen that, despite the fairly large range in spectral type and the even larger spread in rotational

velocities, there are quite strong similarities between the different objects. The main similarities are:

- Almost all of the stars show low-latitude structure at or near the equator.
- Almost all of the stars have high-latitude spots and/or a polar spot.
- Most stars have some degree of intermediate latitude structure, although the amount can vary considerably.

This last point is significant for our study of BD+22° 4409 (presented in Chapter 3) from Doppler images obtaining using the process of least-squares deconvolution on the raw spectra. The images show a lot less intermediate latitude structure than is seen on stars of similar spectral type, age and rotation rate such as AB Dor, PZ Tel and some of the α Persei G dwarfs. It was postulated in Section 3.6 that this may be due to BD+22° 4409 being in a different part of its activity cycle.

On the Sun spots emerge at higher latitudes at the start of a spot cycle than they do at later times in the cycle and they also drift to lower latitudes during their time on the surface. A similar scenario was postulated by Barnes (1999) to explain the different distribution of surface features on a number of α Persei G-dwarfs and the young, active dwarfs PZ Tel and Speedy Mic. However in almost all cases only one map at a given epoch is available and until the detection of a stellar analogue of the solar 'butterfly' diagram, this remains conjecture. Continued monitoring will be needed to determine if the very active, young stars show cyclical behaviour in the various diagnostics of magnetic activity.

As discussed in Section 1.2.1, observations of a large number of stars by the Mount Wilson HK Project have shown that about 25% of the monitored stars have variations but no apparent periodicity; these tend to be the youngest and most active stars. However, the majority of stars of all spectral types and ages show periodicities with periods of 2.5 yr up to the length of the sample ($\sim$30 years), with the older stars in the sample all having periods greater than 7 years. Although these results do not rule out the possibility of cyclic behaviour in young active stars, it may have consequences for understanding the nature of the dynamo processes that operate in these active stars (cf. Section 1.4).

For binary stars there is the advantage of having times of minima that can stretch back over a century available for use as a diagnostic of long-term activity. This timebase

is many times greater than that of Doppler images of active stars for example. The theoretical work of Applegate (1992) and later improvements by Lanza, Rodonò & Rosner (1998) and Lanza & Rodonò (1999) has provided a natural link between the O-C variations seen in many binaries with magnetic activity cycles (Sections 1.2.2.1 and 1.2.2.3).

The first observation verification of the Applegate mechanism was provided by Hall (1991b) for CG Cyg and since then further tests have been carried out with both positive (Rodonò, Lanza & Catalano 1995) and unclear results (Šimon 1997a, Šimon 1997b). The main problem is that, although the baselines of eclipse timings is longer than other methods, the timescale of the variations in binaries also appears to be longer than single stars and we are in a similar situation in terms of numbers of complete cycles. An additional problem is that discriminating tests of the Applegate mechanism require contemporaneous photometry to determine if the light and orbital period variations are in step, and the availability of suitable photometry tends to be patchy. Several groups have long-term programs to obtain photometry of active stars and these have started to yields results for long-term photometric variations (cf. Section 1.2.2.1).

Of the systems presented in this work, GSC2807-1423 in Chapter 4 has too short an observational history for long-term photometric or orbital period variations to have been detected. However with the observed changes in the brightest quadrature between this work and that of Robb (1998) (Section 4.6), the chances of long-term variations are high.

Further monitoring of the light curve for changes in morphology and the O'Connell effect caused by spot evolution and/or migration should be carried out to establish if there is an activity cycle on this unusual object. Additional spectroscopic and photometric efforts would also help clarify the discrepancies found in the analysis of the existing data and confirm whether it is a member of the very small class of eclipsing RS CVn binaries with periods less than a day, or possibly an even rarer example of a PMS binary.

These differences in the brightness of maxima (the O'Connell effect) and swapping between two preferred longitudes for spot activity has been observed on a wide variety of objects (see Section 1.2.2.2), including single stars as well as binary systems. Berdyugina & Tuominen (1998) presented the best evidence for cyclic switching of active longitudes (which they called a "flip-flop") on 4 RS CVn binaries. Multiple switches were found on all the systems and the timescales varied from 9.0 yrs for EI Eri up to $\simeq$ 17.5 yrs for HR 7275 (V1762 Cyg). Apart from σ Gem which had the longest orbital period ($P = 19.6$ d) of the

four, no synchronization of the active longitudes to the orbital motion was found.

This is in contrast to the short-period class ($P \leq 1$ day) of RS CVn binaries which have mainly been studied by Zelik and collaborators using two spot photometric models. Although these models have limitations which are discussed in Section 2.5, they are still useful for studying the coarse longitude distribution of spots and Zelik et al. found exclusive preference for active longitudes at 90° and 270° in these stars. There have also been been theoretical calculations by Moss & Tuominen (1997) which have shown that close late-type binaries should show large-scale nonaxisymmetric magnetic fields with maxima at the conjunctions, corresponding to the longitudes 0°and 180°. Although this is not supported by the observations, both the theory and the analysis of the observations are in a somewhat immature state and further work in both areas is required.

The technique of eclipse mapping described in Section 2.5 has the potential to allow much more detailed studies of the spot distributions and evolution on short-period active binaries. This was applied to XY UMa (Chapter 5) to produce surface maps at 10 epochs covering 4 years, which show evidence for short and long-term evolution of the spot distribution and a preference for activity at longitudes 90° and 270°.

The greater brightness of XY UMa compared to the other binary stars included in this work means that it has been better studied and there is evidence of both long-term photometric and orbital period variation. The orbital period variation is roughly cyclic and covers roughly 1.9 cycles if the older, less accurate visual times are excluded. However there are large gaps and at least half of the observed cycle is based on a handful of early data points. This has been postulated to be the effect of a third body by Chochol et al. (1998) and related to changes in activity by Jeffries et al. (1995). We find that any third body must have a minimum mass of 0.17 $M_{\odot}$ and $\Delta v = 2.89$ km s^{-1} and although the effect on the spectra and radial velocities is likely to be minimal, there is the possibility it could be detected with near-IR adaptive optics.

There is also a complicated pattern of brightness variation, which does not as yet have a simple explanation in terms of a long-term activity cycle. In addition, there is also evidence of switching between the active longitudes seen on the star. However as we have less than a full cycle of activity and a complicated situation with additional growth and decline of spots in the eclipsed region, it is too early for definitive conclusions.

The two W UMa systems discussed in Chapter 6, V523 Cas and TY UMa, also show signs of long-term changes in brightness and orbital period. There is the possibility of a cycle in orbital-period variation in TY UMa and one in the brightness of the maxima in V523 Cas. The problem with these two systems is the faintness of the two stars and the "unfashionable" nature of W UMa systems meaning that the studies are much more intermittent and irregular, leading to large gaps in the O-C curve and the photometric history. This complicates any interpretation of the evidence for long-term variations.

There is a need to extend the baseline of high precision times of eclipse minima that have been obtained from photoelectric or CCD data. In many binary systems, most of the baseline of the O-C timings is based on older, less precise photographic and visual timings of minima. The wider availability and lower cost of CCD cameras in the present time may well improve this situation, increasing the number of systems that can be studied with modest professional and semi-professional equipment.

7.3 Future work

Improvements to LIGHT2

The future analysis of light curves of eclipsing binaries such as those undertaken here, could be significantly improved by an update of the internal data used by LIGHT2. LIGHT2 uses 4 data files for storage of the limb-darkening parameters, bolometric corrections, colour vs. temperature relation and the model atmosphere data. These data were taken from Carbon & Gingerich (1969), Popper (1980), Popper (1980), Carbon & Gingerich (1969) combined with Kurucz (1979) respectively and most of the data is over twenty years old. Many improvements have been made in the treatments of limb-darkening and huge leaps forward have been made in the physics incorporated in the latest stellar atmospheres and utilization of this modern data would bring LIGHT2 right up-to-date.

The light coming from a binary system does not only depend on the physical geometry and sizes of the system, but also on how the intensity varies across the stellar disks. Limb-darkening, which is symmetric with respect to longitude, is one of the main effects, the other being gravity-darkening which will be discussed later. The most recent and comprehensive computation and tabulation of limb-darkening coefficients were pre-

sented by Diaz-Cordoves, Claret & Giménez (1995) and Claret, Diaz-Cordoves & Giménez (1995) who used ATLAS9 model atmospheres (Kurucz 1993) and computed values of the coefficients for linear, quadratic and square-root limb-darkening laws. The use of different limb-darkening laws in different temperature regimes has been examined by Claret (1998) who concluded that linear limb-darkening fitting is not adequate in any temperature or wavelength regime especially for longer wavelengths ($\geq R$). In general it was found that the square-root law performed better than the quadratic law and both were superior to a linear approximation.

Model atmosphere calculations have undergone a huge increase in sophistication in the twenty-odd years since the results of Kurucz (1979). Greatly improved opacity calculations by the Opacity Project (Rogers & Iglesias 1992) and large improvements in the molecular data, particularly the important molecules of CO (Goorvitch & Chackerian 1994a, Goorvitch & Chackerian 1994b), CN (Jørgensen & Larsson 1990), TiO (Jørgensen 1994) and H_2O (Allard et al. 1994, Partridge & Schwenke 1997).

The huge increase in the speed of computers means that atomic and molecular line opacities can be treated by direct opacity sampling rather than using opacity distribution functions such as the Rosseland mean opacity. With direct opacity sampling the relevant background lines are selected from master line lists at each iteration and the contribution of every line within a window is summed to obtain the total line opacity at arbitrary wavelength points, the latter feature being crucial for NLTE calculations. This leads to a more accurate and rigorous treatment of the opacity, at the expense of increased computing time. For stars with effective temperatures greater than 7000–10,000 K NLTE effects become increasingly important and above 18,000 K Aufdenberg et al. (1998) and Aufdenberg, Hauschildt & Baron (1999) have shown that effects of line blanketing and spherical geometry are vitally important.

At the lower temperature end, the increasing number of very low mass objects (late M, L, T and brown dwarfs) that are being discovered in deep cluster searches and infrared sky surveys has required improvements in the equation of state (Chabrier & Baraffe 1997) to incorporate molecules, coupling of the atmospheric model with the interior as a boundary condition and the inclusion of dust formation and opacity which becomes important below 3000 K (Chabrier et al. 2000).

The current state of the art in stellar atmosphere codes is probably the PHOENIX

code (for a review see Allard et al. 1997) which is capable of solving NLTE relativistically expanding stellar atmospheres, including dust formation and opacity, for plane-parallel or spherical geometries. Results for LTE plane-parallel atmospheres in the temperature range $3000 \leq T_{eff} \leq 10,000$ K (the "NextGen" grid) were presented by Hauschildt, Allard & Baron (1999) and these could be incorporated into LIGHT2 as a replacement for the Kurucz (1979) atmospheres presently used.

In addition to the limb-darkening discussed above, the other effect which alters the intensity across the stellar surface is gravity-darkening. The original work in this area is due to von Zeipel (1924) who showed that the flux distribution depends on the surface gravity as $T_{eff}^4 \propto g^{\beta_1}$ where $\beta_1 = 1$ for radiative atmospheres. This means that the polar regions are hotter than the equatorial ones in distorted stars. This was extended to stars with convective envelopes by Lucy (1967) who found an average value of $\beta_1 = 0.32$.

Recent work and calculations by Claret (2000) have given for the first time values of β_1 as a function of mass, chemical composition and time and investigated the effect of different input physics and differential rotation on the gravity-darkening exponents. Although it would be possible to incorporate gravity-darkening exponents as a function of mass into LIGHT2 it is probably unnecessary because as pointed out by Claret (2000) there are several correlations between the parameters in a light curve solution and gravity-darkening is a 2nd order effect. Variations in the gravity-darkening exponents caused by changing chemical compositions, different metallicities and differences in the mixing length parameter α will be a 3rd order effect and it will probably not be possible to discriminate these effects until the advent of micro-magnitude precision photometry from space.

Improved bolometric corrections and broad-band colours have been compiled by Bessell, Castelli & Plez (1998) for stars of spectral type O–M based on ATLAS9 (Kurucz 1993) and NMARCS (Plez, Brett & Nordlund 1992) atmospheres. Results are available in the $UBVRIJHKL$ passbands defined by Bessell (1990), which could be used to extend LIGHT2 to allow solutions of IR data, a wavelength region which is becoming increasingly important. Bessell (1990) also analysed and compared theoretical colour vs. temperature relations with observation and found good agreement for almost all the relations.

This proposed upgrade to LIGHT2, which we christen "LIGHT2000", would improve the program greatly and permit more accurate and meaningful comparisons of new, hopefully high precision data, with theoretical models. Most of the proposed modifications

listed above could be accomplished relatively easily with little modification of the existing code, apart from minor changes in the datafile reading routines. Addition of limb-darkening laws other than the standard linear law would require more modification, including some changes to the parser but this would not be too difficult.

Extension of observational baselines

One recurring theme throughout this work has been that, no matter the method or diagnostic of long-term activity, we often seem to be in the situation of not quite having enough data or timebase to make definite statements about the long-term behaviour. The case is either that we have less than 1 complete cycle of a putative periodic signal and desire additional data to confirm and refine the period or we have a few objects with likely cycles and require additional objects to broaden the sample and investigate the dependence of cycles on other parameters.

Examples of the first case are the orbital period variations of binary systems discussed in Section 1.2.2.3 and the systems in Table 1.3, particularly the W UMa systems, which are bright, short-period and span an interesting range of cycle periods. Their probable periods could be confirmed and refined with a small amount of observational effort and broaden the sample space of systems with long-period variations considerably.

Another example of the first case is XY UMa, where we have ~ 1.9 cycles of orbital period variation and perhaps half a cycle of possible activity switching between active longitudes from the surface maps. In addition there is a long-term variation in system brightness which is not well understood and easily relatable to the other pieces of evidence. The continuation of the observing program to obtain surface maps at roughly monthly intervals for a few more years would clear up the situation of the growth and decline of active regions on the surface, and as a bonus, increase the baseline of precise times of eclipse minima and extend the O-C diagram.

The area of Doppler imaging, including Zeeman-Doppler Imaging and detections of differential rotation, fits into both of the above categories of incomplete results. We have systems such as HR 1099, II Peg, LQ Hya and AB Dor where cycles are just starting to become detectable and verifiable and the observational efforts should be continued. We also have a need to expand the parameter space to investigate topics such as the spot

evolution and distribution at the ends of the spectral type range where the dynamo is expected to operate, the effects of binarity and rotational velocity on the surface differential rotation and the formation, evolution and variation of the dynamo processes. Another necessary observational test is to determine the coincidence (or not) of magnetic and spot features. On the Sun the two coincide closely, but the results from the few Zeeman-Doppler Imaging studies that are able to map the magnetic field and surface spot distribution suggest this is not the case on rapidly-rotating active stars (Donati et al. 1999) and this needs further investigation.

The overall situation within the field of activity cycles in late-type stars is one of great potential with a large number of possible cycles on a wide variety of objects on the brink of confirmation or refinement. In addition the field of surface imaging is reaching maturity with an ever increasing number of high quality results being obtained. New developments in telescopes, instrumentation and analysis techniques will enable more information and understanding to be extracted and results obtained for a much broader sample of stars.

It will then become possible to really probe the parameter space and to establish the effect on the dynamo processes of the parameters that enable us to distinguish individual stars from each other.

REFERENCES

Agerer F., Huebscher J., 1997, Inf. Bull. Variable Stars, 4472

Agerer F., Huebscher J., 1998, Inf. Bull. Variable Stars, 4562

Akalin A., Derman E., 1997, A&AS, 125, 407

Allard F., Hauschildt P. H., Miller S., Tennyson J., 1994, ApJ, 426, L39

Allard F., Hauschildt P. H., Alexander D. R., Starrfield S., 1997, ARA&A, 35, 137

Anders G. J., Coates D. W., Thompson K., Innis J. L., 1999, MNRAS, 310, 377

Applegate J. H., Patterson J., 1987, ApJ, 322, L99

Applegate J. H., 1992, ApJ, 385, 621

Arévalo M. J., Lázaro C., 1999, AJ, 118, 1015

Arzoumanian Z., Fruchter A. S., Taylor J. H., 1994, ApJ, 426, L85

Aufdenberg J. P., Hauschildt P. H., Baron E., 1999, MNRAS, 302, 599

Aufdenberg J. P., Hauschildt P. H., Shore S. N., Baron E., 1998, ApJ, 498, 837

Baliunas S. L., Soon W., 1995, ApJ, 450, 896

Baliunas S. L., Donahue R. A., Soon W., Henry G. W., 1998, in Donahue R. A., Bookbinder J. A., eds, ASP Conference Series Vol. 154: 10th Cambridge Workshop on Cool Stars, Stellar Systems and the Sun. ASP Conference Series, San Francisco, p. 153

Banks T. S. Master's thesis, Victoria Univ. Wellington, Wellington, New Zealand, 1989

Barnes J. R., Collier Cameron A., 2000, in Boffin H., Steeghs D., Guypers J., eds, Astro Tomography: An International Workshop on Indirect Imaging - Lecture Notes in Physics Series. Springer-Verlag, Berlin, In press

Barnes T. G., Evans D. S., Moffett T. J., 1978, MNRAS, 183, 285

Barnes J. R., Collier Cameron A., Unruh Y. C., Donati J.-F., Hussain G. A. J., 1998, MNRAS, 299, 904

Barnes J. R., Collier Cameron A., James D. J., Donati J.-F., 2000a, MNRAS, In press

Barnes J. R., Collier Cameron A., James D. J., Donati J.-F., 2000b, MNRAS, 314, 162

Barnes J. R., 1999, PhD thesis, University of St. Andrews, St. Andrews, Scotland

Bedford D. K., Jeffries R. D., Geyer E. H., Vilhu O., 1990, MNRAS, 243, 557

Beichman C. A., Chester T. J., Skrutskie M., Low F. J., Gillett F., 1998, PASP, 110, 480

Beljawsky S., 1933, NNVS, 4, 196

Bell S. A., Hilditch R. W., Edwin R. P., 1993, MNRAS, 260, 478

Berdyugina S. V., Tuominen I., 1998, A&A, 336, L25

Berdyugina S. V., Berdyugin A. V., Ilyin I., Tuominen I., 1998a, A&A, 340, 437

Berdyugina S. V., Berdyugin A. V., Ilyin I., Tuominen I., 1998b, A&A, 350, 626

Berdyugina S. V., Berdyugin A. V., Ilyin I., Tuominen I., 2000, A&A, 360, 272

Berdyugina S. V., 1998, A&A, 338, 97

Bessell M. S., Castelli F., Plez B., 1998, A&A, 333, 231

Bessell M. S., 1990, PASP, 102, 1181

Bondar' N. I., 1992, Inf. Bull. Variable Stars, 3767

Bondar' N. I., 1995, A&AS, 111, 259

Bopp B. W., Africano J. L., Stencel R. E., Noah P. V., Klimike A., 1983, ApJ, 275, 691

Borra E. F., Edwards G., Mayor M., 1984, ApJ, 284, 211

Bouvier J., Forestini M., Allain S., 1997, A&A, 326, 1023

Bradstreet D. H., 1981, AJ, 86, 98

Broglia P., Conconi P., 1981, Inf. Bull. Variable Stars, 1949

Broglia P., Conconi P., 1983, A&AS, 51, 97

Brown D. N., Landstreet J. D., 1981, ApJ, 246, 899

Bruls J. H. M. J., Solanki S. K., Schüssler M., 1998, A&A, 336, 231

Budding E., Zeilik M., 1987, ApJ, 319, 827

Budding E., 1986, Ap&SS, 118, 241

Byrne P. B., 1996, in Strassmeier K., Linsky J., eds, IAU Symposium No. 176: Stellar Surface Structure. Kluwer, Dordrecht, p. 299

Caligari P., Moreno-Insertis F., Schüssler M., 1995, ApJ, 441, 886

Carbon D. F., Gingerich O. J., 1969, in Gingerich O. J., ed, Theory and Observation of Normal Stellar Atmospheres. M.I.T. Press, Cambridge, Mass., p. 377

Chabrier G., Baraffe I., 1997, A&A, 327, 1039

Chabrier G., Baraffe I., Allard F., Hauschildt P. H., 2000, ApJ, In press

Chochol D., Pribulla T., Teodorani M., Errico L., Vittone A. A., Milano L., Barone F., 1998, A&A, 340, 415

Claret A., Diaz-Cordoves J., Giménez A., 1995, A&AS, 114, 247

Claret A., 1998, A&A, 335, 647

Claret A., 2000, A&A, 359, 289

Collier Cameron A., Hilditch R. W., 1997, MNRAS, 287, 567

Collier Cameron A., Unruh Y. C., 1994, MNRAS, 269, 814

Collier Cameron A., Jeffery C. S., Unruh Y. C., 1992, in Jeffery C. S., Griffin R. E. M., eds, Stellar Chromospheres, Coronae and Winds. Institute of Astronomy, Cambridge, p. 81

Collier Cameron A., 1992, in Byrne P. B., Mullan D. J., eds, Surface Inhomogeneities on Late-type Stars. Springer-Verlag, Berlin, p. 33

Collier Cameron A., 1995, MNRAS, 275, 534

Collier Cameron A., 1997a, private communication

Collier Cameron A., 1997b, MNRAS, 287, 556

Collier Cameron A., 2000, in Boffin H., Steeghs D., Guypers J., eds, Astro Tomography: An International Workshop on Indirect Imaging - Lecture Notes in Physics Series. Springer-Verlag, Berlin, In press

Currie M. J., Berry D. S., 1999, Starlink User Note 95.14, Rutherford Appleton Laboratory

Cutispoto G., 1998a, A&AS, 127, 207

Cutispoto G., 1998b, A&AS, 131, 321

Delfosse X., Forveille T., Perrier C., Mayor M., 1998, A&A, 331, 581

Delfosse X., Forveille T., Mayor M., Burnet M., Perrier C., 1999, A&A, 341, L63

DeLuca E., Fan Y., Saar S., 1997, ApJ, 481, 369

Demicran O., Derman E., Akalin A., 1991, AJ, 101, 201

Demircan O., Gürol B., 1996, A&AS, 115, 333

Demircan O., Selam S., 1993, A&A, 267, 107

Deutsch A., 1958, in Lehnert B., ed, Proceedings, IAU Symposium No. 6: Electromagnetic Phenomena in Cosmological Physics. Cambridge University Press, Cambridge, p. 209

Diaz-Cordoves J., Claret A., Giménez A., 1995, A&AS, 110, 329

Dobson A. K., Radick R. R., 1989, ApJ, 344, 907

Donahue R. A., 1998, in Donahue R. A., Bookbinder J. A., eds, ASP Conference Series Vol. 154: 10th Cambridge Workshop on Cool Stars, Stellar Systems and the Sun. ASP Conference Series, San Francisco, p. CD1235

Donati J.-F., Collier Cameron A., 1997, MNRAS, 291, 1

Donati J.-F., Brown S. F., Semel M., Rees D. E., Dempsey R. C., Matthews J. M., Henry G. W., Hall D. S., 1992, A&A, 265, 682

Donati J.-F., Semel M., Carter B., Rees D. E., Collier Cameron A., 1997, MNRAS, 291, 658

Donati J.-F., Cameron A. C., Hussain G. A. J., Semel M., 1999, MNRAS, 302, 437

Donati J.-F., Mengel M., Carter B. D., Marsden S., Collier Cameron A., Wichmann R., 2000, MNRAS, 316, 699

Donati J.-F., Semel M., Praderie F., 1989, A&A, 225, 457

Donati J.-F., 1999, MNRAS, 302, 457

Draper P. W., Eaton N., 1998, Starlink User Note 109.9, Rutherford Appleton Laboratory

Duerbeck H. W., 1978, Acta Astron., 28, 49

Eddy J. A., 1977, in White O. R., ed, The Solar Output and Its Variation. Colo. Assoc. Univ. Press, Boulder, p. 51

Eggleton P. P., 1996, in Milone E. F., Mermilliod J.-C., eds, ASP Conference Series Vol. 90: The origins, evolution, and destinies of binary stars in clusters. ASP Conference Series, San Francisco, p. 257

Eibe M. T., Byrne P. B., Jeffries R. D., Gunn A. G., 1999, A&A, 341, 527

Epchtein N. et al., 1994, Ap&SS, 217, 3

Epchtein N., 1998, in The Impact of Near-Infrared Sky Surveys on Galactic and Extragalactic Astronomy. Kluwer, Dordrecht, p. 3

Erdem A., Güdür N., 1998, A&AS, 127, 257

Falk A. E., Wehlau W. H., 1974, ApJ, 192, 409

Frieboes-Conde H., Herczeg T. J., 1973, A&AS, 12, 1

Geyer E. H., 1976, in Eggleton P. P., Mitton S., Whelan J., eds, IAU Symposium No. 73: Structure and Evolution of Close Binary Stars. Reidel, Dordrecht, p. 313

Geyer E. H., 1980, in Plavec M. J., Popper D. M., Ulrich R. K., eds, Proc. IAU Symp. 88, Close Binary Stars: Observations and Interpretation. Reidel, Dordrecht, p. 423

Gleissberg W., 1944, Pub. Istanbul Univ. Obs., No. 27

Gleissberg W., 1971, Solar Phys., 21, 240

Gliese W., Jahreiss H., 1992, Third Catalogue of Nearby Stars. Veröff. Astron. Rechen-Instit., Heidelberg

Goncharsky A. V., Stepanov V. V., Khokhlova V. L., Yagola A. G., 1982, SvA, 26, 690

Gondoin P., 1986, A&A, 160, 73

Gondoin P., 1999, A&A, 352, 217

Goorvitch D., Chackerian C., 1994a, ApJS, 91, 483

Goorvitch D., Chackerian C., 1994b, ApJS, 92, 311

Granzer T., Schüssler M., Caligari P., Strassmeier K. G., 2000, A&A, 355, 1087

Gray D. F., 1992, The observation and analysis of stellar photospheres, 2nd edition. CUP, University of Cambridge

Greimel R., Robb R. M., 1998, Inf. Bull. Variable Stars, 4652

Griffin R. F., Griffin R. E. M., Gunn J. E., Zimmerman B. A., 1985, AJ, 90, 609

Hale G. E., Nicholson S. B., 1925, ApJ, 62, 270

Hall D. S., 1989, Space Sci. Rev., 50, 219

Hall D. S., 1991a, in Tuominen I., Moss D., Rüdiger R., eds, IAU Colloquim No. 130, The Sun and Cool Stars: Activity, Magnetism, Dynamos. Springer-Verlag, Berlin, p. 353

Hall D. S., 1991b, ApJ, 380, L85

Hanzl D., 1991, Inf. Bull. Variable Stars, 3615

Hartmann L., Bopp B. W., Dussault M., Noah P. V., Klimke A., 1981, ApJ, 249, 662

Hatzes A. P., Kürster M., 1999, A&A, 346, 432

Hatzes A. P., Vogt S. S., 1992, MNRAS, 258, 387

Hatzes A. P., Vogt S., Ramseyer T., Misch A., 1996, A&A, 469, 808

Hatzes A. P., 1993, ApJ, 410, 777

Hatzes A. P., 1995a, in Strassmeier K. G., ed, IAU Symposium No. 176: Poster Proceedings: Stellar Surface Structure. Kluwer, Dordrecht, p. 87

Hatzes A. P., 1995b, in Strassmeier K. G., ed, IAU Symposium No. 176: Poster Proceedings: Stellar Surface Structure. Kluwer, Dordrecht, p. 90

Hatzes A. P., 1995c, AJ, 109, 350

Hatzes A. P., 1998, A&A, 330, 541

Hauschildt P. H., Allard F., Baron E., 1999, ApJ, 512, 377

Heckert P., Zeilik M., 1988, Inf. Bull. Variable Stars, 3253

Hempelmann A., Hatzes A. P., Kuerster M., Patkos L., 1997, A&A, 317, 125

Hendry P. D., Mochnacki S. W., 2000, ApJ, 531, 467

Henry G. W., Eaton J. A., Hamer J., Hall D. S., 1995, ApJS, 97, 513

Hilditch R. W., Bell S. A., 1994, MNRAS, 267, 1081

Hilditch R. W., Collier Cameron A., 1995, MNRAS, 277, 747

Hilditch R. W., Collier Cameron A., Hill G., Bell S. A., Harries T. J., 1997, MNRAS, 291, 749

Hilditch R. W., 2001, An Introduction to Close Binary Stars. CUP, University of Cambridge

Hill G., Rucinski S. M., 1993, in Milone E. F., ed, Lightcurve modelling of eclipsing binary stars. Springer-Verlag, Berlin, p. 135

Hill G., 1979, Publ. Dom. Astrophys. Obs., 15, 297

Hill G. User Guide to RVORBIT. Dominion Astrophysical Observatory, 1986

Hoffman M., 1981a, Inf. Bull. Variable Stars, 1976

Hoffman M., 1981b, Inf. Bull. Variable Stars, 1978

Horne K. D., 1986, PASP, 98, 609

Howarth I. D., Murray J., Mills D., Berry D. S., 1997, Starlink User Note 50.20, Rutherford Appleton Laboratory

Huang S.-S., 1963, ApJ, 138, 471

Hussain G. A. J., Unruh Y. C., Collier Cameron A., 1997, MNRAS, 288, 343

Innis J. L., Coates D. W., Evans T. L., 1990, MNRAS, 242, 306

Jankov S., Donati J.-F., 1995, in Proceedings of 4th MUSICOS Workshop, Beijing 1994. Beijing Astronomical Observatory, Beijing, p. 143

Jankov S., Foing B. H., 1992, A&A, 256, 533

Jaschek C., Jaschek M., 1987, The classification of stars. CUP, University of Cambridge

Jassur D. M. Z., 1986, Ap&SS, 128, 369

Jeffries R. D., Jewell S. J., 1992, in Giampapa M. S., Bookbinder J. A., eds, ASP Conference Series Vol. 26: 7th Cambridge Workshop on Cool Stars, Stellar Systems and the Sun. ASP Conference Series, San Francisco, p. 77

Jeffries R. D., James D. J., Bromage G. E., 1994, MNRAS, 271, 476

Jeffries R. D., Byrne P. B., Doyle J. G., Anders G. J., James D. J., Lanzafame A. C., 1994, MNRAS, 270, 153

Jeffries R. D., Collins C., Elliot K. H., Pittard J. M., Taylor S. B., 1995, Inf. Bull. Variable Stars, 4277

Jeffries R. D., 1998, MNRAS, 295, 825

Jetsu L., Pelt J., Tuominen I., 1993, A&A, 278, 449

Jetsu L., Pelt J., Tuominen I., 1999, A&A, 351, 212

Jetsu L., 1996, A&A, 314, 153

Jørgensen U. G., Larsson A., 1990, A&A, 238, 424

Jørgensen U. G., 1994, A&A, 284, 179

Kalimeris A., Mitrou C. K., Doyle J. G., Antonopoulou E., Rovithis-Livaniou H., 1995, A&A,

293, 371

Kalimeris A., Rovithis-Livaniou H., Rovithis P., 1994, A&A, 282, 775

Kaufer A., Pasquini L., 1998, in Proceedings of SPIE 3355: Optical Astronomical Instrumentation. SPIE, Bellingham, WA, p. 844

Khalesseh B., Hill G., 1992, A&A, 257, 199

Kholopov P. N. et al., 1985, General Catalogue of Variable Stars, 4th Edition. Nauka, Moscow

Kővári Z., 1999, in Butler C. J., Doyle J. G., eds, ASP Conference Series Vol. 158: Solar and Stellar Activity: Similarities and Differences. ASP Conference Series, San Francisco, p. 166

Kitchatinov L. L., Rüdiger G., 1995, A&A, 299, 446

Kitchatinov L. L., Rüdiger G., 1999, A&A, 344, 911

Kitchatinov L. L., Jardine M., Donati J.-F., 2000, MNRAS, 318, 1171

Kjurkchieva D., Marchev D., Ogloza W., 2000, A&A, 354, 909

Korhonen H., Berdyugina S. V., Hackman T., Duemmler R., Ilyin I. V., Tuominen I., 1999, A&A, 346, 101

Korhonen H., Berdyugina S. V., Hackman T., Strassmeier K. G., Tuominen I., 2000, A&A, 360, 1067

Kuklin G. V., 1976, in Bumba V., Kleczek J., eds, IAU Symposium No. 71: Basic Mechanisms of Solar Activity. Reidel, Boston, p. 147

Kupka F., Piskunov N., Ryabchikova T. A., Stempels H. C., Weiss W. W., 1999, A&AS, 138, 119

Kürster M., Dennerl K., 1993, in Linsky J., Serio S., eds, Physics of Solar and Stellar Coronae. Kluwer Academic Publishers, Dordrecht, p. 443

Kürster M., Schmitt J. H. M. M., Cutispoto G., 1994, A&A, 289, 899

Kürster M., 1993, A&A, 274, 851

Kurucz R. L., 1979, ApJS, 40, 1

Kurucz R. L., 1993, CDROM # 13 (ATLAS9 atmospheric models) and # 18 (ATLAS9 and SYNTHE routines, spectral line database), Cambridge, MA

Lang K. R., 1992, Astrophysical Data: Planets & Stars. Springer-Verlag, Berlin

Lanza A. F., Rodonò M., 1999, A&A, 349, 887

Lanza A. F., Rodonò M., Rosner R., 1998, MNRAS, 296, 893

Lavrov M. I., Zhukov G. V., 1976, Pub. Kazan University Obs., 42, 46

Lazáro C., Arévalo M. J., Fuensalida J. J., 1987, Ap&SS, 134, 347

Lee W.-B., 1985, PhD thesis, Universität Bonn, Bonn, Germany

Lee W. B., 1993, in Leung K. C., Nha I.-S., eds, New Frontiers in Binary Star Research. Astron. Soc. Pac., San Francisco, p. 334

Leggett S. K., Allard F., Dahn C., Hauschildt P. H., Kerr T. H., Rayner J., 2000, ApJ, 535, 965

Li Q., Zhang R., Zhang X., 1989, Inf. Bull. Variable Stars, 3374

Lister T. A., Collier Cameron A., Bartus J., 1999, MNRAS, 307, 685

Lister T. A., McDermid R. M., Hilditch R. W., 2000, MNRAS, 317, 111

Lockwood G. W., Skiff B. A., Radick R. R., 1997, ApJ, 485, 789

Lu W., Rucinski S. M., 1999, AJ, 118, 515

Lucy L. B., 1967, Z. für Astrophysik, 65, 89

Lucy L. B., 1976, ApJ, 205, 208

Maceroni C., van't Veer F., 1996, A&A, 311, 523

Maceroni C., Vilhu O., van't Veer F., van Hamme W., 1994, A&A, 288, 529

Malina R. F. et al., 1994, AJ, 107, 751

Marsh T. R., 1989, PASP, 101, 1032

Matese J. J., Whitmire D. P., 1983, A&A, 117, L7

Mills D., 1994, Starlink User Note 152, Rutherford Appleton Laboratory

Milone E. F., Hrivnak B. J., Fisher W. A., 1985, ApJ, 90, 354

Montes D., Martin E. L., 1998, A&AS, 128, 485

Moss D., Tuominen I., 1997, A&A, 321, 151

Narayan R., Nityananda R., 1986, ARA&A, 24, 127

Neff J. E., O'Neal D., Saar S. H., 1995, ApJ, 452, 879

Nesci R., Maceroni C., Milano L., Russo G., 1986, A&A, 159, 142

Noah P. V., Bopp B. W., Fekel F., 1987, in Linsky J. L., Stencel R. E., eds, Fifth Cambridge Workshop on Cool Stars, Stellar Systems and the Sun. Springer-Verlag, Berlin, p. 506

Nolthenius R., 1991, Inf. Bull. Variable Stars, 3589

Noyes R. W., Hartmann L., Baliunas S. L., Duncan D. K., Vaughan A. H., 1984, ApJ, 279, 763

O'Connell D. J. K., 1951, Pub. Riverview College Obs., 2, 85

Oláh K., Hall D. S., Henry G. W., 1991, A&A, 251, 531

Oláh K., Kolláth Z., Strassmeier K. G., 2000, A&A, 356, 643

Oláh K., Panov K. P., Pettersen B. R., Valtaoja E., Valtaoja L., 1989, A&A, 218, 192

Oláh K., Kővári Z., Bartus J., Strassmeier K. G., Hall D. S., Henry G. W., 1997, A&A, 321, 811

O'Neal D., Saar S. H., Neff J. E., 1996, ApJ, 463, 766

Partridge H., Schwenke D. W., 1997, J. Chem. Phys., 106, 4618

Petrova A. V., 1995, SvA, 39, 825

Pettersen B. R., Oláh K., Sandmann W. H., 1992, A&AS, 96, 497

Phillips M. J., Hartmann L., 1978, ApJ, 224, 182

Piskunov N. E., Huenemoerder D. P. Saar S. H., 1994, in ASP Conference Series Vol. 64: 8th Cambridge Workshop on Cool Stars, Stellar Systems and the Sun. ASP Conference Series, San Francisco, p. 661

Piskunov N. E., Kupka F., Ryabchikova T. A., Weiss W. W., Jeffery C. S., 1995, A&AS, 112, 525

Piskunov N. E., Tuominen I., Vilhu O., 1990, A&A, 230, 363

Piskunov N. E., 1991, in Tuominen I., Moss D., Rüdiger R., eds, IAU Colloquim No. 130, The Sun and Cool Stars: Activity, Magnetism, Dynamos. Springer-Verlag, Berlin, p. 309

Piskunov N. E., 1996, in Strassmeier K. G., Linsky J. L., eds, IAU Symposium No. 176: Stellar

Surface Structure. Kluwer, Dordrecht, p. 45

Plavec M. J., 1962, Bull. Astron. Inst. Czech., 13, 224

Plez B., Brett J. M., Nordlund A., 1992, A&A, 256, 551

Pojmanski G., Geyer E. H., 1990, Acta Astron., 40, 245

Popper D. M., 1980, ARA&A, 18, 115

Press W. H., Teukolsky S. A., Vetterling W. T., Flannery B. P., 1992, Numerical Recipes: The Art of Scientific Computing (Second Edition). Cambridge University Press, Cambridge

Pribulla T., Chochol D., Parimucha, Š, 1999, Inf. Bull. Variable Stars, 4751

Radick R. R., Lockwood G. W., Baliunas S. L., 1990, Sci, 247, 39

Rafert J. B., 1982, PASP, 94, 485

Rainger P. P., Hilditch R. W., Edwin R. P., 1991, MNRAS, 248, 168

Ribes J. C., Nesme-Ribes E., 1993, A&A, 276, 549

Rice J. B., Strassmeier K. G., 1998, A&A, 336

Rice J. B., Wehlau W. H., Khokhlova V. L., 1989, A&A, 208, 179

Robb R. M., Cardinal R. D., 1995a, Inf. Bull. Variable Stars, 4221

Robb R. M., Cardinal R. D., 1995b, Inf. Bull. Variable Stars, 4270

Robb R. M., Balam D. D., Greimel R., 1999, Inf. Bull. Variable Stars, 4714

Robb R. M., 1998, Inf. Bull. Variable Stars, 4560

Robinson R. D., 1980, ApJ, 239, 961

Rodonò M., Cutispoto G., 1994, Mem. Soc. Astron. Ital., 65, 83

Rodonò M., Lanza A. F., Catalano S., 1995, A&A, 301, 75

Rogers F. J., Iglesias C. A., 1992, ApJS, 79, 507

Rovithis-Livaniou H., Rovithis P., Bitzaraki O., 1992, Ap&SS, 189, 237

Rucinski S. M., Lu W., 1999, AJ, 118, 2451

Rucinski S. M., Lu W., Mochnacki S. W., 2000, AJ, 120, 1133

Rucinski S. M., 1976, PASP, 88, 777

Rucinski S. M., 1986, in Cottrell P. L., Hearnshaw J. B., eds, IAU Symposium No. 118: Instrumentation and Research Programmes for Small Telescopes. Reidel, Dordrecht, p. 159

Rucinski S. M., 1994, in Sahade J., McCluskey J. E., Kondo Y., eds, The Realm of Interacting Binary Stars. Kluwer, Dordrecht, p. 111

Saar S. H., Butler R. P., Marcy G. W., 1998, ApJ, 498, L153

Saar S. H., Piskunov N. E., Tuominen I., 1994, in ASP Conference Series Vol. 64: 8th Cambridge Workshop on Cool Stars, Stellar Systems and the Sun. ASP Conference Series, San Francisco, p. 661

Saar S. H., 1988, ApJ, 324, 441

Saar S. H., 1998, Inf. Bull. Variable Stars, 4580

Samec R. G., Bookmyer B. B., 1987, PASP, 99, 1310

Samec R. G., Banks D. W., Hernandez R. B., Bright L. A., Faulkner D. R., Williams D. B., 1999,

American Astronomical Society Meeting No. 194 #75.06

Samec R. G., Stoddard M. L., Faulkner D. R., 2000, American Astronomical Society Meeting No. 196 #46.01

Samec R. G., van Hamme W., Bookmyer B. B., 1989, AJ, 98, 2287

Santos N. C., Mayor M., Naef D., Pepe F., Queloz D., Udry S., Blecha A., 2000, A&A, 361, 265

Sarna M. J., Fedorova A. V., 1989, A&A, 208, 111

Schüssler M., Solanki S. K., 1992, A&A, 264, L13

Schüssler M., Caligari P., Ferriz-Mas A., Solanki S. K., Stix M., 1996, A&A, 314, 503

Schwabe H., 1843, Astron. Nachr., 20, No. 285

Semel M., 1989, A&A, 225, 456

Shortridge K., Meyerdierks H., Currie M., Clayton M., Lockley J., Charles A., Davenhall C., 1995, Starlink User Note 86.11, Rutherford Appleton Laboratory

Šimon V., 1997a, A&A, 319, 886

Šimon V., 1997b, A&A, 327, 1087

Skilling J., Bryan R. K., 1984, MNRAS, 211, 111

Skrutskie M. F. et al., 1998, in The Impact of Large Scale Near-Infrared Sky Surveys on Galactic and Extragalactic Astronomy. Kluwer, Dordrecht, p. 25

Soderblom D. R., Stauffer J. R., MacGregor K. B., Jones B. F., 1993, ApJ, 409, 624

Soon W. H., Baliunas S. L., Zhang Q., 1993, ApJ, 414, L33

Stauffer J. R., Hartmann L. W., 1987, ApJ, 318, 337

Stauffer J. R., Hartmann L. W., Jones B. F., 1989, ApJ, 346, 160

Stout-Batalha N. M., Vogt S. S., 1996, in Strassmeier K. G., ed, IAU Symposium No. 176: Stellar Surface Structure. Kluwer, Dordrecht, p. 337

Stout-Batalha N. M., Vogt S. S., 1999, ApJS, 123, 251

Strassmeier K. G., Bartus J., 2000, A&A, 354, 537

Strassmeier K. G., Rice J. B., 1998, A&A, 330

Strassmeier K. G., Rice J. B., 2000, A&A, 360, 1019

Strassmeier K. G., Hubl B., Rice J. B., 1997, A&A, 322, 511

Strassmeier K. G. et al., 1991, A&A, 247, 130

Strassmeier K. G., Rice J. B., Wehlau W. H., Hill G. M., Matthews J. M., 1993, A&A, 268, 671

Strassmeier K. G., Bartus J., Cutispoto G., Rodonò M., 1997a, A&AS, 125, 11

Strassmeier K. G., Boyd L. J., Epand D. H., Granzer T., 1997b, PASP, 109, 697

Strassmeier K. G., Bartus J., Kovari Z., Weber M., Washuettl A., 1998, A&A, 336, 587

Strassmeier K. G., Lupinek S., Dempsey R. C., Rice J. B., 1999, A&A, 347, 212

Strassmeier K. G., 1994, A&A, 281, 395

Strassmeier K. G., 1996a, in Strassmeier K., Linsky J., eds, IAU Symposium No. 176: Stellar Surface Structure. Kluwer, Dordrecht, p. 289

Strassmeier K. G., 1996b, A&A, 314, 558

Strassmeier K. G., 1999, A&A, 347, 225

Strassmeier K. G., 2000, A&A, 357, 608

Tikhonov A. N., 1963, Soviet Math. Dokl., 4, 1624

Unruh Y. C., Collier Cameron A., 1995, MNRAS, 273, 1

Unruh Y. C., Collier Cameron A., 1997, MNRAS, 290, L37

Unruh Y. C., Collier Cameron A., Cutispoto G., 1995, MNRAS, 277, 1145

Unruh Y. C., 1996, in IAU Symposium No. 176: Stellar Surface Structure. Kluwer, Dordrecht, p. 35

van Hamme W., Wilson R. E., 1985, A&A, 152, 25

van Leeuwan F., Alphenaar P., Meys J. M. M., 1987, A&AS, 67, 483

Vilhu O., 1982, A&A, 109, 17

Vilhu O., 1984, A&A, 133, 117

Vincent A., Piskunov N. E., Tuominen I., 1993, A&A, 278, 523

Voges W. et al., 1996, IAU Circ., 6420

Vogt S. S., Hatzes A. P., 1991, in Tuominen I., Moss D., Rüdiger R., eds, IAU Colloquim No. 130, The Sun and Cool Stars: Activity, Magnetism, Dynamos. Springer-Verlag, Berlin, p. 297

Vogt S. S., Penrod G. D., 1983, PASP, 95, 565

Vogt S. S., Penrod G. D., Hatzes A. P., 1987, ApJ, 321, 496

Vogt S. S., Hatzes A. P., Misch A. A., Kürster M., 1999, ApJS, 121, 547

Vogt S. S., 1980, ApJ, 240, 567

Vogt S. S., 1988, in Cayrel de Strobel G., Spite M., eds, IAU Symposium No. 132: The Impact of Very High S/N Spectroscopy on Stellar Physics. Kluwer Academic Publishers, Dordrecht, p. 253

von Zeipel H., 1924, MNRAS, 84, 665

Wade R. A., Rucinski S. M., 1985, A&AS, 60, 471

Walker D. D., Diego F., Charalambous A., Hirst C. J., Fish A. C., 1986, in Proceedings of SPIE 627: Instrumentation in Astronomy VI. SPIE, Bellingham, WA, p. 291

Wallace P. T., 1998, Starlink User Note 5.17, Rutherford Appleton Laboratory

Washuettl A., Strassmeier K. G., Collier Cameron A., 1998, in Donahue R. A., Bookbinder J. A., eds, ASP Conference Series Vol. 154: 10th Cambridge Workshop on Cool Stars, Stellar Systems and the Sun. ASP Conference Series, San Francisco, p. CD2073

Weber M., Strassmeier K. G., 1998, A&A, 330, 1029

Weber R., 1958, J. des Observateurs, 41, 4.74

Wilson O. C., 1978, ApJ, 226, 379

Wolf R., 1856, Astron. Mitt. Zurich, No. 14

Worek T. F., 1996, PASP, 108, 962

Young A., Skumanich A., MacGregor K. B., Temple S., 1990, ApJ, 349, 608

Zeilik M., Elston R., Henson G., 1983, AJ, 88, 532

Zeilik M., Cox D., de Blasi C., Ledlow M., Rhodes M., Williams T., 1988a, Inf. Bull. Variable Stars, 3200

Zeilik M., de Blasi C., Rhodes M., Budding E., 1988b, ApJ, 332, 293

Zeilik M., Cox D. A., de Blasi C., Rhodes M., Budding E., 1989, ApJ, 345, 991

Zeilik M., Cox D. A., Ledlow M. J., Rhodes M., Heckert P. A., Budding E., 1990a, ApJ, 363, 647

Zeilik M., de Blasi C., Gordon S., Ledlow M., 1990b, Inf. Bull. Variable Stars, 3535

Zeilik M., Ledlow M., Rhodes M., Arevalo M. J., Budding E., 1990c, ApJ, 354, 352

Zeilik M., Gordon S., Jaderlund E., Ledlow M., Summers D. L., Heckert P. A., Budding E., Banks T. S., 1994, ApJ, 421, 303

Zhai D., Zhang R., Leung K.-C., 1984, A&AS, 57, 487

Zhukov G. V., 1985, Soviet Astron. Lett., 11, 42

APPENDIX A

Times of minima

A.1 XY UMa

Table A.1: Published times of primary minimum for XY UMa and residuals calculated from the ephemeris of Hilditch & Bell (1994).

HJD −2400000.0	Cycle No.	Computed	O-C residuals (days)	Reference
35216.50420	-28608.0	35216.49466	0.009537	Pojmanski & Geyer (1990)
35217.46400	-28606.0	35217.45265	0.011348	Pojmanski & Geyer (1990)
35246.44000	-28546.5	35246.43185	0.008154	Pojmanski & Geyer (1990)
35258.41470	-28521.5	35258.40672	0.007981	Pojmanski & Geyer (1990)
36229.57430	-26493.0	36229.56894	0.005360	Pojmanski & Geyer (1990)
36231.49090	-26489.0	36231.48492	0.005981	Pojmanski & Geyer (1990)
36604.62690	-25710.0	36604.62197	0.004930	Pojmanski & Geyer (1990)
39876.39650	-18880.5	39876.39684	-0.000339	Pojmanski & Geyer (1990)
39913.51820	-18802.0	39913.51895	-0.000746	Pojmanski & Geyer (1990)
42452.67660	-13501.0	42452.67107	0.005530	Pojmanski & Geyer (1990)
42716.60740	-12950.0	42716.59728	0.010123	Pojmanski & Geyer (1990)
42728.58220	-12925.0	42728.57215	0.010050	Pojmanski & Geyer (1990)
42738.63900	-12904.0	42738.63104	0.007957	Pojmanski & Geyer (1990)
42741.51350	-12898.0	42741.50501	0.008487	Pojmanski & Geyer (1990)
43947.86910	-10380.5	43947.85374	0.015356	Pojmanski & Geyer (1990)
44258.49650	-9731.0	44258.48196	0.014544	Pojmanski & Geyer (1990)

continued on next page

continued from previous page

HJD −2400000.0	Cycle No.	Computed	O-C residuals (days)	Reference
44266.39790	-9715.5	44266.38537	0.012527	Pojmanski & Geyer (1990)
44288.43150	-9669.5	44288.41914	0.012361	Pojmanski & Geyer (1990)
44288.67240	-9668.0	44288.65864	0.013763	Pojmanski & Geyer (1990)
44634.26320	-8947.5	44634.25348	0.009721	Pojmanski & Geyer (1990)
45001.64930	-8180.5	45001.64259	0.006710	Pojmanski & Geyer (1990)
45036.38360	-8107.0	45036.36972	0.013878	Pojmanski & Geyer (1990)
45061.52740	-8055.5	45061.51696	0.010444	Pojmanski & Geyer (1990)
45064.40030	-8049.5	45064.39093	0.009374	Pojmanski & Geyer (1990)
45384.60720	-7380.0	45384.59904	0.008163	Pojmanski & Geyer (1990)
45743.37350	-6631.0	45743.36624	0.007261	Pojmanski & Geyer (1990)
45743.62020	-6631.5	45743.60574	0.014463	Pojmanski & Geyer (1990)
46854.64010	-4311.0	46854.63448	0.005623	Heckert & Zeilik (1988)
47593.24890	-2769.0	47593.24466	0.004241	Pojmanski & Geyer (1990)
47594.20670	-2767.0	47594.20265	0.004051	Li, Zhang & Zhang (1989)
47616.23980	-2721.0	47616.23642	0.003385	Li, Zhang & Zhang (1989)
47617.19780	-2719.0	47617.19441	0.003395	Li, Zhang & Zhang (1989)
47618.15560	-2717.0	47618.15240	0.003205	Li, Zhang & Zhang (1989)
47944.35260	-2036.0	47944.34794	0.004657	Hanzl (1991)
47964.47000	-1994.0	47964.46573	0.004270	Pojmanski & Geyer (1990)
47966.38580	-1990.0	47966.38171	0.004091	Pojmanski & Geyer (1990)
48918.62352	-2.0	48918.62363	-0.000110	Hilditch & Bell (1994)
48919.58162	0.0	48919.58162	0.000000	Hilditch & Bell (1994)
49055.61830	284.0	49055.61618	0.002120	Jeffries et al. (1995)
49433.54360	1073.0	49433.54318	0.000420	Erdem & Güdür (1998)
49436.41750	1079.0	49436.41715	0.000351	Erdem & Güdür (1998)
49775.54690	1787.0	49775.54556	0.001340	Jeffries et al. (1995)
50026.54050	2311.0	50026.53890	0.001597	Collier Cameron (1997a)
50048.57450	2357.0	50048.57267	0.001830	Collier Cameron (1997a)
50118.51090	2503.0	50118.50593	0.004970	Collier Cameron (1997a)

continued on next page

continued from previous page

HJD −2400000.0	Cycle No.	Computed	O-C residuals (days)	Reference
50422.43640	3137.5	50422.42821	0.008187	Kjurkchieva et al. (2000)
50422.67540	3138.0	50422.66771	0.007690	Kjurkchieva et al. (2000)
50478.71867	3255.0	50478.71012	0.008553	this work
50482.55260	3263.0	50482.54208	0.010523	Kjurkchieva et al. (2000)
50483.51070	3265.0	50483.50007	0.010634	Kjurkchieva et al. (2000)
50493.56671	3286.0	50493.55896	0.007750	this work
50508.41499	3317.0	50508.40780	0.007187	this work
50528.53215	3359.0	50528.52559	0.006560	this work
50532.36397	3367.0	50532.35755	0.006421	this work
50540.50612	3384.0	50540.50046	0.005657	this work
50542.42183	3388.0	50542.41644	0.005387	this work
50814.49340	3956.0	50814.48556	0.007837	Chochol et al. (1998)
50815.45100	3958.0	50815.44355	0.007447	Chochol et al. (1998)
50833.65213	3996.0	50833.64536	0.006770	this work
50837.48420	4004.0	50837.47732	0.006880	Chochol et al. (1998)
50839.64500	4008.5	50839.63280	0.012203	Chochol et al. (1998)
50852.33261	4035.0	50852.32616	0.006447	this work
50869.57575	4071.0	50869.56998	0.005770	this work
50872.45092	4077.0	50872.44395	0.006970	this work
50872.69155	4077.5	50872.68345	0.008103	this work
50877.72004	4088.0	50877.71289	0.007146	this work
50881.55155	4096.0	50881.54485	0.006697	this work
50888.50010	4110.5	50888.49028	0.009820	Chochol et al. (1998)
50891.61207	4117.0	50891.60375	0.008323	this work
51130.63569	4616.0	51130.62222	0.013473	Pribulla et al. (1999)
51141.65114	4639.0	51141.63910	0.012040	Pribulla et al. (1999)
51150.50720	4657.5	51150.50051	0.006694	Pribulla et al. (1999)
51158.41647	4674.0	51158.40392	0.012547	Pribulla et al. (1999)
51158.65230	4674.5	51158.64342	0.008880	Pribulla et al. (1999)

continued on next page

continued from previous page

HJD −2400000.0	Cycle No.	Computed	O-C residuals (days)	Reference
51177.57570	4714.0	51177.56372	0.011980	Pribulla et al. (1999)
51183.32460	4726.0	51183.31166	0.012941	Pribulla et al. (1999)
51200.56777	4762.0	51200.55548	0.012293	Pribulla et al. (1999)
51203.44206	4768.0	51203.42945	0.012614	Pribulla et al. (1999)
51211.34858	4784.5	51211.33286	0.015717	this work
51211.58497	4785.0	51211.57236	0.012610	this work
51215.41681	4793.0	51215.40432	0.012491	this work
51237.45080	4839.0	51237.43809	0.012714	Pribulla et al. (1999)
51250.38368	4866.0	51250.37095	0.012731	Pribulla et al. (1999)
51256.37190	4878.5	51256.35839	0.013514	Pribulla et al. (1999)
51267.38870	4901.5	51267.37527	0.013431	this work
51268.34744	4903.5	51268.33326	0.014181	this work
51273.37538	4914.0	51273.36271	0.012674	Pribulla et al. (1999)
51274.33357	4916.0	51274.32070	0.012874	Pribulla et al. (1999)
51278.41180	4924.5	51278.39215	0.019647	Pribulla et al. (1999)
51559.33552	5511.0	51559.32268	0.012841	this work
51621.60549	5641.0	51621.59202	0.013470	this work
51628.55820	5655.5	51628.53745	0.020753	this work

A.2 V523 Cas

Table A.2: Published times of minima for V523 Cas and residuals calculated from the ephemeris of Lavrov and Zhukov (1976).

HJD −2400000.0	Cycle No.	Computed	O-C residuals (days)	Reference
41213.52710	-29.0	41213.52658	0.000524	Lavrov & Zhukov (1976)
41220.30360	0.0	41220.30360	0.000000	Lavrov & Zhukov (1976)
41223.45700	13.5	41223.45842	-0.001422	Lavrov & Zhukov (1976)

continued on next page

continued from previous page

HJD −2400000.0	Cycle No.	Computed	O-C residuals (days)	Reference
41225.44300	22.0	41225.44479	-0.001791	Lavrov & Zhukov (1976)
41226.49440	26.5	41226.49640	-0.001998	Lavrov & Zhukov (1976)
41585.44470	1562.5	41585.44501	-0.000306	Lavrov & Zhukov (1976)
41588.24700	1574.5	41588.24929	-0.002292	Lavrov & Zhukov (1976)
41593.39010	1596.5	41593.39048	-0.000383	Lavrov & Zhukov (1976)
41599.35030	1622.0	41599.34959	0.000709	Lavrov & Zhukov (1976)
41942.52470	3090.5	41942.52409	0.000610	Lavrov & Zhukov (1976)
41945.33000	3102.5	41945.32838	0.001624	Lavrov & Zhukov (1976)
41945.44800	3103.0	41945.44522	0.002779	Lavrov & Zhukov (1976)
41950.35350	3124.0	41950.35272	0.000778	Lavrov & Zhukov (1976)
41966.36060	3192.5	41966.36052	0.000079	Lavrov & Zhukov (1976)
41968.46400	3201.5	41968.46374	0.000264	Lavrov & Zhukov (1976)
41972.55310	3219.0	41972.55332	-0.000220	Lavrov & Zhukov (1976)
41973.48760	3223.0	41973.48808	-0.000481	Lavrov & Zhukov (1976)
41975.59250	3232.0	41975.59130	0.001204	Lavrov & Zhukov (1976)
41983.41880	3265.5	41983.41993	-0.001128	Lavrov & Zhukov (1976)
41985.52150	3274.5	41985.52314	-0.001642	Lavrov & Zhukov (1976)
42036.46680	3492.5	42036.46767	-0.000871	Lavrov & Zhukov (1976)
42037.16870	3495.5	42037.16874	-0.000043	Lavrov & Zhukov (1976)
44060.81340	12155.0	44060.81163	0.001772	Bradstreet (1981)
44062.80040	12163.5	44062.79800	0.002403	Bradstreet (1981)
44102.76090	12334.5	44102.75907	0.001828	Bradstreet (1981)
44117.71800	12398.5	44117.71526	0.002736	Bradstreet (1981)
44132.67420	12462.5	44132.67146	0.002744	Bradstreet (1981)
44133.84240	12467.5	44133.83991	0.002491	Bradstreet (1981)
44136.64690	12479.5	44136.64419	0.002705	Bradstreet (1981)
44136.76330	12480.0	44136.76104	0.002260	Bradstreet (1981)
44136.88010	12480.5	44136.87789	0.002215	Bradstreet (1981)
44140.73520	12497.0	44140.73378	0.001421	Bradstreet (1981)

continued on next page

continued from previous page

HJD −2400000.0	Cycle No.	Computed	O-C residuals (days)	Reference
44154.64090	12556.5	44154.63836	0.002537	Bradstreet (1981)
44154.75730	12557.0	44154.75521	0.002091	Bradstreet (1981)
44162.58580	12590.5	44162.58384	0.001960	Bradstreet (1981)
44162.70302	12591.0	44162.70069	0.002334	Bradstreet (1981)
44191.32910	12713.5	44191.32777	0.001328	Hoffman (1981a)
44194.48280	12727.0	44194.48259	0.000207	Hoffman (1981a)
44195.53630	12731.5	44195.53420	0.002099	Hoffman (1981a)
44200.32620	12752.0	44200.32486	0.001344	Hoffman (1981a)
46706.66820	23477.0	46706.65547	0.012731	Samec & Bookmyer (1987)
46707.71910	23481.5	46707.70708	0.012024	Samec & Bookmyer (1987)
46707.83670	23482.0	46707.82392	0.012779	Samec & Bookmyer (1987)
46707.95310	23482.5	46707.94077	0.012334	Samec & Bookmyer (1987)
46708.65440	23485.5	46708.64184	0.012562	Samec & Bookmyer (1987)
46708.77120	23486.0	46708.75868	0.012517	Samec & Bookmyer (1987)
51071.68810	42155.5	51071.64347	0.044627	Samec et al. (1999)
51071.80460	42156.0	51071.76032	0.044282	Samec et al. (1999)
51072.73950	42160.0	51072.69508	0.044420	Samec et al. (1999)
51072.85660	42160.5	51072.81193	0.044675	Samec et al. (1999)
51073.79280	42164.5	51073.74669	0.046113	Samec et al. (1999)
51073.90810	42165.0	51073.86353	0.044567	Samec et al. (1999)
51142.26200	42457.5	51142.21800	0.043996	this work
51142.37950	42458.0	51142.33485	0.044651	this work
51146.46946	42475.5	51146.42443	0.045027	this work
51146.58551	42476.0	51146.54128	0.044232	this work
51162.36093	42543.5	51162.31539	0.045543	this work
51162.47682	42544.0	51162.43223	0.044588	this work
51171.35786	42582.0	51171.31247	0.045389	this work

A.3 TY UMa

Table A.3: Published times of minima for TY UMa and residuals calculated from the ephemeris of Broglia & Conconi (1983).

HJD −2400000.0	Cycle No.	Computed	O-C residuals (days)	Reference
39532.49710	0.0	39532.49650	0.000600	Broglia & Conconi (1981)
39532.67270	0.5	39532.67377	-0.001070	Broglia & Conconi (1981)
39561.56850	82.0	39561.56877	-0.000271	Broglia & Conconi (1981)
39562.45450	84.5	39562.45512	-0.000621	Broglia & Conconi (1981)
39563.51790	87.5	39563.51874	-0.000840	Broglia & Conconi (1981)
39566.53280	96.0	39566.53233	0.000471	Broglia & Conconi (1981)
39614.39550	231.0	39614.39521	0.000285	Broglia & Conconi (1981)
39643.46730	313.0	39643.46749	-0.000186	Broglia & Conconi (1981)
39648.43060	327.0	39648.43104	-0.000444	Broglia & Conconi (1981)
39673.42470	397.5	39673.42611	-0.001406	Broglia & Conconi (1981)
39676.44070	406.0	39676.43970	0.001005	Broglia & Conconi (1981)
39681.40230	420.0	39681.40325	-0.000954	Broglia & Conconi (1981)
44634.49830	14390.5	44634.50279	-0.004487	Broglia & Conconi (1983)
44634.67400	14391.0	44634.68006	-0.006057	Broglia & Conconi (1983)
44635.56210	14393.5	44635.56641	-0.004307	Broglia & Conconi (1983)
44641.58880	14410.5	44641.59358	-0.004785	Broglia & Conconi (1983)
44642.47520	14413.0	44642.47993	-0.004735	Broglia & Conconi (1983)
44649.38900	14432.5	44649.39346	-0.004462	Hoffman (1981b)
44649.56400	14433.0	44649.57073	-0.006732	Hoffman (1981b)
44723.48700	14641.5	44723.49230	-0.005299	Broglia & Conconi (1983)
44724.37350	14644.0	44724.37865	-0.005149	Broglia & Conconi (1983)
44725.43660	14647.0	44725.44227	-0.005669	Broglia & Conconi (1983)
44730.40050	14661.0	44730.40583	-0.005327	Broglia & Conconi (1983)
50192.52780	30067.5	50192.62464	-0.096843	Agerer & Huebscher (1998)
50193.58940	30070.5	50193.68826	-0.098862	Agerer & Huebscher (1998)
50194.47970	30073.0	50194.57461	-0.094912	Agerer & Huebscher (1998)

continued on next page

continued from previous page

HJD −2400000.0	Cycle No.	Computed	O-C residuals (days)	Reference
50195.36510	30075.5	50195.46096	-0.095862	Agerer & Huebscher (1998)
50195.54170	30076.0	50195.63823	-0.096532	Agerer & Huebscher (1998)
51262.37684	33085.0	51262.44876	-0.071921	this work
51262.55370	33085.5	51262.62603	-0.072331	this work
51265.39007	33093.5	51265.46235	-0.072280	this work
51265.56764	33094.0	51265.63962	-0.071980	this work
51278.86260	33131.5	51278.93487	-0.072266	Samec et al. (2000)
51279.74951	33134.0	51279.82122	-0.071705	Samec et al. (2000)
51279.92670	33134.5	51279.99849	-0.071785	Samec et al. (2000)
51280.81240	33137.0	51280.88483	-0.072435	Samec et al. (2000)
51531.47882	33844.0	51531.54454	-0.065717	this work
51561.61504	33929.0	51561.68043	-0.065388	this work
51561.79173	33929.5	51561.85770	-0.065968	this work
51564.62856	33937.5	51564.69402	-0.065457	this work
51569.59186	33951.5	51569.65758	-0.065715	this work
51569.77004	33952.0	51569.83485	-0.064805	this work
51623.48351	34103.5	51623.54764	-0.064129	this work
51624.37021	34106.0	51624.43399	-0.063778	this work
51638.37443	34145.5	51638.43831	-0.063884	this work
51639.61570	34149.0	51639.67920	-0.063504	this work